ISSN:2538-516X

Journal of Civil Engineering Researchers

Volume: 6; Number: 4; December 2024

J-Researchers

J-Researchers

JOURNAL OF CIVIL ENGINEERING RESEARCHERS

Volume 6, Number 4, December 2024

Contents

J-Researchers

Journal of Civil Engineering Researchers

Journal homepage: www.journals-researchers.com

Evaluation of Shape Memory Alloys in the Performance of Reinforced Concrete Frames under Near-Fault Earthquakes

Seyed Ahmad Mazloum,[a] Mahdi Mashhadiyan,[a,*] Elham Rajabpour,[b]

[a] *Department of Civil Engineering, Ramsar Branch, Islamic Azad University, Ramsar, Iran*

[b] *Department of Civil Engineering, Chalous Branch, Islamic Azad University, Chalous, Iran*

ABSTRACT

This study investigates and compares the performance of reinforced concrete buildings containing SMA bars and steel bars as longitudinal reinforcement of column. The use of this type of material is to reduce permanent deformation in the structure due to the reversible properties of these materials. First, a laboratory specimen of a reinforced concrete column with shape memory alloy bars was modeled in the OPENSEES software and the modeling method was validated. Then, 3- and 5-story concrete frames, in two states, reinforced with steel bars and SMA bars, under nonlinear static and nonlinear time history analyses with near-fault records were analyzed. The results of the time history analyses showed that, although the use of SMA bars significantly reduces the residual deformation of the structure, it does not show a significant effect on reducing the maximum displacement of the structure. The maximum rotational deformation of columns in frames with SMA bars is greater than of frames with steel bars. However, SMA bars have greatly reduced the permanent rotational deformation of columns and reduced it to zero. The maximum drift of floors in frames with SMA bars increases slightly. The permanent drift of the structure in frames with SMA bars is significantly reduced.

ARTICLE INFO

Received: July 14, 2024
Accepted: August 20, 2024

Keywords:
Concrete Frames
Nonlinear Static Analysis
Time History Dynamic Analysis
Shape Memory Alloy
Seismic Performance

DOI: 10.61186/JCER.6.4.1
DOR: 20.1001.1.2538516.2024.6.4.1.6

1. Introduction

During an earthquake, heavy structures, especially concrete structures, are subjected to significant forces due to their large mass [1,2]. The ways to dissipate the energy imposed on structures during an earthquake without destroying the stability of the structure are important. One of the ways to reduce the concrete structures damage is to use shape memory alloys (SMA) [3,4,5]. These materials are smart metals that have two different crystal structures, one of which is stable at high stresses and the other at low stresses. This reversible phase transformation has led to the emergence of special mechanical properties in them, which can improve the seismic performance of structures.

Shape memory alloys (SMAs) are a class of materials that have unique properties, including Young's modulus-temperature relations, shape memory effects, superelastic effects, and high damping characteristics [6]. Superelastic

* Corresponding author. Tel.: +98-911-196-2921; e-mail: mahdi.mashhadiyan@gmail.com.

shape memory alloys (SMAs) have the ability to undergo large deformations and recover all plastic deformations upon unloading. Their utilization in steel structures can significantly reduce seismic residual deformations, which will facilitate post-seismic retrofitting [7]. Experimental results by Sharabash & Andrawes, 2009 showed that the SMA braced frame could withstand several strong earthquakes with very limited capacity degradation [8]. The investigations by Abdulridha et al., 2013 and Abraik & Youssef, 2018 demonstrate the superior seismic performance of superelastic SMA RC as compared to steel RC. The results show that the crack widths and crack spacing were larger in the SMA beams; however, upon removal of load, the crack openings were recovered, Energy dissipation was lower in the SMA beams [9,10]. The results by Nikbakht et al., 2015 indicate that in high seismicity zones, bridge columns with SMA bars have a superior performance against earthquake loading [11]. Recent studies showed that concrete confinement using shape memory alloy (SMA) spirals is a promising technique for seismic retrofitting of reinforced concrete columns that lack flexural ductility [12]. Test results by Jung et al., 2018 show that SMA confinement is highly effective in mitigating the seismic damage and improving the seismic performance of retrofitted RC columns, subjected to strong earthquakes [13]. The analyses by Cortés-Puentes & Palermo, 2017 showed that the SMA braces can improve the lateral strength capacity, energy dissipation, and re-centering of reinforced concrete shear walls, while reducing strength and stiffness degradation associated with shear-related damage [14]. Elbahy, 2019 investigated the seismic performance of RC frames retrofitted using external superelastic SMA bars and compared to the behaviour of a regular steel RC frame structure. Analysis results show improved seismic performance for the retrofitted frames as compared to the original steel RC frame. This improvement was represented by lower level of damage at the same earthquake intensity and increased seismic capacity [15].

In this study, the effectiveness of shape memory alloys as longitudinal bars to improve the flexural performance of reinforced concrete beams and columns has been investigated. For this purpose, the performance of reinforced concrete frames with columns equipped with shape memory alloys and conventional ones has been evaluated.

2. Shape Memory Alloys

In general, two distinct behaviors can be defined for shape memory materials:

- Shape memory effect: When these materials are in the Martensite state, after applying stress and reaching a nonlinear state and creating residual strain by unloading, the residual strain of the material can be eliminated by applying temperature and the material will return to its original state [16].
- Superelastic behavior: Another important property of these materials that has attracted attention in civil engineering is superelastic behavior. This means that a sample of shape memory materials which is initially in the austenite state, upon applying stress, is converted to a less symmetrical Martensite state with lower stiffness. This behavior will cause nonlinear behavior. If the structure is unloaded at this time, the structure will return to the initial point in a path other than the loading path and no residual strain will be created [16].

3. Modeling

3.1. Structural Specifications

In this study, two 3- and 5-story buildings are modeled with steel bars in the beam, and in order to compare the performance, the columns of each of these buildings are modeled separately with steel bars and with SMA bars. The specifications of the buildings are as follows:

Each building has four spans in the X direction and three spans in the Y direction. The length of all spans is 5 meters and the height of the floors is 2.3 meters. The lateral load-bearing system of the building is a reinforced concrete frame. The connection of the column feet to the foundation is modeled as a bracket and the foundation of the structure is assumed to be rigid. The P-Δ effect is considered for the columns. The dead load applied to the floor of the floors is 550 kg/m^2 and the live load applied is 200 kg/m^2. The nodes at each floor level are interconnected in such a way that they can represent the behavior of a rigid roof. Concrete with a strength of 25 MPa has been used. The yield strength of steel bars and SMA bars has been considered to be 400 MPa. The modeling and cross-sectional characteristics of columns in the 3-story and 5-story frames are presented in Figure and Table 1.

The period of rotation obtained from 3- and 5-story frames in two cases including steel rebar and SMA rebar is presented in Table 2.

3.2. Selection of accelerograms and their scaling

Using nonlinear time history analysis in the OPENSEES software, the response of the structure is obtained as a function of time during the seismic event. To perform such an analysis, the nonlinear behavior of the materials is modeled and the accelerogram is defined.

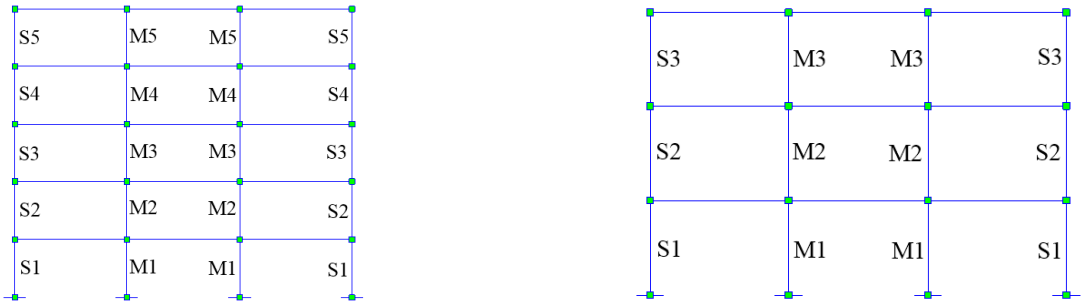

Figure 1: Modeling frame view

Table 1

Column cross-section specifications in 3- and 5-story frames

3-Storey					5-Storey				
Frame sections	b (mm)	h (mm)	Beams reinforced with steel bars ρs	ρs	Frame sections	b (mm)	h (mm)	Beams reinforced with steel bars ρs	ρs
S1	400	400	1.37	1.51	S1	450	450	1.59	1.73
S2	350	350	1.15	1.35	S2	450	450	1.00	1.00
S3	350	350	1.59	1.66	S3	400	400	1.00	1.00
M1	400	400	1.39	1.57	S4	400	400	1.00	1.00
M2	350	350	1.33	1.47	S5	400	400	1.10	1.06
M3	350	350	1.00	1.09	M1	450	450	1.76	2.11
---	---	---	---	---	M2	450	450	1.00	1.00
---	---	---	---	---	M3	400	400	1.21	1.28
---	---	---	---	---	M4	400	400	1.00	1.00
---	---	---	---	---	M5	400	400	1.00	1.00

Table 2

Period and frequency

Building	3 floors with steel rebar	3 floors with SMA rebar	5 floors with steel rebar	5 floors with SMA rebar
Period	0.84	0.79	1.15	1.08

To select the accelerograms and determine their characteristics and distance from the fault, is applied the set of records classified in FEMA P695, which was presented in 2009 under the title “Measurement of Building Seismic Performance Factors”. For this study, seven near-fault earthquake records are considered according to Table 3.

The soil type, fault type, and distance from the epicenter for the near-fault accelerometer set are as follows. The selected earthquakes are related to soil type D according to the NEHRP standard. In the time history analysis method, the structural analysis is performed by giving the effect of ground acceleration as a function of time, at the base level of the building, and using conventional structural dynamics calculations. To achieve this goal, it is necessary to select at least three pairs of accelerometers belonging to the horizontal components of three different earthquakes recorded to satisfy the design earthquake conditions and in which the magnitude, distance from the fault, and the mechanism of the seismic source are considered.

3.3. Validation

Nakashoji et al. in 2014 tested a reinforced concrete column with a circular cross-section and a scale of one-third. The column diameter and height was selected 457 mm and 1.57 m, respectively. Sixteen SMA bars with a diameter of 13 mm were used for longitudinal reinforcement. Concrete with a strength of 47.5 MPa was used in this test [17].

Table 3

Earthquake name and station for the set of near-fault accelerograms

ID NO.	Earthquake		
	M	Year	Name
1	7.1	1999	Duzce
2	6.8	1990	Gazli
3	6.5	1979	Imperial
4	6.8	1985	Nahanni
5	6.9	1989	Loma
6	7.0	1992	Cape
7	6.7	1994	Northridge

Numerical modeling was performed in the OPENSEES software. In concrete modeling, nonlinear behavior of materials was considered. The well-known Kent & Park model was used to define the behavior curve of uniaxial concrete. The relationship of this model is as follows:

$$\sigma_c = f_c' \times \left[2\left(\frac{\varepsilon_c}{\varepsilon_c'}\right) - \left(\frac{\varepsilon_c}{\varepsilon_c'}\right)^2\right] \quad (1)$$

In this relation, σ_c and ε_c are the compressive stress and strain, respectively, f_c' and ε_c' are the compressive strength of the unconfined concrete cylindrical specimen and its corresponding strain, respectively.

In Figure 3, the base-drift shear curve obtained from the experiment is plotted next to the base-drift shear curve obtained from the OPENSEES model. According to the curves in Figure 3, the OPENSEES model was able to simulate the behavior of the reference specimen in an acceptable manner. The stiffness (initial slope) of both graphs coincided and the strength of the finite element model was able to predict the strength of the reference model with a difference of less than 5%.

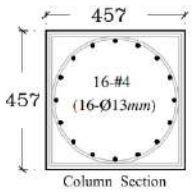

Figure 2: Column cross-section characteristics

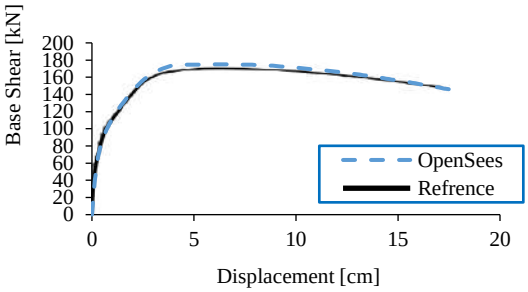

Figure 3: Base shear-drift curve obtained from the experiment next to the base shear-drift curve obtained from the OPENSEES model

4. Time history analysis

4.1. Three-story building

Time history analysis of the three-story model was performed in two cases of steel rebar and alloy rebar using seven different earthquake records. In Figure 4, the time history curve related to the base shear and roof floor displacement of the three-story frame under the effect of a two-three earthquake is plotted. The green graph is for the frame with steel rebars and the blue graph is for the frame with SMA rebars in the column.

According to Figure 4, the maximum base shear applied to steel bars is greater than that of SMA bars and the maximum displacements are not much different between the two types of bars. In Figure 5, the lateral displacement curve of the floors (drift) in a three-story building with a column with steel bars and SMA bars under the effect of a two-magnitude earthquake is plotted next to each other. According to the obtained graphs, the maximum drift in both structures is similar to each other and the overall behavior of the two structures is not much different. However, the permanent drift of the structure with SMA bars is less compared to the structure with steel bars.

The maximum rotation of beams and columns at different floors of a three-story frame is plotted in Figure 6 (a) and (b), respectively. The blue graph is for the frame with steel rebar in the column and the orange graph is for the frame with SMA rebar in the column.

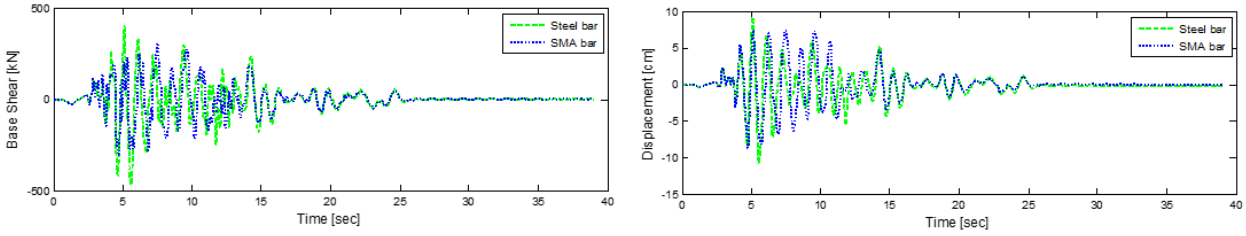

Figure 4: Three-story frame under the influence of Duzce earthquake (a) Base shear (b) Roof displacement

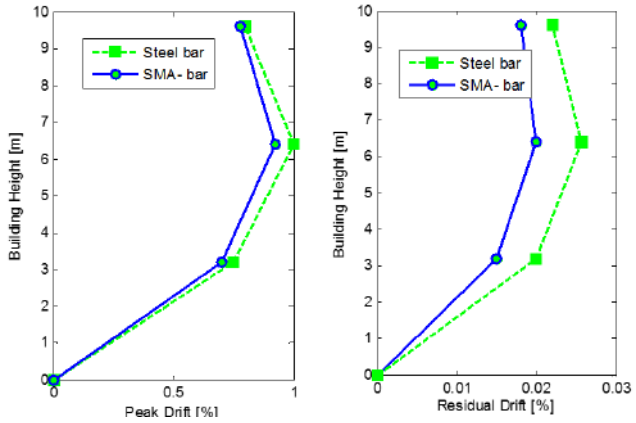

Figure 5: Drift curve of floors in a three-story building with a column with steel rebar and SMA rebar

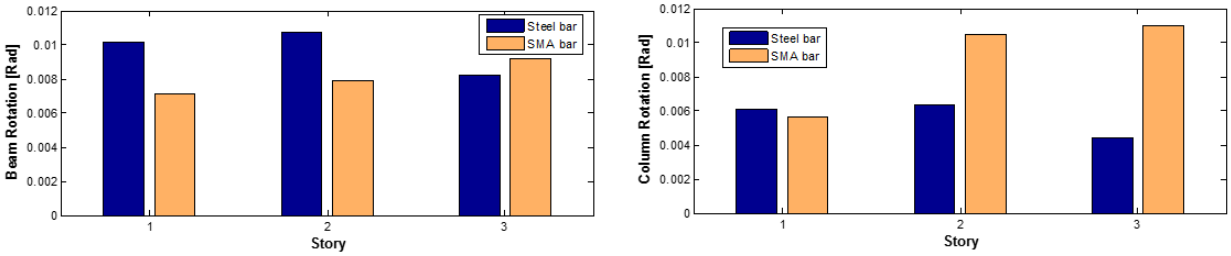

Figure 6: Maximum rotation at different floors (average of seven records) (a) Beam rotation (b) Column rotation

According to figure 6, the use of SMA rebar has reduced the rotation of beams and the use of SMA rebar has increased the rotation of columns.

4.2. Five-story building

In Figure 7-9, the time history curve of the base shear of the five-story frame under the effects of the Duzce, Northridge, and Imperial earthquakes is plotted and the difference in the performance of steel rebar and SMA in these three types of earthquakes is clearer. As shown in the figure, the maximum base shear applied to steel rebar is higher.

Figure 10(a) and (b) show the time history curves of the roof displacement of the five-story frame under the Northridge and Imperial earthquakes, respectively. The steel-reinforced column (green curve) has undergone permanent displacement and its final displacement is not zero and in fact the building has not returned to its original state. But, the building with the SMA-reinforced column has returned to its original state.

Figure 11 shows the lateral displacement curve of the floors (drift) in the five-story building with the steel-reinforced column and the SMA-reinforced column under the Imperial earthquake. According to the obtained graphs, the maximum drift in both structures is similar to each other and the overall behavior of the two structures is not much different, but the permanent drift of the structure with the SMA-reinforced has decreased sharply and the structure has returned to its original state, while the permanent drift has occurred in the steel-reinforced structure.

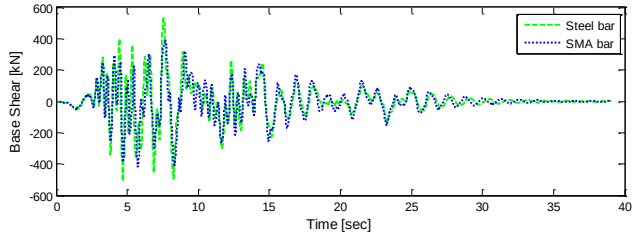

Figure 7: Base shear of the Duzce earthquake

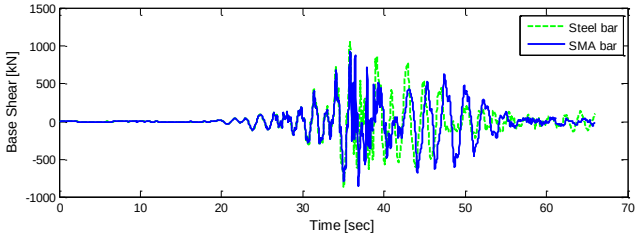

Figure 8: Base shear of the Northridge earthquake

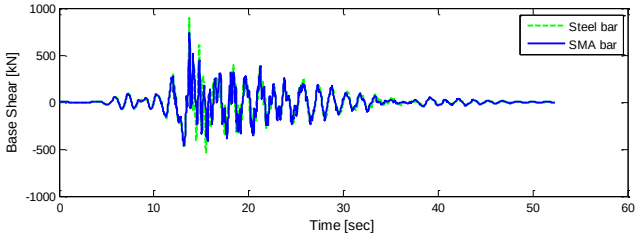

Figure 9- Base shear of the Imperial earthquake

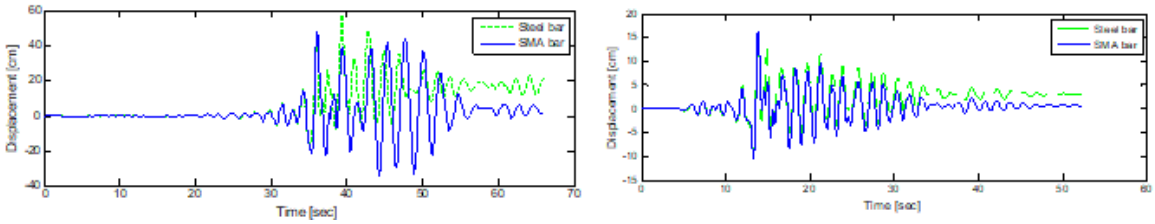

Figure 10- Roof displacement (a) Northridge earthquake (b) Imperial earthquake

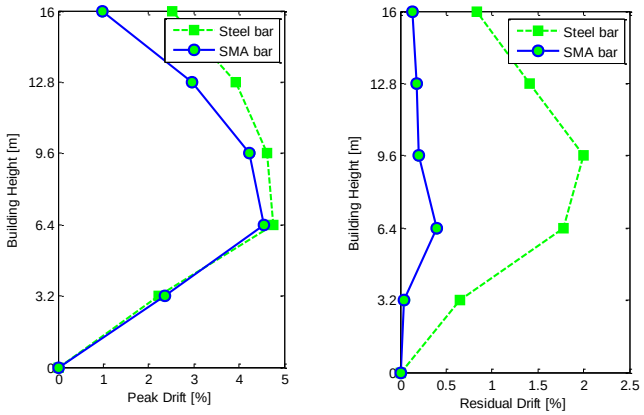

Figure 11- Lateral displacement of floors (drift) in a five-story building under Imperial earthquake

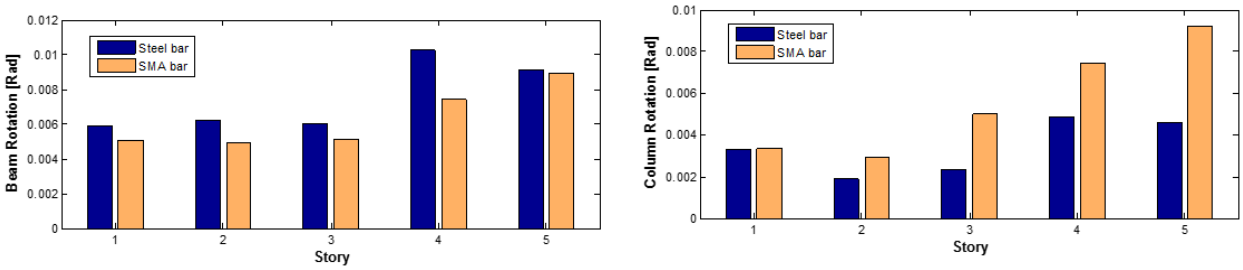

Figure 12- Maximum rotation at different floors (average of seven records) (a) Beam rotation (b) Column rotation

The maximum rotation of beams and columns in different floors of the five-story frame are plotted in Figure 12 (a) and (b), respectively. According to this figure, the use of SMA rebar has reduced the rotation of beams and increased the rotation of columns.

5. Investigation of the effect of the ratio of shape memory alloy

In order to investigate the effect of the ratio of shape memory alloy, a 5-story frame with an average rebar ratio of 1.4% and 2.1% for columns was analyzed using pushover analysis and the deformation of beams and columns in these two cases was compared. According to Figure 13, the maximum frame capacity in the model with an average rebar ratio of 2.1% was obtained as 770 kN, which shows a 15% increase compared to the model with an average rebar ratio of 1.4%. According to Figure 14, in the model with an average rebar ratio of 2.1%, a slight increase in the rotation of beams and a slight decrease in the rotation of columns occurred.

6. Conclusion

This study investigates the performance of reinforced concrete buildings with SMA bars in columns under near-fault earthquakes. For this purpose, two three-story and five-story buildings were considered. These buildings were analyzed once using steel bars and once using SMA bars in seven near-fault accelerograms. The following results is obtained:

- The performance of SMA bars did not differ significantly compared to steel bars in reducing the maximum displacements of the structure and their effectiveness was almost similar. However, the use of SMA bars has greatly reduced the permanent deformation of the structure.

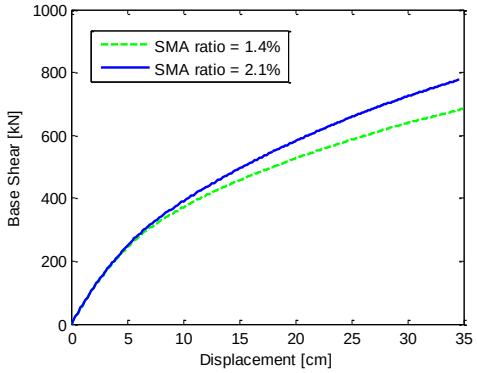

Figure 13 : Pushover curve

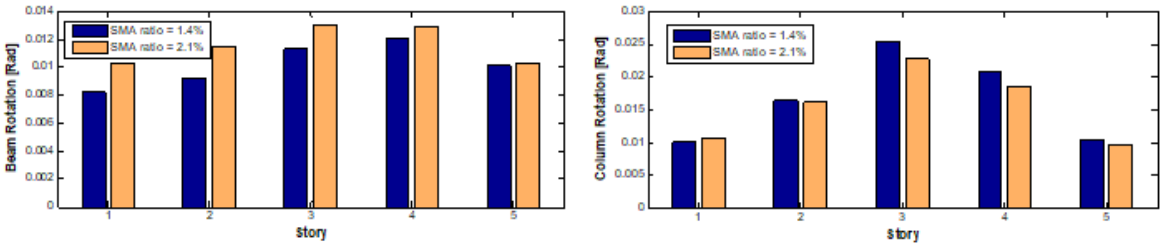

Figure 14 : Maximum rotation at different floors (average of seven records) (a) Beam rotation (b) Column rotation

- In frames with SMA bars in columns, the maximum rotational deformation of the columns was greater than that of frames with steel bars. However, SMA bars have greatly reduced the permanent rotational deformation of the columns and brought them to zero.
- The maximum lateral displacement or maximum drift of the floors in frames with SMA bars has slightly increased. However, the permanent drift of the structure in frames with SMA reinforcement is greatly reduced. This is due to the elastic recovery of strain in SMA materials, which reduces the permanent deformation of the structure.

References

[1] Jha, Nitya Nand, Rohit Kumar Singh, and Sushila Sharma. "Behaviour and design of a (G+ 5) multi storey framed structure under different loading condition." Asian Journal of Civil Engineering 25.7 (2024): 5293-5305. https://doi.org/10.1007/s42107-024-01113-w

[2] Anas, S. M., Mehtab Alam, and Messaoud Saidani. "Prediction of impact response of square reinforced concrete (RC) slab with square/circular opening under drop-weight impact using FEM simulation." Asian Journal of Civil Engineering 25.2 (2024): 2189-2208. https://doi.org/10.1007/s42107-023-00903-y

[3] Elroby, Shaimaa A., et al. "Experimental and machine learning-based model for large-scale reinforced concrete shear walls strengthened with CFRP sheets and shape memory alloys." Asian Journal of Civil Engineering (2024): 1-19. https://doi.org/10.1007/s42107-024-01135-4

[4] Fawzy, Khaled, et al. "Overview of the punching capacity of the flat slab under reversed cyclic loading and methods of improvement." Asian Journal of Civil Engineering 25.3 (2024): 2641-2652. https://doi.org/10.1007/s42107-023-00934-5

[5] Kiani, Mahdi, and Hamed Enayati. "Evaluation of a nonlinear TMD seismic performance for multi-degree of freedom structures." Asian Journal of Civil Engineering 25.2 (2024): 1395-1412. https://doi.org/10.1007/s42107-023-00850-8

[6] DesRoches, R., and B. Smith. "Shape memory alloys in seismic resistant design and retrofit: a critical review of their potential and limitations." Journal of earthquake engineering 8.3 (2004): 415-429. https://doi.org/10.1080/13632460409350495

[7] Sultana, Papia, and Maged A. Youssef. "Seismic performance of steel moment resisting frames utilizing superelastic shape memory alloys." Journal of Constructional Steel Research 125 (2016): 239-251. https://doi.org/10.1016/j.jcsr.2016.06.019

[8] Sharabash, Alaa M., and Bassem O. Andrawes. "Application of shape memory alloy dampers in the seismic control of cable-stayed bridges." Engineering Structures 31.2 (2009): 607-616. https://doi.org/10.1016/j.engstruct.2008.11.007

[9] Abdulridha, Alaa, et al. "Behavior and modeling of superelastic shape memory alloy reinforced concrete beams." Engineering Structures 49 (2013): 893-904. https://doi.org/10.1016/j.engstruct.2012.12.041

[10] Abraik, Emad, and Maged A. Youssef. "Seismic fragility assessment of superelastic shape memory alloy reinforced concrete shear walls." Journal of building engineering 19 (2018): 142-153. https://doi.org/10.1016/j.jobe.2018.05.009

[11] Nikbakht, Ehsan, et al. "Application of shape memory alloy bars in self-centring precast segmental columns as seismic resistance." Structure and Infrastructure Engineering 11.3 (2015): 297-309. https://doi.org/10.1080/15732479.2013.876056

[12] Chen, Qiwen, and Bassem Andrawes. "Cyclic stress–strain behavior of concrete confined with NiTiNb-shape memory alloy spirals." Journal of Structural Engineering 143.5 (2017): 04017008. https://doi.org/10.1061/(ASCE)ST.1943-541X.0001728

[13] Jung, Donghyuk, James Wilcoski, and Bassem Andrawes. "Bidirectional shake table testing of RC columns retrofitted and repaired with shape memory alloy spirals." Engineering structures 160 (2018): 171-185. https://doi.org/10.1016/j.engstruct.2017.12.046

[14] Cortés-Puentes, W. Leonardo, and Dan Palermo. "SMA tension brace for retrofitting concrete shear walls." Engineering Structures 140 (2017): 177-188. https://doi.org/10.1016/j.engstruct.2017.02.045

[15] Elbahy, Yamen Ibrahim, Maged A. Youssef, and M. Meshaly. "Seismic performance of reinforced concrete frames retrofitted using external superelastic shape memory alloy bars." Bulletin of Earthquake Engineering 17 (2019): 781-802. https://doi.org/10.1007/s10518-018-0477-7

[16] Brinson, L. Catherine. "One-dimensional constitutive behavior of shape memory alloys: thermomechanical derivation with non-constant material functions and redefined martensite internal variable." Journal of intelligent material systems and structures 4.2 (1993): 229-242. https://doi.org/10.1177/1045389X9300400213

[17] Nakashoji, Brian A. Seismic performance of square nickel-titanium reinforced ECC columns with headed couplers. University of Nevada, Reno, 2014.

J-Researchers

Journal of Civil Engineering Researchers

Journal homepage: www.journals-researchers.com

The Use of Machine Learning, Computational Methods, and Robotics in Bridge Engineering: A Review

Parankush Koul[a,*]

[a] *Department of Mechanical and Aerospace Engineering, Illinois Institute of Technology, 3201 South State Street, Chicago, 60616, Illinois, United States of America*

ABSTRACT

In this review paper, the applications of machine learning, computational methods, and robotics to bridge design are considered to help improve structure integrity and resilience. It describes a variety of computational methods, including finite element analysis (FEA) and computational fluid dynamics (CFD), that have been used to calculate failure modes and evaluate the dynamic behavior of bridge structures in extreme conditions, such as earthquakes and floods. It also highlights robotics' potential to streamline inspection techniques, showing new robotic systems for effective bridge monitoring. Additionally, it points out issues related to data shortages and implementation difficulty and presents future research priorities, such as the need for powerful machine learning algorithms and the use of Internet of Things (IoT) solutions for real-time monitoring. In summary, the paper highlights the life-changing impact of these technologies on the safety and reliability of bridge systems.

ARTICLE INFO

Received: November 02, 2024
Accepted: November 24, 2024

Keywords:
Machine Learning
Computational Methods
Robotics
Structural Integrity
Resilience

DOI: 10.61186/JCER.6.4.9
DOR: 20.1001.1.2538516.2024.6.4.2.7

1. Introduction

Machine learning, computation, and robotics combined have revolutionized so many disciplines that bridge engineering does not have any place. In recent years, these technologies have increasingly been used to design, monitor, service, and inspect bridges. Machine learning is a subset of artificial intelligence (AI), and it uses algorithms that can look at enormous data sets, learn from them, and make inferences or decisions based on them [1]. With this feature, engineers can measure structural health with greater precision and accuracy, which increases the life-cycle safety of bridges.

Computational tools such as numerical simulations and optimization techniques are used to develop and analyze bridge systems. They allow engineers to simulate advanced behaviors with multiple load loads and make better design decisions [2]. Combining computing hardware with machine learning algorithms, engineers can produce predictive maintenance algorithms to increase the service life of bridges at reduced costs and operating times [3].

The history of bridge engineering is shaped by robotics, too. Thanks to the use of robotics, automation has become

* Corresponding author. Tel.: +1 (630) 341-7082; e-mail: pkoul2.iit@gmail.com.

possible for automatic inspection in real time and early detection of any potential problems in bridge structures [4]. These robots could even do something dangerous or challenging for human inspectors, like navigating narrow hallways or performing inspections in severe weather.

The combination of machine learning, robotics, and computation improves the quality of bridge tests as well as reduces administrative work in the engineering industry [5]. Keeping pace with this interdisciplinary process, the new best practice in bridge engineering will be safer, more effective, and more predictive. Thus, an exhaustive review of applications, limitations, and future challenges of these technologies in bridge engineering is needed.

Overall, combining machine learning, computational techniques, and robotics in bridge engineering is a revolutionary step toward better design, repair, and management of bridge infrastructure and is therefore an emerging field of research and application [6].

2. Applications of Machine Learning in Bridge Engineering

Structural Health Assessment: Machine learning algorithms are used to use the real-time data from bridge sensors to monitor the bridge's health and integrity. This way it can be used to catch problems before they become more severe.

Bridge Inspection and Condition Forecast: Machine learning algorithms are used to optimize bridge inspection and condition forecast models. By considering historical inspection data, these algorithms will predict possible future states, saving time on maintenance and money.

Reinforced Concrete (RC) Bridge Design and Inspection: Machine learning technology is applied in RC bridge design and inspection. These procedures help in resilient design decisions and accurate inspections [7].

Wind Engineering: Machine learning models in bridge wind engineering are used to model the impact of wind loads on bridges. It is an application that is very important for keeping bridges safe and stable in the face of changing wind conditions.

Load Capacity Rating: Decision trees and random forests are used to rank bridge populations on their load capacity. This application optimizes the usage by giving reliable estimations of current bridges' load-bearing capacity.

Time Series Prediction: Machine learning is used to implement time series prediction methods in coastal bridge engineering to be proactive based on time-series trends [8].

Bridge Pier Scour Prediction: Machine learning tools can help in scour around bridge piers by going through all models' reviews. This information is essential for keeping bridge foundations in excellent shape and avoiding catastrophic erosion failure [9].

Monitoring Technology Selection: Use case of concrete and steel bridge structural health monitoring (SHM) using machine learning infers monitoring technologies. This technique of tuning gives accurate data collection and analysis for structural evaluation.

3. Applications of Computational Methods in Bridge Engineering

Computational tools like FEA and CFD play an important role in bridge design in terms of design cost, safety, and performance. Below are some of the primary uses of these techniques:

3.1. Applications of FEA in Bridge Engineering

FEA is also very widely used in bridge design as it can simulate sophisticated geometries and behavior of materials under different loads. Key applications include:

- Structural Design: FEA permits you to model bridge structures in detail to determine the response to dead, live, wind, and seismic loads. This facilitates discovering stress points and failure modes.
- Design Optimization: FEA can be used to optimize bridge designs through material and geometry selections in order to obtain the most cost-effective structure meeting safety and performance standards at a minimal material usage and cost [10].
- Preliminary Evaluation of Existing Bridges: FEA plays an important role in evaluating existing bridges for structural integrity. Engineers can mimic the condition and stress and then suggest reinforcement or repair where needed [11].
- Construction Simulation: FEA can simulate the building of the bridge to enable engineers to predict how different ways or sequences of construction might affect its performance [12].

3.2. Applications of CFD in Bridge Engineering

CFD is required to determine the flow behavior around bridges. Key applications include:

- Wind Load Simulation: CFD is used to evaluate the impact of wind on bridge stability and performance. Simulating wind over bridge models will help designers discover aerodynamic properties and design bridges to deal with the heaviest wind [13].

- Hydrodynamic Impact: For bridges over the ocean, CFD helps in modeling the hydrodynamic effects of waves and currents so that the bridge can resist these environmental stresses [14].
- Scour Analysis: The scour around the piers and foundations of bridges, driven by the flow of water, can be calculated using CFD, important for the bridge's stability.
- Thermal Impacts: CFD can also simulate the thermal impacts of materials on bridges based on environmental factors and help determine potential expansion and contraction problems that can weaken the structure.

4. Applications of Robotics in Bridge Engineering

For bridge engineering, robots contribute to the increase of productivity, safety, and precision in many activities. Below are the major robotic applications in this context.

- *Bridge Deck Construction*: Robots are used to automate the construction of bridge decks, with more accuracy and a shorter time to build [15].
- *Testing and Inspection*: The bridges are now increasingly tested and inspected by robots, which provide non-destructive testing methods that can evaluate structural integrity without destroying it [16].
- *SHM*: Intelligent robotic devices perform the continuous SHM and provide instantaneous data and information about the functioning and state of bridges [17].
- *Bridge Automation*: Roadside robots enable bridge automated inspections with much faster and more accurate assessments compared to the manual method [18].
- *Inspection data collection*: Robotic technology is providing better data collection solutions in robot bridge inspections to perform more effective and detailed analysis [19].
- *Robust Robot Selection for Restoration*: Genetic algorithms are employed to choose robotics best suited for restoration of bridges and provide optimal robotic solutions according to requirements [20].
- *Non-destructive Inspection*: Robot platforms armed with the best sensors and algorithms perform non-destructive inspection of bridges that allows thorough inspection without degrading the structure [21].
- *Cable Inspection Robots*: Cable-stayed bridge inspection robots can also monitor the critical elements, such as cables, and lead to an increase in maintenance operations [22].
- *Smart Material Adoption*: Robotics, along with smart materials, are emerging as major parts of construction engineering, enabling new designs and construction of bridges [23].

5. Industrial Case Studies for the Application of Machine Learning, Computational Techniques and Robotics in Bridge Engineering

5.1. Applications of Machine Learning in Bridge Engineering

Machine learning has been used in various ways to improve bridge engineering performance, stability, and safety.

- AMC Bridge: It offers software development solutions like machine learning solutions in bridge design. They use AI to simplify operations and process quality, allowing them to get the most out of data and optimize engineering processes [24].
- Rowan CREATES: They are exploring machine learning methods for structural health assessment of bridge infrastructure in highly seismically active areas. This program seeks to enhance the resilience of bridge constructions through rapid decision support tools that use predictive analytics [25].
- Imetrum and University of Exeter Collaboration: a project that creates a new technology for long-term bridge condition monitoring via machine learning. The technology also has intelligent features that automatically interpret data, report problems, and predict potential issues of condition in the future, thus saving on maintenance expenses and improving safety [26].

5.2. Applications of Computational Techniques like FEA and CFD in Bridge Engineering

The computational methods of FEA and CFD are used to analyze and optimize bridge designs for safety and efficiency.

- *DH Glabe & Associates*: DH Glabe & Associates apply FEA to the structural analysis of bridges. Their engineers compute complicated bridge structures for load-bearing conditions such as wind and earthquakes using sophisticated software such as LUSAS [27].

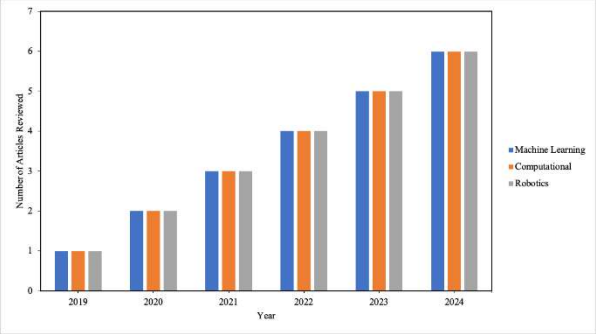

Fig. 1. Articles reviewed (2019-2024) for applications of machine learning, computational techniques and robotics in bridge engineering.

- *Predictive Engineering*: They are quite proficient in using FEA for bridges and other projects. They consider the stress, vibration, and fatigue effects needed to prevent or prolong the life of bridges [28].
- *Resolved Analytics*: This company uses CFD modeling to model scour and erosion at bridges. As they model fluid dynamics, they can predict erosion that could compromise bridge foundations to enhance design and maintenance plans [29].

5.3. Applications of Robotics in Bridge Engineering

This trend of using robots to improve productivity, tackle labor issues, and make bridge construction safer continues.

- *Advanced Construction Robotics*: They've created TyBot, a robot for rebar tiedown in bridge construction. TyBot ties up to 1,000 intersections per hour, which is an impressive savings in labor and keeps workers away from dangerous situations at the site [30, 31].

- *Autodesk and USC Collaboration*: Autodesk collaborated with USC during the Arroyo Pedestrian Bridge Project in Los Angeles, which involved using a robotic arm to raise and install special steel girders for welding. Such cooperation among human and robot hands simplified the manufacturing of this complex design.

- *MX3D*: A Dutch firm that's innovating with 3D printing of bridges. They built a 3D-printed steel bridge by industrial robots, which demonstrates new construction technologies and will contribute to sustainability through reduced material waste [32].

6. Literature Review on Applications of Machine Learning, Computational Techniques and Robotics in Bridge Engineering

The number of articles covered for the applications of machine learning, computational techniques and robotics in bridge engineering in this review are shown in Figure 1 from 2019 through 2024.

6.1. Leveraging Machine Learning for Optimized Bridge Design, Adaptive Smart Infrastructure, and Predictive Maintenance in Dynamic Environmental Conditions

Table 1 below shows a quantitative distribution by publisher of the number of articles related to machine learning advancements in bridge engineering.

Table 1
Number of articles from different publishers reviewed for advancements of machine learning in bridge engineering

Publisher	Number of Articles Reviewed
Springer	5
Elsevier	4
IEEE	2
MDPI	2
SPIE	2
ASCE	1
IOP Publishing	1
Sage Journals	1
Structurae	1
Wiley	1
Zenodo	1
Total	21

Mathern et al. (2019) designed a model using AI and machine learning to design bridges that are sustainable and buildable to accelerate structural decision-making and improve the environmental impacts through fast design evaluation [33]. In contrast, Pan et al. (2020) focused on conditional infrastructure evaluation of massive infrastructure such as high bridges with deep learning and specifically convolutional neural networks (CNNs). This research used satellite images to improve the feature extraction for safety analysis and showed that AI could be applied to continuous spatial and temporal infrastructure health monitoring [34]. Moon et al. (2020) used recurrent neural networks (RNNs) and active learning to extract damage objects from inspection reports for bridges, using Named Entity Recognition (NER) to automated extraction of entities caused by damage. Such automation enabled more reliable and timely maintenance programs that made structural integrity calculations more accurate [35].

Xu et al. (2021) covered all the machine learning use cases in construction, from shallow to deep learning. They showed how site monitoring, automatic structural defect

detection, and predictive maintenance can make construction and infrastructure work safer, more efficient, and more structurally sound [36]. Nguyen (2021) was interested in material evaluation on bridge spans by using a data-driven method with a new viscosity resistance coefficient (IC), deep learning, and balancing composite motion optimization (BCMO) to investigate material performance and safety in bridges in Ho Chi Minh City. It was shown that IC values calculated from real-time vibration data could be used as an indicator for long-term structural monitoring [37]. Meanwhile, Moon et al. (2021) used artificial neural networks (ANN) to estimate dynamic displacements in bridges during heavy traffic. They used the correlated measured strains with displacement data to confirm the performance of the ANN model in predicting structural responses to loads in real time, enabling more responsive smart bridges [38].

The paper by Wang et al. (2022) used a gray neural network for designing recycled concrete bridges with sustainability and recycling in mind by making predictions of durability. In this study, we observed that the AI algorithm improved construction control by predicting the longevity of recycled concrete bridges to encourage green bridge design [39]. Meanwhile, Kumar et al. (2022) built a modified CNN for bridge condition measurement using a large dataset from the National Bridge Inventory. Their model with the Firefly algorithm to improve feature selection, predictability of 97.49%, which was a high improvement over the regular CNN model, showed that machine learning can be applied to adaptive infrastructure monitoring without physical inspection [40]. In contrast, Entezami et al. (2022) implemented a three-stage machine learning system for SHM for damage detection in environmental uncertainty with very limited sensor information. Using autoregressive spectra, log-spectral distance, and auto-associative neural networks (AANN), they controlled for environmental perturbations and performed accurate damage quantification on rarely seen structures [41].

The article by Zhou et al. (2022) concerned creating maintenance policies with the best possible policy by modeling bridge component degradation. This method used Q-learning algorithms coupled with matrix updates in real time and was verified by simulating a simple supported beam bridge and a cable-stayed bridge—far superior to the existing methods in making dynamic decisions on larger bridge designs [42]. Dolui et al. (2023) used machine learning classifiers—one such being a decision tree—to compute bridge health from galfenol-based magnetostrictive sensors. With structural vibration converted to electrical signals with an accuracy of 98.72%, this technique showed the effectiveness of connecting sensor data with machine learning to give an accurate, live structural health report [43]. Giglioni et al. (2023) took the lack of labeled data for damage detection and applied domain adaptation within a transfer learning framework. This approach relied on vibration measurements and damage features by domain to pass health-state labels from one structure to the next, proven by testing it on the Z24 and S101 bridges, and was suitable for sparse data [44].

Xie et al. (2023): machine learning applied for severe wind conditions to construction of fast railway bridges over typhoon zones with safety and proactive action via the Back Propagation-Genetic Algorithm model for wind speed prediction. This model was practical as it related actual wind measurements to predefined standards and so supported adaptive building practices [45]. Meanwhile, Ghafoori et al. (2023) leveraged historical bridge condition information using a machine learning framework for bridge maintenance optimization. They modeled degradation through random forests and linear programming to forecast it, prioritize maintenance resources, and deliver maximum infrastructure performance under budget constraints [46]. In contrast, Tai et al. (2023) focused on the economic cost minimization of stochastic optimization algorithms for cable-stayed bridge designs. They proposed two stochastic conjugate gradient algorithms—Modified Armijo and Modified Weak Wolfe-Powell line search algorithms—which improved global convergence and robustness in minimizing construction cost under uncertainty [47].

Zhang et al. (2024) addressed wind-bridge dynamics and applied machine learning for wind field simulation and aerodynamic control to refine insights on wind-induced bridge vibrations and make design responses to changing winds more responsive. Similarly, Nguyen et al. (2024) using ANN and adaptive neuro-fuzzy inference systems (ANFIS) for SHM of Dbica railway bridge produced predictive precision (up to 85%) in diagnosis of dynamic bridge behavior, thus improving maintenance practices and lowering failure probability [48]. Bai et al. (2024), by contrast, focused on the conceptual design of bridges, automating beam type choice with graph neural networks (GNNs) via AutoDis Graph Ontology Attention Matching (AGOAM). This change dramatically accelerated and optimized design choices by mapping attribute interactions to structural demands, a revolution in automated, scalable conceptual design [49].

Yang, Wang, and Nassif (2024) studied the environmental causes of bridge decay by applying XGBoost to condition predictions of RC bridge decks and identified age, freeze-thaw cycles, and rain as major factors contributing to decay. Their result confirmed that feature weighting supports efficient resource allocation for predictive maintenance [50]. In contrast, Gunderia et al. (2024) were focused on sustainable predictive maintenance with different AI-based models such as ANN and CNN. They suggested a combined ANN, CNN and life cycle

assessment-based integrated model for maintenance best practices based on sustainability in prediction [51]. Giglioni et al. (2024) adapted transfer learning as a domain adapter to enhance damage classification and generalized machine learning algorithms from well-labeled data to unlabeled data over bridge networks. This was proven to work on prototype bridges, improving damage classification and compute speed of SHM with inadequate labeled data [52].

6.2. Leveraging Computational Techniques like FEA and CFD in Bridge Engineering: Predicting Failure Modes and Enhancing Structural Integrity for Long-Lasting Resilience

Table 2 presents the number of articles reviewed for computational techniques' advancements in bridge engineering, by publisher.

Table 2
Number of articles from different publishers reviewed for advancements of computational techniques in bridge engineering

Publisher	Number of Articles Reviewed
IOP Publishing	4
MDPI	3
ASCE	2
Elsevier	2
Springer	2
Copernicus Meetings	1
IJIREM	1
Sage Journals	1
Sciendo	1
Structurae	1
Taylor & Francis	1
TU Delft Open Publishing	1
University of Toledo	1
Total	21

In the study by El-Ghandour and Foster (2019), FEA and Multibody Systems Dynamics (MSD) were combined to explain the bridge approach problem in railroad systems, that is, the detrimental effects of abrupt stiffness changes at bridge entrances. They found that installing an inclined concrete slab greatly reduced stress and vertical deformations, making railroads safer and more durable [53]. In contrast, Izvekov et al. (2020) focused on a metallurgical crane's girder using FEA to detect the zones of failure at static loads. Their probabilistic model elucidated important risks for the integrity of the girder, which was a precursor to appropriate reinforcement, pointing towards the necessity of continuous maintenance to extend service life [54]. Sharma and Guner (2020) were pioneers of this field when they proposed a nonlinear FEA approach for the strength analysis of deep bridge bent caps that are typically placed under loads beyond their design limits. Their findings showed more accurate prediction of cracking and modes of failure than the older approaches, which gave bridge engineers a strong basis for measuring deep concrete components [55].

Liu et al. (2021) devised a coupled CFD-FEM simulation technique for bridge fire performance and showed how previous tests had often missed the dynamic interactions between heat and structure. Their study showed that the coupled method accurately predicted vulnerability under fire conditions—and hence safety studies and design guidelines for bridges that are vulnerable to fire [56]. Sengsri and Kaewunruen (2021) tested the local failure modes and critical buckling loads of a meta-functional auxetic sandwich core for composite bridge bearings. They used three-dimensional finite element models, which they verified using experimental results, and they showed that the novel auxetic design led to a major increase in crashworthiness and structural strength through local buckling failures that could occur before yielding when compressed [57]. Ko (2021) looked at the seismic behavior of RC single-column bridge bents under near-fault ground movement. By using nonlinear fiber finite element models without bond-slip effect, Ko's study accurately predicted the modes of failure; modeling without it could overestimate the strength of structures [58].

Zhu and Wu Tian (2022) applied CFD to the main girder of cable-stayed bridges to study vortex-induced vibrations (VIV). Their numerical models, derived using a bidirectional fluid-structure coupling process, had shown the importance of wind loads on bridge safety in construction and operation by modeling the vortex vibration behavior of the main girder [59]. Parallax-style, Yoneda et al. (2022) focused on a 3D finite-element modeling generation system with data processing platform (DPP) for fatigue evaluation of reinforced concrete bridges. Their results showed the DPP can be used to improve the structural model's predictive power under various stress conditions, resulting in a more accurate and effective modeling of real bridge structures compared with conventional modeling [60]. Meanwhile, Tang et al. (2022) carried out a reliability-based vulnerability study of bridge piers damaged by debris flow using FEA to simulate fluid-solid effects. Their study—through a finite element model and impact forces using a two-phase flow theory, distilled into an easy-to-understand 2D model—determined critical velocity and failure modes of bridge piers in debris flows and helped provide safer infrastructures [61].

Quan et al. (2022) conducted a comprehensive study of the seismic mitigation of a long-travel high-speed railway continuous beam bridge by using FEA to model the behavior of the bridge under earthquake loads with viscous dampers as an essential design element. They discovered that the dampers acted as good absorbers, with damping

rates up to 81% on some seismic waves, which enhanced structural stability and dynamic response [62]. Duan and Tao (2023), meanwhile, considered flood resilience using both CFD and Fluid-Structure Interaction (FSI) modeling to analyze flood damage to bridge piers and came up with the best design for piers in flood areas. Their parametric analysis found that wave height and speed were critical parameters that determined structural integrity, which is important for the infrastructure resilience to floods [63]. Similarly, Fleit et al. (2023) studied flows and local scour in a multiphase hydro- and morpho-dynamic numerical model (REEF3D) of submerged bridge decks. They made it clear that the transport of sediment was a significant factor and backed up their model with experimental evidence, highlighting the challenge of modeling scouring [64].

Kaushal et al. (2023) dynamically simulated bridge geometry with ANSYS FEA and observed natural frequencies and mode forms that highlighted zones at high deformation and potential resonance. Their result called for the development of damping and vibration damping controls for long-term stability [65]. In contrast, Malekghaini et al. (2023) used Bayesian model updating to bridge FEA and data from the real world to identify damage in bridges using a robust model validated on synthetic data and adapted to the real structure. Their findings showed that the framework was useful in determining damage, and so SHM systems became dramatically better [66]. Meanwhile, Dong et al. (2023) focused on the seismic failures of river-spanning girder bridges in the presence of soil liquefaction. Their two-dimensional finite element model revealed that soil liquefaction influenced the response to an earthquake with increased displacements and deformation of important elements, which increased the risk of bridge collapse during a seismic event [67].

Zhu et al. (2024) did a detailed CFD simulation to quantify aerodynamic forces on tall cars crossing the Queensferry Crossing Bridge in different wind loads. The truck's ability to withstand aerodynamic instability, they discovered, was particularly at risk, and hence vehicle dynamics must be taken into account in bridge design to maximize safety [68]. In contrast, Petruccelli et al. (2024) dealt with the hydrodynamic loads acting on bridges in flood events and used CFD to calculate stress conditions and carrying capacity. Their simulations offered important details on drag and lift coefficients for several different submergence scenarios that were used to devise strategies for strengthening bridges against floods [69]. Han and Wang (2024) used FEA to explore failure modes of rock slopes around bridge anchorage foundation pits. They combined limit equilibrium and finite difference techniques to discover major causes of slope failure, such as rain and earthquakes, providing an overview of slope mechanics in vulnerability geological systems [70].

Fusco et al. (2024) were focused on an efficient beam finite element model of the nonlinear structure of existing prestressed RC bridges. They applied a damage-plasticity model on OpenSees, and they showed how their model saves computing time without sacrificing accuracy during inspections [71]. Jia et al. (2024) examined seismic faulting for a simple-supported beam bridge by modeling it using a three-dimensional FEA model in LS-DYNA under real-world conditions. The key variables they found, for example, fault-crossing angle and ground surface permanent rupture displacement, indicated that the position of the bridge in relation to seismic faults had a significant effect on stability [72]. Zhu et al. (2024) investigated the dynamic response of a cable-stayed pipe bridge in seismic loading using a large-scale FEA simulation in ANSYS Workbench, including fluid-structure dynamics. They showed that the FSI approach is more successful at modeling the dynamic behavior of the bridge [73].

6.3. Enhancing Bridge Safety: The Role of Robotics in Inspection Engineering

Table 3 presents the number of articles reviewed for robotics' advancements in bridge engineering, by different publishers.

Table 3
Number of articles from different publishers reviewed for advancements of robotics in bridge engineering

Publisher	Number of Articles Reviewed
IEEE	9
ASCE	2
Emerald	2
MDPI	2
arXiv (Cornell University)	1
ASNT	1
Intelligence Science and Technology Press Inc.	1
SPIE	1
Springer	1
Wiley	1
Total	21

Charron et al. (2019) addressed accessibility and data collection by using mobile ground and air robots. These results showed more direct access to difficult-to-access locations and more consistent data, and consequently, bridge inspections became more efficient than before. Potenza et al. (2020) developed a novel technique using unmanned aerial vehicles (UAVs) with new image processing methods. This method was able to quantify defects and shows that automated inspection and defect classification are much improved. The results showed the

method was robust, in particular when it came to finding repeatable flaws in the infrastructure of the Italian railway network [74]. Wang et al. (2020) scanned steel box girders using a deep learning computer vision tool. It had a predictive accuracy rate of more than 90% in detecting structural decay, which indicates the potential of deep learning in bridge inspections [75].

Yan et al. (2021) talked about UAV automated bridge detection, a new path planning algorithm for UAV flight paths optimized to move through more challenging environments, such as pier jams. Their simulations showed successful full-coverage detection of bridges, proving the UAVs performance in infrastructure monitoring [76]. Gallegos Garrido and Sattar (2021), on the other hand, built SIRCAUR, a self-assisted wall-climbing robot that inspects RC buildings. They focused on improving adhesion forces through simulation and experimental testing so that the robot carried ground-penetrating radar (GPR) for corrosion and concrete degradation detection. These tests proved that the robot was capable of performing accurate and safe inspections, and therefore SHM became better [77]. Meanwhile, Lin et al. (2021) studied using flying robots to do full bridge inspections, automating the entire process of visual information capture, 3D mapping, destructibility detection, analysis, and reporting. They discovered that drones have dramatically increased the inspection speed and quality of data by picking up defects with high sensitivity and avoiding human error [78].

Ahmed et al. (2022) presented a bicycling robot designed for maintenance on steel-reinforced bridges. The sophisticated steel defect detection system was built using deep learning techniques such as LinkNet and UNet. Their study primarily focused on the robot's strength in operating through high-pressure steel buildings and showed promising results in defect detection by fully testing its visual sensor system [79]. In contrast, Zheng et al. (2022) launched the CCRobot-IV, a climbing robot that climbs over obstructions during cable inspections, which improved operational safety substantially. It was built with a quad-ducted propeller system so that the robot didn't need friction to run, carrying heavier loads while traversing rough terrain. It passed its navigation and inspection tests with success through experimental and field tests, which also prove to be useful [80]. Similarly, Motley et al. (2022) worked on a high-powered multi-steering climbing robot with a novel adhesion mechanism and different steering modes for greater control and stability while inspecting steel bridges. The design of the robot was subsequently proven, and they further showed how they could make substantial improvements in inspection methods in the industry [81].

Li et al. (2022) built a circularly rotating cable inspection robot with elastic suspension that was able to scale taller obstacles and ascend stable on vertical cables. They showed their experiments were able to carry a 12.4 kg payload and maneuver through obstacles without any harm to the robot, demonstrating its practical usage for real-world inspection [82]. In contrast, Gong et al. (2023) explored Building Information Modeling (BIM) and robotic mapping to reduce risk in bridge construction. Their study pointed out how critical it was to keep the industry safe and even used AI-powered nanobots to improve detection of hazards. Results suggested that the integrated model resulted in stricter on-site safety management solutions [83]. Meanwhile, Hoxha et al. (2023) were focused on a robotic system for mapping subsurface defects using impact-echo and GPR. They were impressed by the speed of the dual-sensor method, which collected data faster than expected and offered complete evaluations of concrete buildings [84].

Gucunski et al. (2023) focused on condition evaluation of RC bridges through nondestructive evaluation (NDE). They found that robots can speed data collection and safety for inspection employees, providing better measurements of bridge status and less costly traffic delays during inspections [85]. Alamdari and Ebrahimkhanlou (2023), on the other hand, combined cameras and LiDAR cameras to develop a novel method of crack detection that combined high-resolution photographs and 3D point clouds. Their results showed a better detection rate and faster data acquisition, and in the end, a more detailed picture of structural integrity than other approaches [86]. Popli et al. (2023) created Robotics-Assisted Onsite Data Collection (ROAD), a system that used deep learning to detect real-time cracks. In their research, they demonstrated that Xception was a better algorithm than others, with more than 90% accuracy and validation of the system in a variety of field conditions [87].

In the paper of Ade-Omowaye et al. (2024), they explored the impact of robotics and automation on engineering and made a literature review on the economic, social, and ethical implications of these technologies for the digital economy. Their results revealed the possibilities of robotics to enhance the efficiency and safety of engineering based on classic inspection issues [88]. In contrast, Lyu et al. (2024) built a wall-climbing, heavy-duty robot to inspect the concrete masonry of huge bridges. They figured out a way to get a similar adsorption force equation to maximize the capacity to carry load and then ran some tests to confirm that the robot was working as it should. The findings showed that this new design made inspection much safer because it accesses hard-to-reach areas without introducing the risks associated with manual inspection [89]. Pham et al. (2024) designed a compact analog magnetic sensing system for structural inspection of steel bridges. Their test was to engineer synthetic cracks in a steel test plate and then find that, coupled to robotic

platforms, the sensor system allowed for the real-time detection of multiple kinds of cracks. This progress further improved the safety and maintenance of steel buildings [90].

Choi et al. (2024) tried to optimize visual inspection with a mixed reality system that used gaze tracking. It was shown that inspectors could directly view holographic data in real time, which improved the decision-making on complex inspections with higher quality outcomes than traditional techniques [91]. Pokhrel et al. (2024) sought to automate concrete bridge deck inspections with UAS and machine learning. This paper demonstrated CNNs and Vision Transformers (ViTs) successfully to find damage with 97% accuracy of the ViT model as compared to CNN. This development made it clear that the combination of UAS and machine learning could yield more accurate and efficient inspections [92]. Finally, Bian et al. (2024) analyzed all the robots currently used for cable inspections and suggested a new non-destructive sensor. This inspection machine that measured cable corrosion efficiently used two data input modules to provide better inspection precision and speed. The study showed that the proposed device exceeded the limitations of the existing techniques and provided a quicker and more accurate measurement of the bridge cable state [93].

7. Challenges and Future Scope in Bridge Engineering

In this article, some problems and opportunities related to applying machine learning, computing, and robotics in bridge engineering are discussed. Here are the main ones:

7.1. Challenges

- Data Availability: One of the biggest bottlenecks is that there is not enough labeled data to train machine learning models on. This dearth can interfere with the detection of damage and maintenance predictive approaches, as in the application of domain adaptation to counteract this.
- Explicitness of Implementation: Integrating new technology like robotics and machine learning in the existing engineering process is tricky. Engineers may struggle to translate old methodologies to implement these new tools, and the adoption rate might be slower.
- Cost and Ethical Issues: When it comes to economic issues associated with the use of robotics and automation in bridge inspection, questions surrounding the cost, and the elimination of human jobs arise. Questions about ethics in the deployment of autonomous systems in critical infrastructure also have to be settled.
- Environmental Issues: Dynamic environment variables influence bridge dynamics and are an obstacle to predictive maintenance models. Weather conditions and other natural disasters make it hard to calculate bridge status and how efficiently repairs were done.

7.2. Future Scope

- More Effective Machine Learning Models: We can next look for stronger machine learning models that can generalize to various bridge types and conditions. That may involve optimizing transfer learning to apply observations of well-observed bridges to assessments of under-observed buildings.
- Embedding of IoT and Real-Time Monitoring: Bridge engineering in the near future may more often include IoT technologies for real-time monitoring. It would provide the data collection and analysis continuously, more early maintenance plans, and better safety precautions.
- Robotics Development: As robotics develops further, we can expect to see even more advanced inspection systems that can do difficult tasks autonomously. That might mean creating drones and ground robots that can work in harsh conditions and make accurate diagnoses of bridge conditions.
- Environmental Concerns: The green credentials are being paid more attention to in bridge design. It can also be investigated in future research to apply machine learning and computations to the optimal maintenance regimes that extend the life of bridges and are sustainable

8. Conclusion

The review paper titled Machine learning, computation, and robotics for bridge engineering provides a detailed description of how these technologies can significantly advance the discipline. The use of machine learning and computational tools, such as FEA and CFD, has been vital to determining the structural behavior and modes of failure of bridges. These techniques allow for more accurate assessments of structural integrity and resilience in diverse environments. This is highlighted as an industry-leading innovation that increases safety and effectiveness when performing bridge inspections by robots. Robots will get

into difficult places, eliminating the risks associated with manual inspections and facilitating accurate assessments of bridge conditions. These results point to the necessity of constructing bridge structures with greater durability in dynamic conditions such as earthquakes and flooding. With the use of advanced modeling, engineers can visualize bridge vulnerabilities and develop effective reinforcements. This paper emphasizes the need to continue exploring and developing them to adapt to changing engineering issues. Together, the use of these technologies enhances current practices and also prepares the ground for future innovations in bridge design. Finally, the review recommends a multidisciplinary approach that leverages machine learning, computation, and robotics to design safer, more efficient, and more durable bridges. This bundled approach is vital for resolving the nuances of the needs of contemporary infrastructure in the long term. Overall, the paper clearly demonstrates how these novel technologies can transform bridge engineering and deliver safer and more resilient infrastructure.

Acknowledgments

This review was conducted independently without external assistance or funding. All work, including the literature review, analysis, and writing, was completed by the author alone, who remains solely responsible for the views expressed and any errors in this article.

References

[1] Reich, Yoram. “Machine learning techniques for civil engineering problems.” Computer-Aided Civil and Infrastructure Engineering 12.4 (1997): 295–310. https://doi.org/10.1111/0885-9507.00065

[2] Alipour, Mohamad, et al., “Load-Capacity Rating of Bridge Populations through Machine Learning: Application of Decision Trees and Random Forests.” Journal of Bridge Engineering 22.10 (2017). https://doi.org/10.1061/(asce)be.1943-5592.0001103

[3] Fang, Jingang, et al. “An Improved Inspection Process and Machine-Learning-Assisted Bridge Condition Prediction Model.” Buildings 13.10 (2023): 1–14. https://doi.org/10.3390/buildings13102459

[4] Xu, Donghui, et al. “Concrete and steel bridge Structural Health Monitoring—Insight into choices for machine learning applications.” Construction and Building Materials 402 (2023): 132596. https://doi.org/10.1016/j.conbuildmat.2023.132596

[5] Zhang, Zeyu, et al. “Machine learning for bridge wind engineering.” Advances in Wind Engineering 1.1 (2024): 1–32. https://doi.org/10.1016/j.awe.2024.100002

[6] Wedel, Frederik, and Steffen Marx. “Application of machine learning methods on real bridge monitoring data.” Engineering Structures 250 (2022): 113365. https://doi.org/10.1016/j.engstruct.2021.113365

[7] Fan, Weiying, et al. “Machine learning applied to the design and inspection of reinforced concrete bridges: Resilient methods and emerging applications.” Structures 33 (2021): 3954–3963. https://doi.org/10.1016/j.istruc.2021.06.110

[8] Yu, Enbo, et al. “Application of time series prediction techniques for coastal bridge engineering.” Advances in Bridge Engineering 2 (2021): 1–18. https://doi.org/10.1186/s43251-020-00025-4

[9] Rahman, Farooque, and Rutuju Chavan. “Machine Learning application in prediction of Scour around Bridge Piers: A Comprehensive review.” Archives of Computational Methods in Engineering, 2024, 1–24. https://doi.org/10.1007/s11831-024-10167-7

[10] Pavlović, Goran, et al. “Optimal solution for the single-beam bridge crane girder using the Moth-Flame algorithm.” Vojnotehnicki Glasnik 72.3 (2024): 1345–1368. https://doi.org/10.5937/vojtehg72-51953

[11] Fedorik, Filip, et al. “FEA in Road Engineering Applications?” Proceedings of the 34rd ISARC, Taipei, Taiwan, 2017, 128–133. https://doi.org/10.22260/isarc2017/0017

[12] Kurowski, Paul M., and Ralph O. Buchal. “REINFORCING LEARNING IN ENGINEERING EDUCATION BY ALTERNATING BETWEEN THEORY, SIMULATION AND EXPERIMENTS.” Proceedings of the Canadian Engineering Education Association (CEEA), 2011, 1–4. https://doi.org/10.24908/pceea.v0i0.3662

[13] Mikheev, G., et al. “Railway vehicle and bridge interaction: some approaches and applications.” WIT Transactions on the Built Environment 114 (2010): 593–604. https://doi.org/10.2495/cr100551

[14] Chong, and Manuel. Construction engineering of steel tub-girder bridge systems for skew effects. Georgia Institute of Technology, 2012, https://www.proquest.com/docview/1221989465?pq-origsite=gscholar&fromopenview=true&sourcetype=Dissertations%20&%20Theses.

[15] Touran, Ali, and Dennis R. Ladick. “Application of robotics in bridge deck fabrication.” Journal of Construction Engineering and Management 115.1 (1989): 35–52. https://doi.org/10.1061/(ASCE)0733-9364(1989)115:1(35)

[16] Bogue, Robert. “Applications of robotics in test and inspection.” Industrial Robot: An International Journal 45.2 (2018): 169–174. https://doi.org/10.1108/ir-01-2018-0012

[17] Tian, Yongding, et al. “Intelligent robotic systems for structural health monitoring: Applications and future trends.” Automation in Construction 139 (2022): 104273. https://doi.org/10.1016/j.autcon.2022.104273

[18] Charron, Nicholas, et al. “Automated Bridge Inspection Using Mobile Ground Robotics.” Journal of Structural Engineering 145.11 (2019): 04019137. https://doi.org/10.1061/(asce)st.1943-541x.0002404

[19] Phillips, Stephen, and Sriram Narasimhan. “Automating data collection for robotic bridge inspections.” Journal of Bridge Engineering 24.8 (2019): 04019075. https://doi.org/10.1061/(asce)be.1943-5592.0001442

[20] McCrea, A., and R. Navon. “Application of GA in optimal robot selection for bridge restoration.” Automation in Construction 13.6 (2004): 803–819. https://doi.org/10.1016/j.autcon.2004.05.002

[21] Ahmed, Habib, et al. “Review of Non-Destructive Civil Infrastructure Evaluation for Bridges: State-of-the-Art Robotic Platforms, Sensors and Algorithms.” Sensors 20.14 (2020): 1–38. https://doi.org/10.3390/s20143954

[22] Xu, Fengyu, et al. “Cable inspection robot for cable-stayed bridges: Design, analysis, and application.” Journal of Field Robotics 28.3 (2011): 441–459. https://doi.org/10.1002/rob.20390

[23] Gupta, Parul, et al. “Structural Applications of Smart Materials in Construction Engineering Using Robotics.” First International Conference on Industrial and Information Systems, 2006, 261–267. https://doi.org/10.1109/iciis.2006.365734

[24] AMC Bridge. "AI and Machine Learning." AMC Bridge, https://www.amcbridge.com/expertise/ai-and-machine-learning. Accessed 26 Oct. 2024.
[25] Rowan University. "Machine Learning In Bridge Design." Rowan University, https://rowancreates.org/research/projects/in-progress/machine-learning-in-bridge-design.html . Accessed 26 Oct. 2024.
[26] UoE Design Studio. "Machine learning set to make bridges safer – and cheaper to maintain." University of Exeter, 2024, https://researchandinnovation.co.uk/machine-learning-helps-improve-safety-of-civil-structures/ . Accessed 26 Oct. 2024.
[27] DH Glabe & Associates. "Finite Element Analysis, FEA & FEM." DH Glabe & Associates, https://www.dhglabe.com/product-design-and-testing/finite-element-analysis . Accessed 26 Oct. 2024.
[28] Predictive Engineering. "Finite element analysis." Predictive Engineering, https://www.predictiveengineering.com/consulting/fea-consulting-services . Accessed 26 Oct. 2024.
[29] Bible, Stewart. "CFD for Bridge Design." Resolved Analytics, https://www.resolvedanalytics.com/cfd-applications/cfd-for-bridges . Accessed 26 Oct. 2024.
[30] Sadlock, Joshua. "Collaboration Between Robots and Humans Makes Complex Bridge Building Easier." Engineering.com, 2021, https://www.engineering.com/collaboration-between-robots-and-humans-makes-complex-bridge-building-easier/ . Accessed 26 Oct. 2024.
[31] Ashcroft, Sean. "Top 10: Construction Robotics Companies." Construction Digital, 2024, https://constructiondigital.com/top10/the-top-10-construction-robotics-companies . Accessed 26 Oct. 2024.
[32] Ali. "Building the bridges of the future using robots." Bulldozair, 2017, https://blog.bulldozair.com/building-the-bridges-of-the-future-using-robots . Accessed 26 Oct. 2024.
[33] Mathern, Alexandre, et al. "Sustainability-driven structural design using artificial intelligence." 2019 IABSE Congress – the Evolving Metropolis, 2019, 1057–1064. https://doi.org/10.2749/newyork.2019.1057
[34] Pan, Hong, et al. "Conditional assessment of large-scale infrastructure systems using deep learning approaches (Conference Presentation)." Smart Structures and NDE for Industry 4.0, Smart Cities, and Energy Systems 11382 (2020): 113820T. https://doi.org/10.1117/12.2560133
[35] Moon, Seonghyeon, et al. "Bridge Damage Recognition from Inspection Reports Using NER Based on Recurrent Neural Network with Active Learning." Journal of Performance of Constructed Facilities 34.6 (2020): 1–10. https://doi.org/10.1061/(asce)cf.1943-5509.0001530
[36] Xu, Yayin, et al. "Machine learning in construction: From shallow to deep learning." Developments in the Built Environment 6 (2021): 1–13. https://doi.org/10.1016/j.dibe.2021.100045
[37] Nguyen, Thanh Q. "A Data-Driven Assessment Based on Viscosity Resistance Coefficient Indicator of Bridge Spans Using Deep Learning and Balancing Composite Motion Optimization." Journal of Vibration Engineering & Technologies 10 (2021): 601–619. https://doi.org/10.1007/s42417-021-00394-8
[38] Moon, Hyun Su, et al. "Application of artificial neural network to predict dynamic displacements from measured strains for a highway bridge under traffic loads." Journal of Civil Structural Health Monitoring 12(2021): 117–126. https://doi.org/10.1007/s13349-021-00531-7
[39] Wang, Guicheng, et al. "Recycled concrete bridge engineering based on artificial intelligence algorithm." International Symposium on Robotics, Artificial Intelligence, and Information Engineering (RAIIE 2022) 12454 (2022): 643–648. https://doi.org/10.1117/12.2658366
[40] Kumar, Amit, et al. "Efficient Prediction of Bridge Conditions Using Modified Convolutional Neural Network." Wireless Personal Communications 125 (2022): 29–43. https://doi.org/10.1007/s11277-022-09539-8
[41] Entezami, Alireza, et al. "A Multi-stage Machine Learning Methodology for Health Monitoring of Largely Unobserved Structures Under Varying Environmental Conditions." In Lecture notes in civil engineering 254 (2022): 297–307. https://doi.org/10.1007/978-3-031-07258-1_31
[42] Zhou, Qi-Neng, et al. "An Advanced Multi-Agent Reinforcement Learning Framework of Bridge Maintenance Policy Formulation." Sustainability 14.16 (2022): 1–18. https://doi.org/10.3390/su141610050
[43] Dolui, Cherosree, et al. "Magnetostrictive Sensor Based Bridge Health Assessment Using Machine Learning Classifiers." 2023 IEEE Pune Section International Conference (PuneCon), 2023, 1–6. https://doi.org/10.1109/punecon58714.2023.10450103
[44] Giglioni, Valentina, et al. "On the use of domain adaptation techniques for bridge damage detection in a changing environment." Ce/Papers 6.5 (2023): 975–980. https://doi.org/10.1002/cepa.2143
[45] Xie, Yishun, et al. "Prediction and Early Warning of Extreme Winds for High-Speed Railway Bridge Construction Using Machine-Learning Methods." Sustainability 15.24 (2023): 1–18. https://doi.org/10.3390/su152416921
[46] Ghafoori, Mahdi, et al. "Machine Learning-Based Bridge Maintenance Optimization Model for Maximizing Performance within Available Annual Budgets [Dataset]." In Zenodo (CERN European Organization for Nuclear Research), 2023. https://doi.org/10.5281/zenodo.10145531
[47] Tai, Linguang, et al. "A Stochastic Algorithm Based on Cable-stayed Bridges Model for Stochastic Optimization in Machine Learning." Journal of Physics: Conference Series 2607 (2023): 1–14. https://doi.org/10.1088/1742-6596/2607/1/012014
[48] Nguyen, Duc C., et al. "Vibration-based SHM of Dębica railway steel bridge with optimized ANN and ANFIS." Journal of Constructional Steel Research 215 (2024): 108505. https://doi.org/10.1016/j.jcsr.2024.108505
[49] Bai, Huajun, et al. "Intelligent Conceptual Design of Railway Bridge Based on Graph Neural Networks." International Journal of Computational Intelligence Systems 17 (2024): 1–15. https://doi.org/10.1007/s44196-024-00584-8
[50] Yang, Chan, et al. "Impact of Environmental Conditions on Predicting Condition Rating of Concrete Bridge Decks." Transportation Research Record, 2024, 03611981241248647. https://doi.org/10.1177/03611981241248647
[51] Gunderia, Amisha, et al. "AI Approaches for Predictive Maintenance in Road Bridge Infrastructure." 2024 International Conference on Smart Applications, Communications and Networking (SmartNets), 2024, 1–6. https://doi.org/10.1109/smartnets61466.2024.10577641
[52] Giglioni, Valentina, et al. "A domain adaptation approach to damage classification with an application to bridge monitoring." Mechanical Systems and Signal Processing 209 (2024): 1–17. https://doi.org/10.1016/j.ymssp.2024.111135
[53] El-Ghandour, Al, and CD Foster. "Coupled finite element and multibody systems dynamics modelling for the investigation of the bridge approach problem." Proceedings of the Institution of Mechanical Engineers Part F Journal of Rail and Rapid Transit 233.10 (2019): 1097–1111. https://doi.org/10.1177/0954409719828599
[54] Izvekov, Yu A., et al. "Probability calculation applied to potential failure zones of the bridge girder of metallurgical crane." IOP

Conference Series: Materials Science and Engineering 971 (2020): 1–6. https://doi.org/10.1088/1757-899x/971/4/042012

[55] Sharma, Anish, and Guner, Serhan. "Numerical Modeling Methodology for Strength Evaluation of Deep Bridge Bent Caps." Special Publication 342 (2020): 162-177. https://www.utoledo.edu/engineering/faculty/serhan-guner/docs/JP18_Sharma_Guner_2020_Bridges.pdf

[56] Liu, Zhi, et al. "Coupled CFD–FEM Simulation Methodology for Fire-Exposed Bridges." Journal of Bridge Engineering 26.10 (2021): 04021074. https://doi.org/10.1061/(asce)be.1943-5592.0001770

[57] Sengsri, Pasakorn, and Kaewunruen, Sakdirat. "Local Failure Modes and Critical Buckling Loads of a Meta-Functional Auxetic Sandwich Core for Composite Bridge Bearing Applications." Applied Sciences 11.22 (2021): 1–15. https://doi.org/10.3390/app112210844

[58] Ko, Yu-Fu. "Finite Element Analysis of Reinforced Concrete Single-Column Bridge Bent with Flexural Failure Under Near-Fault Ground Motion." International Journal of Civil Engineering 20 (2021): 237–256. https://doi.org/10.1007/s40999-021-00648-2

[59] Zhu, Na, and Tian, Jun. "Numerical simulation of vortex vibration in main girder of cable-stayed bridge based on bidirectional fluid–structure coupling." Applied Mathematics and Nonlinear Sciences 8.2 (2022): 561–570. https://doi.org/10.2478/amns.2021.2.00220

[60] Yoneda, Taiju, et al. "Development of a 3D Finite-Element Modelling Generation System Based on Data Processing Platform and Fatigue Analysis of Full-Scale Reinforced-Concrete Bridge." IABSE Symposium Prague 2022 - Challenges for Existing and Oncoming Structures, 2022, 415–422. https://doi.org/10.2749/prague.2022.0415

[61] Tang, Hao, et al. "Reliability-based vulnerability analysis of bridge pier subjected to debris flow impact." Structure and Infrastructure Engineering 20.1 (2022): 1–12. https://doi.org/10.1080/15732479.2022.2074468

[62] Quan, W., et al. "Study on seismic mitigation Performance of Long-span High-speed Railway Continuous Beam Bridge with Viscous Damper." Journal of Physics: Conference Series 2158 (2022): 1–9. https://doi.org/10.1088/1742-6596/2158/1/012022

[63] Duan, Junyi, and Chengcheng Tao. "Enhancing Bridge Infrastructure Flood Resilience through Fluid-Structure Interaction Modeling." ASCE Inspire 2023, 2023, 666–672. https://doi.org/10.1061/9780784485163.078

[64] Fleit, Gábor, et al. "CFD modeling of flow and local scour around submerged bridge decks." Journal of Coastal and Hydraulic Structures 3 (2023): 1–19. https://doi.org/10.48438/jchs.2023.0026

[65] Kaushal, Harwinder Singh, et al. "Structural Stability Analysis of Bridge Structure Using FEA." International Journal of Innovative Research in Engineering & Management 10.4 (2023): 152–155. https://doi.org/10.55524/ijirem.2023.10.4.19

[66] Malekghaini, Niloofar, et al. "Bayesian Model Updating for System and Damage Identification of Bridges Using Synthetic and Field Test Data." In Conference proceedings of the Society for Experimental Mechanics, 2023, 41–44. https://doi.org/10.1007/978-3-031-37003-8_7

[67] Dong, Zhaoxian, et al. "Influence of soil liquefaction effect on seismic failure mechanism of river-crossing simply-supported girder bridges subjected to near-fault ground motions." Engineering Failure Analysis 154 (2023): 107664. https://doi.org/10.1016/j.engfailanal.2023.107664

[68] Zhu, Licheng, et al. "A full-scale numerical study on aerodynamic force conditions of high sided vehicles on the Queensferry Crossing Bridge." Journal of Physics: Conference Series 2647 (2024): 1–8. https://doi.org/10.1088/1742-6596/2647/4/042001

[69] Petruccelli, Natasha, et al. "CFD modelling to investigate hydrodynamic forces on bridges in case of submergence and material deposition." EGU General Assembly 2024, Vienna, Austria, 14–19 Apr 2024, EGU24-1081, 2024. https://doi.org/10.5194/egusphere-egu24-1081

[70] Han, Songling, and Changming Wang. "Numerical Investigation of Bedding Rock Slope Potential Failure Modes and Triggering Factors: A Case Study of a Bridge Anchorage Excavated Foundation Pit Slope." Applied Sciences 14.16 (2024): 1–24. https://doi.org/10.3390/app14166891

[71] Fusco, D., et al. "High-performance beam finite element for predictive response in monitoring existing bridges." Journal of Physics: Conference Series 2647 (2024): 1–10. https://doi.org/10.1088/1742-6596/2647/18/182020

[72] Jia, Hongyu, et al. "Numerical simulation and damaged analysis of a simply-supported beam bridge crossing potential active fault." Engineering Structures 301 (2024): 117283. https://doi.org/10.1016/j.engstruct.2023.117283

[73] Zhu, Xiyu, et al. "Study of the Dynamic Reaction Mechanism of the Cable-Stayed Tube Bridge under Earthquake Action." Buildings 14.7 (2024): 1–34. https://doi.org/10.3390/buildings14072209

[74] Potenza, Francesco, et al. "A robotics and computer-aided procedure for defect evaluation in bridge inspection." Journal of Civil Structural Health Monitoring 10 (2020): 471–484. https://doi.org/10.1007/s13349-020-00395-3

[75] Wang, Dalei, et al. "An Automated Inspection Method for the Steel Box Girder Bottom of Long-Span Bridges Based on Deep Learning." IEEE Access 8 (2020): 94010–94023. https://doi.org/10.1109/access.2020.2994275

[76] Yan, Yuchen, et al. "The Navigation and Control Study of UAV for Cross-domain Bridge Collaboration Detection." 2021 IEEE International Conference on Real-time Computing and Robotics (RCAR), 2021, 788–793. https://doi.org/10.1109/rcar52367.2021.9517661

[77] Garrido, Gabriela Gallegos, and Sattar, Tariq Pervez. "An Autonomous Wall Climbing Robot for Inspection of Reinforced Concrete Structures: SIRCAUR." Journal of Artificial Intelligence and Technology 1.3 (2021): 188–196. https://doi.org/10.37965/jait.2021.0016

[78] Lin, Jacob J., et al. "Bridge Inspection with Aerial Robots: Automating the Entire Pipeline of Visual Data Capture, 3D Mapping, Defect Detection, Analysis, and Reporting." Journal of Computing in Civil Engineering 35.2 (2021): 04020064. https://doi.org/10.1061/(asce)cp.1943-5487.0000954

[79] Ahmed, Habib, et al. "Multi-directional Bicycle Robot for Bridge Inspection with Steel Defect Detection System." 2022 IEEE/RSJ International Conference on Intelligent Robots and Systems (IROS), 2022, 4617–4624. https://doi.org/10.1109/iros47612.2022.9981325

[80] Zheng, Zhenliang, et al. "CCRobot-IV: An Obstacle-Free Split-Type Quad-Ducted Propeller-Driven Bridge Stay Cable-Climbing Robot." IEEE Robotics and Automation Letters 7.4 (2022): 11751–11758. https://doi.org/10.1109/lra.2021.3099872

[81] Motley, Cadence, et al. "Design of A High Strength Multi-Steering Climbing Robot for Steel Bridge Inspection." 2022 IEEE/SICE International Symposium on System Integration (SII), 2022, 323–328. https://doi.org/10.1109/sii52469.2022.9708750

[82] Li, Jie, et al. "Circumferentially rotatable inspection robot with elastic suspensions for bridge cables." Industrial Robot 49.5 (2022): 981–993. https://doi.org/10.1108/ir-11-2021-0261

[83] Gong, Guilin, et al. "Discovery and Discrimination of Bridge Engineering Safety Issues by BIM Virtual Scene Combined with Robotic Mapping." Journal of Robotics 2023.1 (2023): 1–12. https://doi.org/10.1155/2023/3028505

[84] Hoxha, Ejup, et al. "Robotic Inspection and Subsurface Defect Mapping Using Impact-Echo and Ground Penetrating Radar." IEEE Robotics and Automation Letters 8.8 (2023): 4943–4950. https://doi.org/10.1109/lra.2023.3290386

[85] Gucunski, Nenad, et al. “Advancing Condition Assessment of Reinforced Concrete Bridge Elements Through Automation, Visualization, and Improved Interpretation of Multi-NDE Technology Data.” Materials Evaluation 81.1 (2023): 56–66. https://doi.org/10.32548/2023.me-04289

[86] Alamdari, Ali Ghadimzadeh, & Arvin Ebrahimkhanlou. “A robotic approach for crack detection through the integration of cameras and LiDARs.” Sensors and Smart Structures Technologies for Civil, Mechanical, and Aerospace Systems 2023 12486 (2023): 21–29. https://doi.org/10.1117/12.2658110

[87] Popli, Renu, et al. “ROAD: Robotics-Assisted Onsite Data Collection and Deep Learning Enabled Robotic Vision System for Identification of Cracks on Diverse Surfaces.” Sustainability 15.12 (2023): 1–17. https://doi.org/10.3390/su15129314

[88] Ade-Omowaye, Joshua, et al. “Robotics and Automation in Engineering: Perspectives for the Digital Economy.” 2024 International Conference on Science, Engineering and Business for Driving Sustainable Development Goals (SEB4SDG), 2024, 1–7. https://doi.org/10.1109/seb4sdg60871.2024.10630219

[89] Lyu, Guizhi, et al. “A heavy-load wall-climbing robot for bridge concrete structures inspection.” Industrial Robot 51.3 (2024): 465–478. https://doi.org/10.1108/ir-11-2023-0273

[90] Pham, Anh Quyen, et al. “Analog Magnetic Sensor-Robotic System for Steel Structure Inspection.” 2024 IEEE/SICE International Symposium on System Integration (SII), 2024, 669–674. https://doi.org/10.1109/sii58957.2024.10417657

[91] Choi, Sunwoong, et al. “Gaze-based Human-Robot Interaction System for Infrastructure Inspections.” arXiv (Cornell University), 2024. https://doi.org/10.48550/arxiv.2403.08061

[92] Pokhrel, Rojal, et al. “Automated Concrete Bridge Deck Inspection Using Unmanned Aerial System (UAS)-Collected Data: A Machine Learning (ML) Approach.” Eng—Advances in Engineering 5.3 (2024): 1937–1960. https://doi.org/10.3390/eng5030103

[93] Bian, Li, et al. “Current Status of Bridge Cable Climbing Robot Technology and Design of Cable Corrosion Detection Device.” 2024 5th International Conference on Mechatronics Technology and Intelligent Manufacturing (ICMTIM), 2024, 542–547. https://doi.org/10.1109/icmtim62047.2024.10629445

Journal of Civil Engineering Researchers

Journal homepage: www.journals-researchers.com

Investigating the Effect of Silica Foam on the Mechanical Properties of Concrete Containing Recycled Glass Shards

Hadi Faghihmaleki,[a,*] Reza Abbasghorbani[a]

[a] *Faculty of Civil Engineering, Ayandegan Institute of Higher Education, Tonekabon, Iran*

ABSTRACT

Recycled glass waste is one of the most attractive waste materials that can be used to create a concrete mix. Therefore, researchers focus on the production of concrete using recycled glass as an abrasive or as a pozzolanic material, but the use of recycled glass in the form of coarser particles to replace sand in concrete increases the alkali-silica reaction and this causes Unfavorable performance in the mechanical properties of concrete. To prevent this, micro silica is used to improve the strength and mechanical properties of concrete .In this research, after building the control mixing design, recycled glass was replaced with sand and silica foam as micro silica in four designs with a fixed ratio of 5% by weight of cement. The compressive strength test was performed at the ages of 7 and 28 days, and three samples were taken in each test, and a total of 24 cubic samples were tested. Tensile test, like compressive strength test, were tested at the ages of 7 and 28 days, which included two cylindrical samples in each test, and a total of 16 cylindrical samples were tested. The presence of silica foam in concrete causes adhesion and reduction of slump fluidity, and the highest slump fluidity was observed at 5% ratio. The result of testing the compressive strength and tensile strength of the concrete containing glass shards and silica foam had decreased in quality compared to the control mixing plan, which shows the unfavorable performance of coarse glass particles in the concrete structure.

ARTICLE INFO

Received: November 06, 2024
Accepted: November 25, 2024

Keywords:
Silica foam
Shards of glass
Durability
Concrete with recycled materials
Compressive and tensile strength

DOI: 10.61186/JCER.6.4.22
DOR: 20.1001.1.2538516.2024.6.4.3.8

1. Introduction

Concrete is one of the most widely used materials in engineering structures [1]. The favorable physical and mechanical properties of concrete and the ease of its production have made concrete the most widely used material in the construction industry. The compressive strength of concrete and bearing high pressures is one of its characteristics [2]; In this way, it shows good resistance against sudden failures and compressive stresses other characteristics of concrete that can be mentioned are high energy absorption and fire resistance [3]. Although concrete works well in civil works, its components are made from natural sources.

Lack of natural resources and over-harvesting can cause great problems in the future. Therefore, an alternative to the materials used in concrete that reduces the damage to the environment is felt more than ever [4]. The volume of industrial and construction waste landfills is expanding [5]. According to the estimates made in the last few years, we

* Corresponding author. Tel.: +989112923228; e-mail: h.faghihmaleki@gmail.com (Associate Prof. Hadi Faghihmaleki).

have faced an increase of 9.2% of natural materials [6]. One of the ways to deal with this important issue is to recycle and reuse it. This will prevent the accumulation of waste materials. Glass is one of the waste materials that we see producing a significant amount of it all over the world. In 2004, the United Nations estimated the production of solid waste in the whole world to be about 200 million tons, of which more than 7% was glass waste [7]. Concrete containing glass shards is one of the modern innovations in the construction industry, which avoids problems related to their burial and recycling by using glass shards as a substitute for traditional aggregates. But concrete containing glass fragments may lose properties such as mechanical resistance and weather resistance compared to traditional concrete. In order to improve the properties of concrete containing glass shards, adding silica foam to it as a strength additive is investigated. Silica foam is a self-compacting filler material that, by adding it to concrete, reduces the porosity and weight of the concrete itself, and as a result improves the mechanical resistance and thermal properties and insulation of concrete.

Bhanja and Sengupta in 2005 [8], conducted experiments on a water ratio of 0.26 to 0.42 and a silica foam ratio of 0.0 to 0.3. and considered compressive, tensile and bending strength for all samples in this research. The obtained results show an increase in compressive and tensile strength with silica foam composition and that the percentage of substitution in the tests is not fixed at one percent but depends on the ratio of water to cement. Compared to split tensile strengths, flexural strengths showed more improvements. Evaldes and Vitoldas in 2021 [9], collected glass from a dump site and crushed it in a ball mill in two ways before and after cleaning, and then the glass shards were analyzed by a scanning electron microscope (SEM) and analyzed by energy dispersive X-ray spectroscopy (EDX).

The effects of waste glass powder before and after cleaning, hydation process of Portland cement were analyzed using semi-adiabatic calorimetric method. For further research, the boiler properties such as density, compressive strength and porosity of ordinary strength concrete with different amounts of glass powder were also investigated. In these tests, it was found that when 25% of the ordinary sand was replaced with waste glass powder after the cleaning process, a slight increase in compressive strength could be expected. Vaitkus and et al., in 2020 [10], in percentages of 0%, 7% and 10% compared to cement and a fixed ratio of 0.4 water to cement ratio. The designs were tested in compression, tension and cyclic loading of production. In addition, the density was determined to identify the difference in concrete microstructure due to the presence of silica fume. The results showed that silica foam significantly increases the performance of high-strength concrete in terms of pressure, stretch, bending and cyclic loading, and the design of 7% is the optimal value.

The use of glass in concrete can be done in two ways: glass shards as a substitute for part of the aggregate and glass powder as a substitute for part of the cement. One of the biggest concerns for replacing glass chips as part of the aggregate is its alkali-silica reaction. This reaction in concrete causes closure of expansion joints, displacement of structural members relative to each other and other adverse effects. One of the ways to reduce the effects of the alkali-silica reaction is to add additional cement materials such as silica foam, which is a powder with very fine silica particles that is obtained from the processing and grinding of nano silica or silica foam.

The addition of silica foam in concrete significantly improves concrete, reduces shrinkage in the drying process, which leads to the reduction of surface cracks and fractures in concrete, and increases the adhesion between cement and minerals. In addition, the presence of silica foam in concrete increases the compressive and tensile strength. Therefore, it is necessary and important to investigate the percentage of replacement and the necessary amount of silica foam to reduce the alkali-silica effect and increase the strength of concrete.

2. Laboratory program

2.1. Specifications of materials used in concrete

2.1.1. Aggregate

The aggregate used in the research concrete is from the sand of the Tonkabon spring river. The rough outer surface of the aggregate provides more surface area for materials such as water and cement to bond. The maximum size of the aggregate is another important factor, which was done by conducting a granulation test and using standard sieves, a mechanical shaking device for sieves and a scale with an accuracy of 0.1, and finally by comparing with the permitted range of ASTM. The used aggregates were completely dried in an oven at a temperature of 110°C before testing, and then they were tested vertically and horizontally in a shaking machine at a speed of 150 rpm for ten minutes.

2.1.2. Cement

The cement used in this research is type 1 Portland cement, this gray cement is called ordinary Portland cement. Type 1 Portland cement is divided into three resistance categories 325, 425 and 525 based on 28 days resistance. This used cement is the first category of type 1 cement and is for general use in making mortar and concrete.

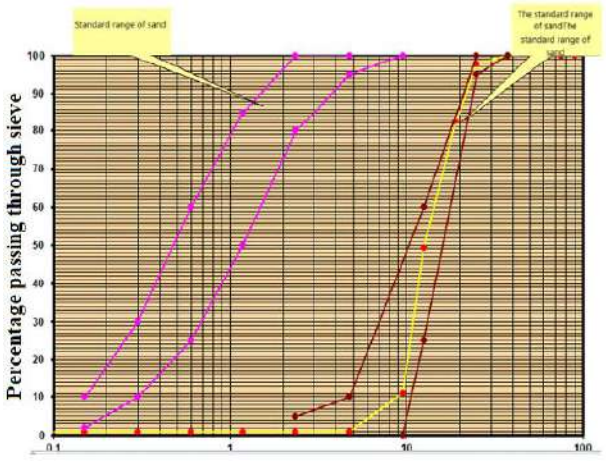

Figure 1: Gravel grading chart compared to ASTM limits

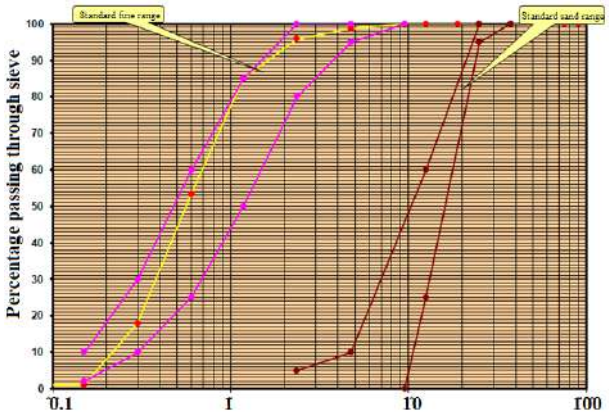

Figure 2: Graph of sand grading compared to ASTM limits

Table 1

Physical properties of cement used in concrete

Physical properties of cement	amount
Initial capture time	100-160minutes
Secondary capture time	180-240minutes
Autoclave volume expansion	0.15-0.05%
Special level	2900cm2/gr

Table 2

Comparison of chemical and physical properties of cement compounds

Feature	Portland cement	Silica fly ash	Lime fly ash	cement slag	Silica foam
SiO2	21.9	52	35	35	85-97
Al2O3	6.9	23	18	12	-
CaO	6.3	5	21	40	<1
SO3	1.7	-	-	-	-
(m2/kg) specific surface	370	420	420	400	30000-15000
Specific density	3.15	2.38	2.65	2.94	2.22
General use in concrete	Primary binder	Cement substitute	Cement substitute	Cement substitute	Amplifier

Figure 3: Appearance of silica foam.

Figure 4: Appearance of used glass shards.

2.1.3. Silica foam

Silica foam is a polymorph of the amorphous (non-crystalline) solid form of silicon dioxide. This ultra-fine powder can be produced as a by-product of silicon and ferrosilicon alloy and consists of spherical particles with an average diameter of 150 nm. The first experiment of silica fume in Portland cement concrete was done in 1952.In early research, an expensive additive called silica foam, an amorphous form of silica, was made and used by burning silicon tetrachloride in a hydrogen-oxygen flame. The specific gravity of silica foam is generally in the range of 2.2 to 2.3. The specific surface area of silica foam can be measured by the BET method or the nitrogen absorption method. It typically ranges from 15,000 to 30,000 square meters/kg.

2.1.4. Glass shards

Aggregates make up almost 70% of concrete composition, for this reason, using glass aggregates in concrete can lead to reduction of glass waste. In this research, it was done by using recycled glass and crushing them manually, and the size of the glass shards was based on the sand grading chart and coordinated with the size of the sand grains. The size of glass shards after final crushing is between 0.5 and 2.5 cm.

2.1.5. Lubricant

The additive used in this research is radon concrete lubricant, which is very suitable for the production of high-strength concrete. The consumption amount of super lubricant in this research is 2% of the cement weight in the mixing plan. Each time the super lubricant was added to the last part of the water sample and then added to the mixture.

2.1.6. Water

The water used in the construction of mixing plans and sample processing was from the drinking water of Tonkabon city.

Table 3

Characteristics of super lubricant

Increase in air percentage	less than 2%
Alkali content	Less than 5 grams of Na2O
Chemical base	Polycarboxylate ether
Chlorine ion	does not have
color	Colorless and transparent
Freezing temperature	minus three degrees Celsius
PH value	3 to 7
physical state	liquid
specific weight	1.18±0.05grams per cubic
brand	RAMKA

2.1.7. mixing designs

In this research, in order to achieve a suitable mixing plan for concrete with a strength of 30 MPa in a period of 28 days, the percentage of water to cement is 0.52 and during four mixing plans with percentages of 5, 7, 10 and 12 percent, silica foam and glass shards with A constant of 5% was considered in four mixing plans, which was done by making cubic and cylindrical samples and performing compressive and tensile strength tests by concrete breaker jack machine at the age of 7 days. The mixing plan of control concrete samples (Table 4) was made to achieve concrete with a strength of 30 MPa. 4 cubic samples 15*15*15 and 4 cylindrical samples 15*30 without lubricant were made. The best compressive strength obtained in the 7-day sample was 262 kg/m^2.

Table 4

Control sample mixing plan

cement	water	sand	sand	Water to cement ratio
380	198	1136	659	0/52

The main mixing plan of the research in Table 5, which includes concrete containing silica foam and glass shards containing lubricant. In this plan, the mixing of silica foam is considered as a percentage of the cement volume. The glass shards used in this mixing design are fixed at 5% and

Figure 5: Cubic and cylindrical samples of control concrete

Table 5
Mixing scheme of concrete containing silica foam and glass shards

Mixing design number	sand	sand	cement	Silica foam	water	shards of glass	lubricant
silica foam 5%	1136	659	361	19	198	56/8	7/6
silica foam 7%	1136	659	353/4	26/6	198	56/8	7/6
silica foam 10%	1136	659	342	38	198	56/8	7/6
silica foam 12%	1136	659	334/4	45/6	198	56/8	7/6

Figure 6: The process of making and processing samples.

have been replaced as a part of coarse sand, and the lubricant used is 2% of the cement volume.

2.1.8. Making samples

After preparing the materials, cement, silica foam, shards of glass, gravel, sand and water are first weighed. After collecting the sand materials, pour it into the mixer and add 80% of the weighed water to it, after a minute, add silica foam to the coarse sand and mix them properly. The mixing process continued for 2-3 minutes. After sand and glass shards are added to the materials in the mixer at the same time and after 2-3 minutes cement is added to it and after 2 minutes the lubricant is added to 20% of the remaining water and allowed to mix. We let the mixer continue to work for another 3-5 minutes and after 3-5 minutes, turn off the mixer and the desired concrete is ready to be placed in the mold. After cleaning the inside of the mold and greasing it with special oil, the made concrete was poured into the molds in three layers and 25 strokes in each layer by the rod and compacted. After 24 hours, the samples were removed from the mold and kept in the water pool with Ph close to 7 for processing (Figure 6).

3. Tests

3.1. Concrete slump test

In this research, to perform the slump test, first, the inside of the cone mold was completely cleaned and moistened, and concrete was poured into the funnel in three layers and with equal volume. The layers were compacted by a rod with 25 strokes. After compaction of the last layer, the slump mold was pulled up vertically without moving the base plate, and then the amount of concrete drop from the height of the rod on the metal plate to the highest point of the concrete was measured and recorded.

Figure 7: Concrete slump test

Figure 8: Cube samples after being taken out of the pond and tested for compressive strength

Figure 9: Cylindrical samples after being taken out of the pond and tested for tensile strength.

Table 6

Conversion coefficients of non-standard samples to standard samples.

150mm cubic compressive strength (MPa)	≤25	30	35	40	45	50	55
Compressive strength of standard cylinder (MPa)	1.25	1.20	1.17	1.14	1.13	1.11	1.1

3.2. Compressive strength test of concrete

In order to control the quality of hardened concrete, a compressive strength test was performed to determine the capacity of concrete made against direct compressive forces on cubic samples by a concrete breaker jack and the possibility of software analysis. Compressive strength depends on several factors, including the quality of consumables, mixing plan and quality control during concrete production. To perform the compressive strength test, after 7 and 28 days of treatment in the pond, the samples were removed from the water one day before the test and placed in the open air to dry (Figure 8). Then put the sample in the place where the sample is placed inside the device and turn on the device. After the device applied force to the sample and the number shown on the device remained constant, the device was turned off and the amount of stress and force was recorded.

3.3. Concrete tensile strength test

In this research, the samples were removed from the pond after 7 and 28 days of treatment and placed in the open space for one day to dry completely. The tensile test of concrete was performed by cutting a cylindrical sample in half based on the ASTM C496 standard. The samples were fixed and tested in the appropriate place with the help of steel rod and bottom plate in the machine. in such a way that the load is applied against the direction of concreting. After performing the test steps, it was recorded with the maximum load and the tensile strength was calculated by halving the Eq. (1).

$$T = \frac{2P}{\pi l d} \quad (1)$$

In Eq. (1):
T = halving tensile strength (kg/cm^3)
P = maximum applied load (kg)
L = length of cylindrical specimen
d = diameter of cylindrical sample (cm)

3.4. Concrete elasticity modulus test

The modulus of elasticity test of concrete is one of the important tests in evaluating the mechanical properties of concrete. The modulus of elasticity indicates the hardness and resistance of concrete against deformation under applied loads. The modulus of elasticity of concrete is defined as the ratio of applied stress to the corresponding strain in concrete. The larger the aggregates used in concrete, the higher the modulus of elasticity of concrete. With higher loading speed, the compressive strength of concrete increases, and in this direction, the modulus of elasticity of concrete also increases. The modulus of elasticity makes it possible to predict the behavior of structures under different loadings and indicates how much concrete can withstand the load without undergoing changes. To check the samples in this research, the compressive strength test results of 28-day cubic samples were used. The coefficients in table (6) were used to convert the resistance of a cubic sample to a cylindrical sample. The modulus of elasticity of concrete under tension or compression is obtained by the slope of the stress-strain curve under uniaxial loading from Eq. (2).

$$E = \left(3300\sqrt{F_c} + 6900\right)\left[\frac{\gamma_c}{23}\right]^{1.5} \quad (2)$$

In Eq. (2):
E = modulus of elasticity of concrete GPa
F_c = compressive strength of concrete MPa
γ_c = specific mass of concrete kN/m^3

4. Results and discussion

4.1. Concrete slump test

The results of the fresh concrete slump test are presented in Table 7. The result of concrete slump in concrete without silica foam has little separation and no water loss, and the amount of fresh concrete slump is 80 mm. Silica foam in concrete caused an increase in concrete slump due to its very high adhesion property. In concrete containing silica foam, concrete slump increased and the slump in concrete containing 5% silica foam was 74 mm. Also, the concrete slump containing 12% silica foam has increased and has shown a number of 50 mm, and this is a reason for the amount of water absorption of silica foam compared to the use of ordinary cement alone. The presence of silica foam in concrete has increased the water consumption.

Table 7
Concrete slump results

The name of the mix	Slump (mm)
Witness concrete	80
Silica foam 5%	74
Silica foam 7%	67
Silica foam 10%	58
Silica foam 12%	53

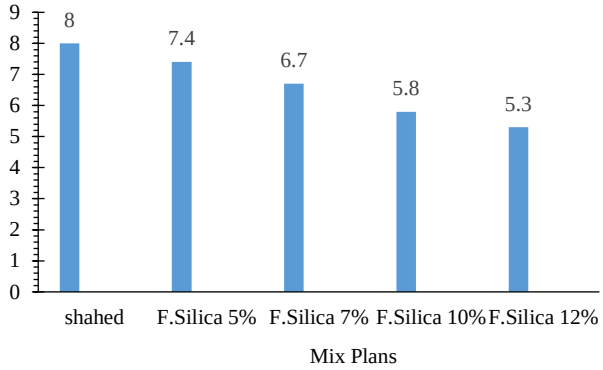

Figure 10: Concrete slump diagram (cm).

According to Figure (10), the concrete sample containing 5% silica foam decreased by 7.5% compared to the control concrete sample, and the fluidity was close to the control concrete. Also, for the concrete sample containing 7% silica foam, 16.25% slump reduction occurred. 10% and 12% silica foam samples have 27.5% and 33.75% slump reduction, respectively. The adhesion of these two samples is much higher due to the presence of more silica foam in its mixing plan.

4.2. Compressive strength test

The results of the compressive strength test show that the strength of the samples has increased due to the increasing age of processing. The strength of the 28-day concrete cube sample has increased by 24.3% compared to the 7-day sample. In the sample containing 5% silica foam, the 28-day compressive strength has increased by 22.39% compared to the 7-day sample, and in the samples with 7, 10, and 12% silica foam, it has increased by 20.93, 17.58, and 22.70%, respectively. These plans have shown a lower initial resistance than the control concrete.

7-day concrete samples containing silica foam and glass shards showed a decrease in compressive strength compared to the 7-day control sample. In the 7-day concrete samples containing 5% silica foam, there was a

34.61% decrease compared to the 7-day control sample. In 7-day concrete samples containing 7% silica foam compared to the 7-day control sample, there was a 35.18% decrease, and in the 7-day concrete samples containing 10 and 12% silica foam compared to the 7-day control sample, there was a 36.21 and 42.24% decrease, respectively. has had

Table 8
Compressive strength test results (Mpa)

No mixing	Compressive strength at 7 days	Compressive strength of 28 days
Concrete sample as witness	25.7	33.9
A sample of 5% silica foam	16.8	21.6
A sample of 7% silica foam	16.6	21
A sample of 10% silica foam	16.4	19.9
A sample of 12% silica foam	14.8	19.2

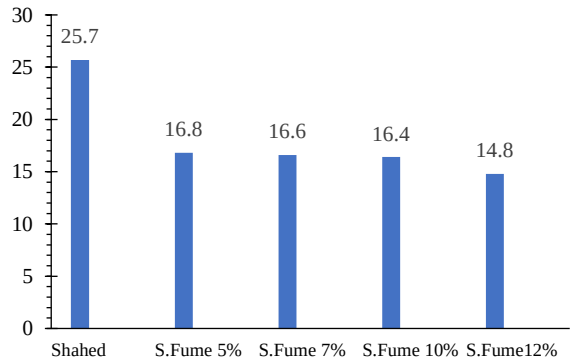

Figure 11: Graph of the 7-day compressive strength results of the samples (MPa).

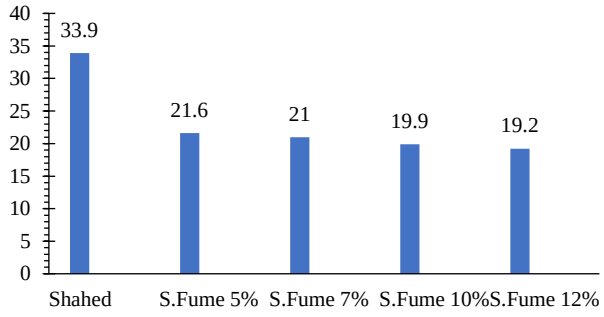

Figure 12: 28-day compressive strength results graph of the samples (MPa).

In the 28-day concrete samples containing silica foam and glass shards, it showed a decrease in compressive strength compared to the 28-day control samples. In the samples of 28 days, 5% silica foam has decreased by 36.21% compared to the control sample of 28 days. In the 7 and 10% silica foam samples, compared to the 28-day control sample, there was a decrease of 37.95 and 41.41%, respectively, and in the 28-day sample containing 12% silica foam, there was a 43.43% decrease compared to the 28-day control sample. The ratio of glass shards in all samples was 5% compared to coarse sand.

4.3. Tensile strength test

The tensile strength of concrete decreased with the decrease of compressive strength compared to control concrete. At the age of 28 days, the tensile strength of concrete in the design containing 5% silica foam and 5% glass shards has decreased by 32.05% compared to the control design, and at the age of 7 days, the 5% sample has shown a 42.8% decrease. Tensile strength of concrete in 7 days 7% and 10% silica foam samples compared to the control sample showed 51.42% and 71.42% decrease in tensile strength, respectively.

Among the samples, the largest reduction in strength was the 12% silica foam sample, which had a 74.85% reduction in strength compared to the control concrete. The highest resistance observed among the samples was the 5% sample with a resistance of 2.01 MPa. The tensile strength of concrete in the 28-day sample containing 5% silica foam has decreased by 32% compared to the control concrete. In the samples containing 7% and 10% silica foam, compared to the control concrete, it showed a 42.3% and 64.1% decrease in tensile strength, respectively. The sample containing 12% silica foam has seen a 71.7% reduction in strength compared to concrete, which is the highest reduction in strength among the samples. The highest tensile strength obtained among the samples of 28 days was related to the sample containing 5% silica foam, which showed a tensile strength of 2.65 MPa.

4.4. Elastic modulus test

The test results of concrete modulus of elasticity at the age of 28 days are presented in the table. According to the obtained results, the modulus of elasticity decreases with the increase of silica foam in concrete. The obtained result shows that the rate of increase of concrete elasticity modulus is lower than the rate of increase of concrete compressive strength and the obtained results are relatively close to each other. In the tests conducted, the modulus of elasticity increased with the increase in compressive strength. The highest number obtained in the results of the tests was related to the witness concrete.

In the design containing 5% silica foam compared to concrete, it has shown a 15.49% decrease in modulus of elasticity. In designs containing 7% and 10% silica foam,

Table 9
Tensile strength results (MPa)

The name of the mix	Witness sample	A sample of 5% silica foam	A sample of 7% silica foam	A sample of 10% silica foam	A sample of 12% silica foam
Tensile strength 28days	3.9	2.65	2.25	1.4	1.1

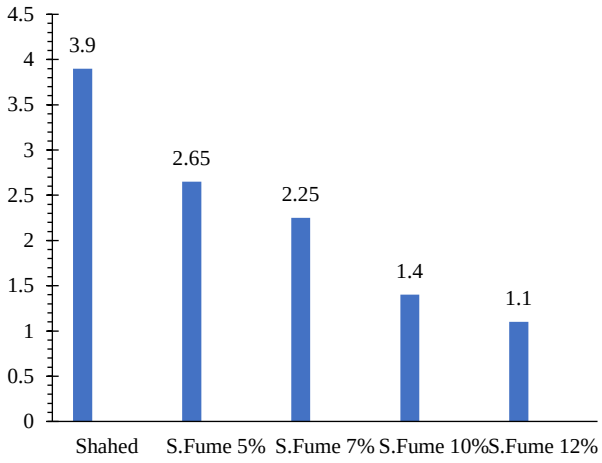

Figure 13: The graph of tensile strength test results at the age of 28 days (MPa)

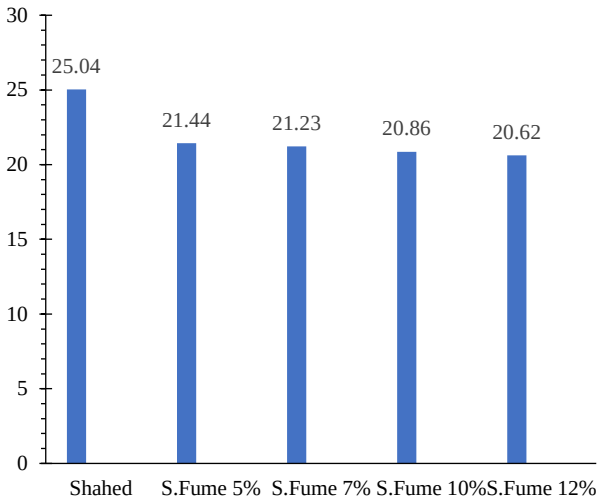

Figure 14: Diagram of modulus of elasticity of concrete at the age of 28 days (MPa)

Table 10: Modulus of elasticity of 28-day concrete (MPa)

The name of the mix	Witness sample	A sample of 5% silica foam	A sample of 7% silica foam	A sample of 10% silica foam	A sample of 12% silica foam
Modulus of elasticity	25.04	21.44	21.23	20.86	20.62

compared to the control concrete, there was a decrease of 16.47 and 18.21%, respectively, and compared to the sample containing 5% silica foam, it showed a decrease of 0.98 and 2.74%, respectively. In the design containing 12% silica foam, compared to the control sample, it has decreased by 19.36% and compared to the sample containing 5%, it has shown a decrease of 3.9%. The sample containing 12% silica foam has the lowest modulus of elasticity of concrete among the samples and the sample containing 5% silica foam has the highest modulus of elasticity of concrete.

5. Conclusions

As a result, the following conclusions were obtained:

1. The presence of silica foam in concrete due to its high adhesion has a negative effect on the mental properties of concrete and reduces the efficiency of concrete, which in concrete samples containing 5% silica foam is 7.5%, 7% silica foam is 16.25, 10% silica foam is 27.5 and the sample of 12% silica foam has decreased by 33.75% compared to the control sample.
2. The best result of compressive strength in concrete samples is related to the strength of the sample containing 5% silica foam with a resistance of 21.6 MPa and the lowest compressive strength obtained among the samples is related to the sample containing 12% silica foam with a resistance It was 19.2 MPa.
3. The highest tensile strength obtained among the samples was related to the sample containing 5% silica foam with a resistance of 2.65 MPa, and the lowest tensile strength was related to the sample containing 12% silica foam with a resistance of 1.1 MPa.
4. The highest modulus of elasticity obtained among the samples was related to the sample containing 5% silica foam with a resistance of

21.44 GPa, and the lowest amount of resistance among the samples was the sample containing 12% silica foam with a resistance of 20.66 GPa.

5. Adding shards of glass to concrete has caused the concrete to break apart and crack, and as a result, it has caused a drop in concrete strength.

References

[1] S., R.D., Investigation of the mechanical properties of self-compacting concrete, containing glass jar under aggressive of sulfuric acid. Sistan and Baluchestan.University, (2015).

[2] Ali, Esraa Emam, and Sherif H. Al-Tersawy. "Recycled glass as a partial replacement for fine aggregate in self compacting concrete." Construction and Building Materials 35 (2012): 785-791. https://doi.org/10.1016/j.conbuildmat.2012.04.117

[3] Borna .,M ,Olapur .,M ,Daszfoli-Abbasi .,K.A. " Managing the construction and development of the use of scrap glass in concrete by determining its physical and mechanical properties." First International Conference on Iran's Environmental Crisis and its Improvement, (2020)

[4] Kavosi, Ali, and S. Yasin Mousavi. "Performance of concrete containing waste glass at a low water/binder ratio." Concrete Research 10.1 (2017): 125-134. https://doi.org/10.22124/jcr.2017.2364

[5] Cartuxo, Francisco, et al. "Increased durability of concrete made with fine recycled concrete aggregates using superplasticizers." Materials 9.2 (2016): 98. https://doi.org/10.3390/ma9020098

[6] de Castro, Sara, and Jorge de Brito. "Evaluation of the durability of concrete made with crushed glass aggregates." Journal of Cleaner Production 41 (2013): 7-14. https://doi.org/10.1016/j.jclepro.2012.09.021

[7] Topcu, Ilker Bekir, and Mehmet Canbaz. "Properties of concrete containing waste glass." Cement and concrete research 34.2 (2004): 267-274. https://doi.org/10.1016/j.cemconres.2003.07.003

[8] Bhanja, S., and B. Sengupta. "Influence of silica fume on the tensile strength of concrete." Cement and concrete research 35.4 (2005): 743-747. https://doi.org/10.1016/j.cemconres.2004.05.024

[9] Serelis, Evaldas, and Vitoldas Vaitkevicius. "Analysis of cleaned waste glass and utilisation in the normal strength concrete." Journal of international scientific publications: materials, methods & technologies 15 (2021): 8-20. https://epubl.ktu.edu/object/elaba:110396111/

[10] Gražulytė, Judita, et al. "Effect of silica fume on high-strength concrete performance." World Congress on Civil, Structural, and Environmental Engineering. 2020.

J-Researchers

Journal of Civil Engineering Researchers

Journal homepage: www.journals-researchers.com

Investigating the Mechanical Properties of Natural Fiber-Reinforced Concrete with Kenaf, Jute, and Coconut Fibers

Sanaz Kameli,[a] Amin H Shahi,[b] Amir Mahboob[c,*]

[a] *School of Civil Engineering, Engineering Campus, University Sains Malaysia, 14300, Nibong Tebal, Penang, Malaysia*

[b] *Municipality of District 8, Shiraz Municipality, Iran*

[c] *Strength of Materials and Structural Engineering Department, Polytechnic University of Catalonia, C/Colom 11, TR45, 08222 Terrassa, Spain*

ABSTRACT

This study investigates the mechanical properties of natural fiber-reinforced concrete (FRC) through the addition of natural fibers such as kenaf (KFRC), jute (JFRC), and coconut (CFRC). The evaluation focused on key properties including compressive strength, split tensile strength, and flexural strength. Fiber combinations were introduced in a fiber volume fraction of 0.5%, with fiber lengths standardized at 20 mm. A water-to-binder ratio of 0.44 was maintained for all mixes. Six specimens were tested for each parameter after a curing period of 28 days. The objective of this research was to assess the potential of natural fibers like kenaf, jute, and coconut for developing sustainable FRC while maintaining or improving its mechanical properties. Results demonstrated that the inclusion of natural fibers at the specified length and concentration positively influenced post-cracking flexural performance and splitting tensile strength. Among the tested combinations, FRC reinforced with jute fibers (JFRC) exhibited superior performance compared to other fiber combinations.

ARTICLE INFO

Received: October 17, 2024
Accepted: November 12, 2024

Keywords:
Natural fiber-reinforced concrete
Kenaf fibers
Jute fibers
Coconut fibers
Sustainable concrete

DOI: 10.61186/JCER.6.4.32
DOR: 20.1001.1.2538516.2024.6.4.4.9

1. Introduction

Natural fibers have been integral to construction materials for centuries, dating back to ancient civilizations where fibers like straw and horsehair were mixed with mud to reinforce walls and roofs [1, 2]. Today, with growing environmental concerns and the need for sustainable building practices, fiber-reinforced concrete (FRC) has gained renewed attention [3, 4]. The construction industry is a major contributor to global carbon dioxide emissions, and traditional FRC like steel FRC not only consume vast amounts of energy but also release significant greenhouse gases during production [5]. In response to these issues, researchers are increasingly focused on developing eco-friendly FRCs that reduce environmental impact while maintaining or even improving the mechanical properties of conventional construction materials [6, 7].

Natural fiber-reinforced concrete (NFRC) has been increasingly explored as a sustainable alternative to traditional synthetic fibers [8-10]. These fibers are not only renewable and biodegradable, but also exhibit several other advantages, including high tensile strength, lower

* Corresponding author. Tel.: +989122444472; e-mail: amir.mahboob@upc.edu.

processing costs and densities compared to synthetic fibers, making them ideal for environmentally friendly building materials [11–13]. The incorporation of natural fibers such as kenaf, jute, coconut, and sisal has been shown to enhance the tensile strength, flexural strength, and overall durability of concrete by preventing the propagation of microcracks [14-16]. Natural fibers help reduce the shrinkage-related cracks that typically occur in concrete during the drying process, providing enhanced resistance to mechanical stresses and improving the post-cracking behavior of concrete [1,12,17].

Advanced materials are essential in seismic regions where reinforced concrete (RC) structures endure repeated loads. Hassanshahi et al. [18] demonstrated that repeated earthquakes significantly damage RC joints by increasing inelastic displacements. This highlights the importance of materials like NFRC, which enhance toughness, ductility, and post-cracking strength, key properties for improving the performance of earthquake-resistant structures.

Despite their potential benefits, the optimization of NFRC remains a challenge. Factors such as fiber volume fraction, fiber length, and distribution within the concrete matrix significantly impact the mechanical properties of NFRC [19]. Excessive fiber content, for example, can result in clumping and reduced workability of the concrete mix, undermining its effectiveness [20, 21]. Moreover, each natural fiber type possesses unique characteristics, necessitating tailored approaches to maximize their reinforcement potential in concrete [16, 22].

This study provides insights into the individual contributions of each natural fiber type such as kenaf, jute, and coconut and their effects on mechanical properties of FRC performance. The research evaluates compressive strength, split tensile strength, and flexural strength, focusing on the feasibility of using natural fibers as a sustainable alternative to synthetic reinforcement in FRC, potentially reducing the carbon footprint of construction projects and enhancing FRC performance. The outcomes will not only advance the understanding of natural fiber applications in concrete but will also serve as a valuable reference for engineers and practitioners seeking to incorporate innovative materials into sustainable construction practices.

2. Materials and Mixture Proportions

The cement used in this study was CEM II/A-L 42.5 R, with a specific gravity of 2.95 g/cm³. Fine aggregates with a specific gravity of 2.63 and a fineness modulus of 2.77 were utilized, while coarse aggregates had a specific gravity of 2.68 and a fineness modulus of 2.62. The grading curves for both fine and coarse aggregates were determined using sieve analysis, as per ASTM C136 standards [23, 24], and complied with the relevant ASTM specifications. Figure 1 illustrates the aggregate combination used.

Natural fibers, including kenaf, jute, and coconut, as illustrated in Figure 2, were incorporated into the concrete mix. Kenaf fibers had an average diameter of 0.2 mm, tensile strength of 500 MPa, and a density of 1.4 g/cm³. Jute fibers had a smaller average diameter of 0.008 mm, with a tensile strength of 700 MPa and a density of 1.5 g/cm³. Coconut fibers were larger, with an average diameter of 0.25 mm, a tensile strength of 220 MPa, and a density of 1.25 g/cm³. All fibers were cut to a length of 20 mm to ensure consistency. However, natural fibers often contain compounds like lignin and hemicellulose, which hinder the cement hydration process, making pre-treatment necessary.

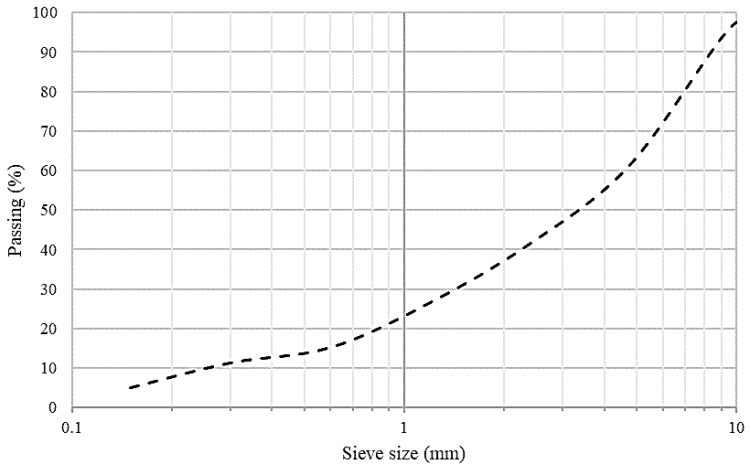

Figure 1. Distribution curve illustrating the particle sizes of the combined aggregates.

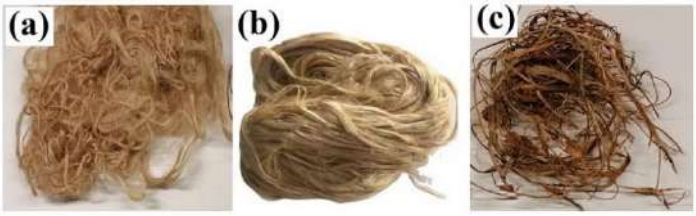

Figure 2. Natural fibers used in the study: a) Kenaf, b) Jute, and c) Coconut.

Table 1.
Proportions of the composite mixtures.

Components	Quantity (kg/m3)			
	PC	KFRC	JFRC	CFRC
Cement	420	420	420	420
Water	185	185	185	185
Superplasticizer	5.0	5.0	5.0	5.0
Crushed granite	700	700	700	700
Coarse river sand	900	900	900	900
Fiber content	0.0	7.0	7.5	6.25
Water / cement	0.44	0.44	0.44	0.44
Dry density	2296	1985	1910	2103

The fibers were subjected to an alkaline treatment by soaking them in a 5% sodium hydroxide (NaOH) solution for one hour. After the treatment, the fibers were air-dried for 24 hours, followed by oven-drying at 85°C for four hours to improve their mechanical properties. Each gram of dry fiber was then processed using a 200 W electric grinder for five seconds to ensure uniform dispersion within the concrete matrix. This process effectively broke down any fiber agglomerates, optimizing their integration into the concrete mix [25- 27].

The concrete mix was prepared using fresh, potable water that was free from organic and acidic contaminants. A superplasticizer (BASF Glenium 313C), with a specific gravity of 1.22 at 25°C, was uniformly added at 8 kg/m³ to all mixtures to enhance the workability of the concrete mix.

To investigate the behavior of NFRC, three distinct mixes were prepared in the laboratory: kenaf fiber-reinforced concrete (KFRC), jute fiber-reinforced concrete (JFRC), and coconut fiber-reinforced concrete (CFRC). Each mix maintained a consistent water-to-binder ratio of 0.44. These fiber-reinforced mixes were compared to a control mix of plain concrete (PC), following the ACI 211.1–91 standard [28] with the goal of achieving a target 28-day compressive strength. The fiber volume fractions for the NFRC mixes were set at 0.5% by volume of concrete. Specimens were labeled based on the type of fiber used in each mix. Cement was used consistently across all four mixtures at a dosage of 420 kg/m³. The quantities of crushed granite and coarse river sand aggregates remained constant in all mixes, at 700 kg/m³ and 900 kg/m³, respectively. The detailed proportions of these composite mixes are detailed in Table 1.

3. Methodology

The specimen preparation began with manually blending cement and fine aggregates (coarse river sand) to create a homogeneous mix. Natural fibers were then added to this blend. At the final stage, coarse aggregates (crushed granite), water, and superplasticizer were introduced. Cylindrical specimens with a diameter of 150 mm and a height of 300 mm were cast for compressive and split tensile strength tests, while prismatic RILEM beam specimens (150 mm width, 150 mm depth, and 600 mm length) were cast for flexural strength testing. These specimens were prepared for all mixes, including PC, KFRP, JFRP, and CFRC. All specimens were stored in an environment with a minimum of 80% relative humidity and a temperature of 27 ± 2°C for 24 hours. They were then moved to a steam-curing room with automatic temperature control, set at 20 ± 2°C and 95% relative humidity. After 28 days of curing, a total of 72 specimens (six for each test type and mix) were tested, and the average results were recorded for evaluation.

3.1. Compressive Strength Tests

The uniaxial compressive strength tests were conducted using a 2000 kN Electro-Hydraulic Pressure testing machine controlled by a computer, applying a steady load until failure. Before testing, all compressive specimens were capped with sulfur for uniform load distribution. The compressive tests followed NP EN 12,390–3:2011 [29] and NP EN 12,390–13:2014 [30] standards. The test control used axial displacement as the control variable, measured by an internal displacement transducer within the loading equipment. The experimental setup for the compressive tests is shown in Figure 3-a.

3.2. Splitting Tensile Strength Tests

Cylindrical specimens were horizontally placed between two hard metal strips, following ASTM C496/C496M [31] guidelines (Figure 3-b). The same

testing machine used for the compressive tests performed the splitting tests, with a jig ensuring specimen alignment. During testing, transversal deformation perpendicular to the load direction was recorded, providing detailed insights into the concrete's tensile response. The tensile strength was calculated from the first peak of the load-deformation curve, representing the material's elastic limit [32-34].

3.3. Flexural Strength Tests

Prismatic beam specimens were prepared with precise dimensions and a standardized notch to ensure controlled crack propagation. The beams were placed in a three-point bending configuration with the notch aligned under the load application point. The load was applied centrally over a 500 mm span at a controlled rate to ensure consistent data collection. The three-point notched beam bending tests (3PNBBT) followed the fib Model Code 2010 [35] recommendations and were conducted using a 300 kN hydraulic jack under monotonic loading.

The tests aimed to assess residual flexural tensile strength parameters (fR,1, fR,2, fR,3, fR,4) at crack mouth opening displacements (CMOD) of 0.5, 1.5, 2.5, and 3.5 mm. The flexural tensile strength (fct,L) was measured at a CMOD of 0.05 mm, which is crucial for understanding post-cracking behavior. Figure 3-c shows the testing setup for the notched beams.

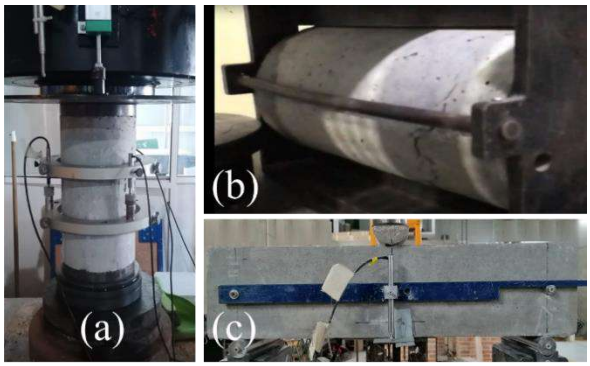

Figure 3. Experimental test setup employed in the study: a) Compressive strength tests, b) Splitting tensile strength tests, c) Flexural strength tests

4. Results and Discussion

4.1. Compressive Strength

The compressive strength results at 28 days (Table 2) demonstrate a noticeable reduction in strength with the incorporation of natural fibers. Plain concrete (PC) exhibited the highest compressive strength of 41.21 MPa, serving as the baseline for comparison. Among the fiber-reinforced concrete mixes, CFRC demonstrated the best performance with a compressive strength of 37.42 MPa, followed by KFRC at 33.1 MPa, and JFRC at 30.53 MPa. The reductions in strength compared to PC were 9.17%, 19.67%, and 25.91% for CFRC, KFRC, and JFRC, respectively. These results highlight the fact that the inclusion of natural fibers reduces the compressive strength, likely due to the increased porosity and fiber-matrix interface discontinuities introduced during mixing.

Table 2.
Compressive strength of all mixes at 28 days: PC, KFRC, JFRC, and CFRC.

Cylinder specimens	Compressive strength	
	$f'c$ (MPa)	CoV (%)
PC	41.21	2.2
KFRC	33.1	7.2
JFRC	30.53	6.9
CFRC	37.42	4.18

Figure 4 further illustrates the stress-strain behavior of all mixes, where it is evident that PC maintained the highest peak compressive stress, while the fiber-reinforced concrete mixes displayed enhanced ductility and post-peak behavior. Coconut fibers, in particular, contributed to CFRC retaining more of its compressive strength due to better bonding with the cement matrix. The lower compressive strengths of KFRC and JFRC can be attributed to the higher water absorption of kenaf and jute fibers, which likely led to the introduction of additional voids within the matrix. These voids act as stress concentrators, contributing to early failure under compressive loads. Overall, while natural fibers reduce compressive strength, they also improve ductility and toughness, which are crucial for applications requiring enhanced crack control and energy absorption.

4.2. Splitting Tensile Strength

The splitting tensile strength results at 28 days (Figure 5) demonstrate that the addition of natural fibers significantly enhanced the tensile capacity of the concrete mixes compared to the PC. Among the mixes, JFRC achieved the highest splitting tensile strength of 4.1 MPa, followed closely by KFRC at 3.9 MPa, and CFRC at 3.7 MPa. PC exhibited the lowest splitting tensile strength of 2.8 MPa, which is consistent with the expectation that natural fibers improve the tensile capacity of concrete due to their ability to bridge cracks and delay crack propagation. However, it is important to note the relatively high coefficient of variation (CoV) observed for the fiber-reinforced mixes, particularly for JFRC and KFRC, which indicates variability in the test results. The CoV reflects the natural variability in fiber properties, such as fiber length, aspect ratio, and dispersion within the matrix, which can

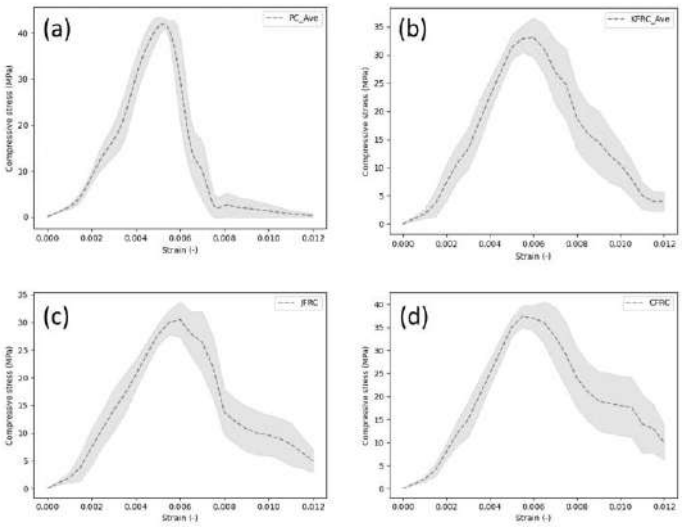

Figure 4. Stress-strain curves for all mixes at 28 days: a) PC, b) KFRC, c) JFRC, d) CFRC.

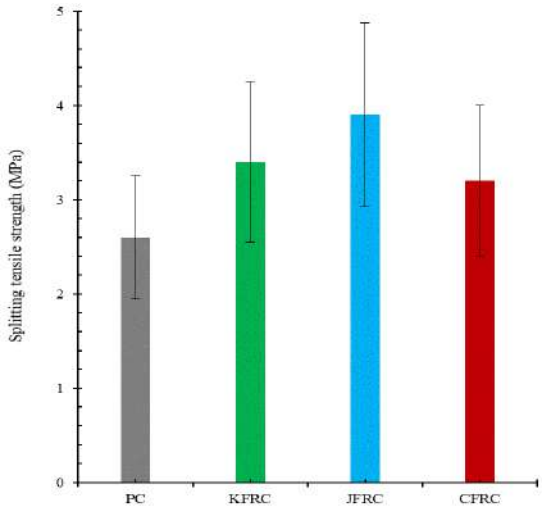

Figure 5. Split tensile strength of all mixes at 28 days: PC, KFRC, JFRC, and CFRC

affect the fiber-matrix bond and ultimately the tensile strength.

The superior performance of JFRC and KFRC can be attributed to the stronger bond between the jute and kenaf fibers and the cement matrix. Jute and kenaf fibers have a high tensile strength and good interaction with the cement matrix, which allows them to absorb and distribute tensile stresses effectively, delaying crack formation. The relatively lower splitting tensile strength of CFRC, although still higher than PC, may be related to the lower aspect ratio and strength of coconut fibers compared to jute and kenaf, leading to less effective crack bridging. Additionally, the variability in tensile strength among the mixes, as indicated by the error bars, suggests that fiber dispersion and the natural variability in fiber properties play a role in the results. Overall, the inclusion of natural fibers significantly enhances the tensile strength of concrete, with jute and kenaf fibers being the most effective.

4.3. Flexural Strength

Figure 6 illustrates the load-CMOD and flexural tensile stress curves for all mixes in the three-point notched RILEM beams at 28 days, while Table 3 provides a detailed comparison of the residual flexural tensile strength parameters for each mix. The results demonstrate that the NFRC mixes exhibited significantly higher residual flexural tensile strengths at various crack mouth opening displacements (CMOD) compared to the PC. Specifically, at CMOD = 0.05 mm, JFRC achieved the highest flexural tensile strength (fct,L = 5.17 MPa), followed by KFRC (4.57 MPa), and CFRC (4.41 MPa), while PC had the lowest value (4.33 MPa). This trend reflects the enhanced ability of the natural fibers to bridge cracks and distribute stresses, particularly at early stages of crack formation, which is reflected in the higher peak load (FL) for the fiber-reinforced mixes.

As the CMOD increases, the residual tensile strengths (fR,1 to fR,4) for the NFRC mixes decline, with JFRC consistently maintaining superior performance. At CMOD1 = 0.5 mm, JFRC shows a residual flexural tensile strength of 3.19 MPa, while KFRC and CFRC also exhibit considerable strength, at 2.16 MPa and 2.02 MPa, respectively, compared to PC's negligible value (0.21 MPa). This significant difference indicates the ability of the natural fibers, particularly jute and kenaf, to provide substantial post-cracking load-bearing capacity, mitigating the rapid degradation of structural integrity seen in PC. However, as crack widths increase, the contribution of

fibers becomes less pronounced, which is evident in the declining residual strengths across all mixes at CMOD3 = 2.5 mm and CMOD4 = 3.5 mm.

Notably, the CoV values for residual flexural tensile strengths are higher at larger CMOD levels, particularly for KFRC and CFRC. This suggests that these natural fibers may exhibit inconsistent behavior during larger deformations, possibly due to variations in fiber orientation, and dispersion, leading to fluctuating crack-bridging efficacy. JFRC, with consistently lower CoV values, shows more stable performance across all CMOD levels, indicating better fiber-matrix interaction and more uniform fiber dispersion. This consistent performance explains JFRC's superior flexural strength and post-cracking load capacity throughout the entire range of crack development.

5. Conclusion

This study successfully evaluated the mechanical properties of natural fiber-reinforced concrete (FRC) incorporating kenaf (KFRC), jute (JFRC), and coconut (CFRC) fibers, highlighting their potential to enhance the sustainability and performance of plain concrete (PC). The research demonstrated that the addition of natural fibers at a volume fraction of 0.5% and a standardized length of 20 mm significantly improved key mechanical properties, including compressive strength, splitting tensile strength, and flexural strength, compared to PC. The results indicated that while the addition of natural fibers reduced compressive strength compared to PC-with compressive strengths of 41.21 MPa for PC, 37.42 MPa for CFRC, 33.1 MPa for KFRC, and 30.53 MPa for JFRC-this reduction was offset by improved ductility and toughness.

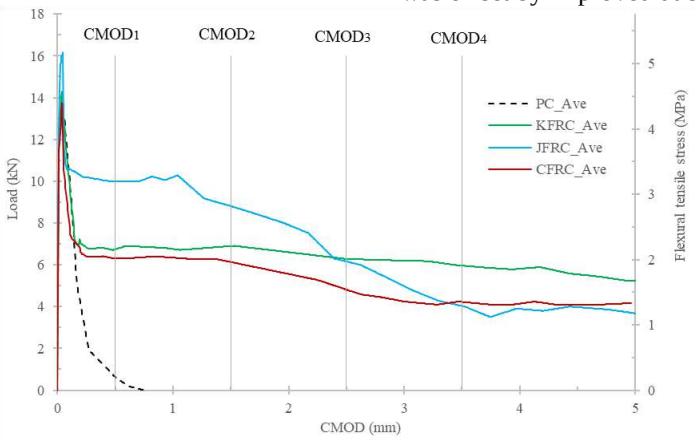

Figure 6. CMOD versus load and flexural stress curves for all mixes in three-point notched RILEM beams at 28 days.

Table 3.
Residual flexural tensile strength parameters for all mixes in three-point notched RILEM beams at 28 days

Flexural tensile strength parameters		RILEM Beams			
		PC	KFRC	JFRC	CFRC
	fct,L (Mpa)	4.33	4.57	5.17	4.41
CMOD = 0.05 mm	FL (kN)	13.52	14.29	16.16	13.77
	CoV (%)	6.38	5.21	3.09	7.4
	fR,1 (Mpa)	0.21	2.16	3.19	2.02
CMOD1 = 0.5 mm	F1 (kN)	0.65	6.74	9.98	6.31
	CoV (%)	7.67	7.52	5.81	8.13
	fR,2 (Mpa)	-	2.21	2.82	1.96
CMOD2 = 1.5 mm	F2 (kN)	-	6.89	8.81	6.13
	CoV (%)	-	12.62	8.79	11.99
	fR,3 (Mpa)	-	2.01	1.97	1.54
CMOD3 = 2.5 mm	F3 (kN)	-	6.28	6.16	4.81
	CoV (%)	-	27.62	20.75	30.19
	fR,4 (Mpa)	-	1.91	1.29	1.35
CMOD4 = 3.5 mm	F4 (kN)	-	5.96	4.03	4.22
	CoV (%)	-	32.71	29.25	32.83

The inclusion of natural fibers significantly enhanced splitting tensile strength, with JFRC achieving the highest value of 4.1 MPa, followed by KFRC at 3.9 MPa and CFRC at 3.7 MPa, compared to PC's 2.8 MPa. This improvement is attributed to the fibers' ability to bridge cracks and delay propagation. In terms of flexural strength,

JFRC consistently outperformed PC, particularly at low crack mouth opening displacements (CMOD), achieving a flexural tensile strength of 5.17 MPa at CMOD = 0.05 mm. The ability of natural fibers to provide significant post-cracking load-bearing capacity demonstrates their effectiveness in enhancing concrete performance. Overall, this research underscores the potential of natural fibers to improve the mechanical properties of concrete while promoting sustainability. Future studies should focus on optimizing fiber combinations and examining long-term durability to validate these findings further.

References

[1] da Fonseca, Régis Pamponet, Janaíde Cavalcante Rocha, and Malik Cheriaf. "Mechanical properties of mortars reinforced with amazon rainforest natural fibers." Materials 14.1 (2020): 155. https://doi.org/10.3390/ma14010155

[2] Juarez, Cesar, et al. "Performance of "Agave lecheguilla" natural fiber in portland cement composites exposed to severe environment conditions." Building and environment 42.3 (2007): 1151-1157. https://doi.org/10.1016/j.buildenv.2005.12.005

[3] Salati, Maryam, Luis Bragança, and Ricardo Mateus. "Sustainability assessment on an urban scale: context, challenges, and most relevant indicators." Applied System Innovation 5.2 (2022): 41. https://doi.org/10.3390/asi5020041

[4] Salles, Adriana, Maryam Salati, and Luís Bragança. "Analyzing the feasibility of integrating urban sustainability assessment indicators with city information modelling (CIM)." Applied System Innovation 6.2 (2023): 45. https://doi.org/10.3390/asi6020045

[5] Pacheco-Torgal, F., and Said Jalali. "Earth construction: Lessons from the past for future eco-efficient construction." Construction and building materials 29 (2012): 512-519. https://doi.org/10.1016/j.conbuildmat.2011.10.054

[6] Mahboob, Amir, et al. "Experimental investigation of eco-friendly fiber-reinforced concrete using recycled and natural fibers, integrated with recycled aggregates." Advanced Composite Materials (2024): 1-30. https://doi.org/10.1080/09243046.2024.2322799

[7] Abedi, Mohammadmahdi, et al. "Three-dimensional braided composites as innovative smart structural reinforcements." Composite Structures 297 (2022): 115912. https://doi.org/10.1016/j.compstruct.2022.115912

[8] Yousefi, Ali, et al. "Experimental investigation on effect of multi-walled carbon nanotubes concentration on flexural properties and microstructure of cement mortar composite." AIP Conference Proceedings. Vol. 1892. No. 1. AIP Publishing, 2017. https://doi.org/10.1063/1.5005663

[9] Abedi, Mohammadmahdi, et al. "Investigation of Mechanical Behavior of a Sustainable Cementitious Composite Reinforced with Natural Fibre: An Experimental and Numerical Study." Available at SSRN 4247583. https://doi.org/10.1016/j.compstruct.2022.115912

[10] Mahboob, Amir, Omid Hassanshahi, and Ashkan Sarabi Tabrizi. "Three-dimensional simulation of granular materials by discrete element method (DEM) by considering the fracture effect of particles." Journal of Civil Engineering Researchers 5.2 (2023): 14-28. https://doi.org/10.61186/JCER.5.2.14

[11] Mahmud, Sakil, et al. "Comprehensive review on plant fiber-reinforced polymeric biocomposites." Journal of Materials Science 56 (2021): 7231-7264. https://doi.org/10.1007/s10853-021-05774-9

[12] Memon, Muhammad Jaffar, et al. "Production of eco-friendly concrete incorporating rice husk ash and polypropylene fibres." Environmental Science and Pollution Research 28 (2021): 39168-39184. https://doi.org/10.1007/s11356-021-13418-3

[13] Olivito, Renato Sante, O. A. Cevallos, and A. Carrozzini. "Development of durable cementitious composites using sisal and flax fabrics for reinforcement of masonry structures." Materials & Design 57 (2014): 258-268. https://doi.org/10.1016/j.matdes.2013.11.023

[14] Poorsaheli, Hadi Bolooki, Amir Behravan, and Seyed Taha Tabatabaei Aghda. "Durability performance of hybrid reinforced concretes (steel fiber+ polyolefin fiber) in a harsh marine tidal zone of Persian Gulf." Construction and Building Materials 266 (2021): 121176. https://doi.org/10.1016/j.conbuildmat.2020.121176

[15] Kumar, K. Senthil, et al. "Layering pattern effects on vibrational behavior of coconut sheath/banana fiber hybrid composites." Materials & Design 90 (2016): 795-803. https://doi.org/10.1016/j.matdes.2015.11.051

[16] Ahamed, M. Shadheer, P. Ravichandran, and A. R. Krishnaraja. "Natural fibers in concrete–A review." IOP Conference Series: Materials Science and Engineering. Vol. 1055. No. 1. IOP Publishing, 2021.

[17] Sathishkumar, T. P., et al. "Mechanical properties of randomly oriented snake grass fiber with banana and coir fiber-reinforced hybrid composites." Journal of composite materials 47.18 (2013): 2181-2191. https://doi.org/10.1177/0021998312454903

[18] Hassanshahi, Omid, et al. "Seismic performance of the typical RC beam–column joint subjected to repeated earthquakes." AIP Conference Proceedings. Vol. 1892. No. 1. AIP Publishing, 2017. https://doi.org/10.1063/1.5005755

[19] Callister Jr, William D., and David G. Rethwisch. Materials science and engineering: an introduction. John wiley & sons, 2007.

[20] Cevallos, O. A., and Renato Sante Olivito. "Effects of fabric parameters on the tensile behaviour of sustainable cementitious composites." Composites Part B: Engineering 69 (2015): 256-266. https://doi.org/10.1016/j.compositesb.2014.10.004

[21] Haseena, A. P., et al. "Mechanical properties of sisal/coir hybrid fibre reinforced natural rubber." Progress in Rubber Plastics and Recycling Technology 21.3 (2005): 155-181. https://doi.org/10.1177/147776060502100301

[22] Izquierdo, Indara Soto, et al. "Sisal fiber reinforced hollow concrete blocks for structural applications: Testing and modeling." Construction and Building Materials 151 (2017): 98-112. https://doi.org/10.1016/j.conbuildmat.2017.06.072

[23] C. Astm, 'Standard test method for sieve analysis of fine and coarse aggregates', ASTM C136-06, (2006).

[24] Oh, Chai Lian, et al. "Shape change analysis of tensegrity models." Latin American Journal of Solids and Structures 16 (2019): e221. https://doi.org/10.1016/j.compstruct.2022.115912

[25] Abedi, Mohammadmahdi, et al. "A sustainable cementitious composite reinforced with natural fibers: An experimental and numerical study." Construction and Building Materials 378 (2023): 131093. https://doi.org/10.1016/j.conbuildmat.2023.131093

[26] Abedi, Mohammadmahdi, et al. "A self-sensing and self-heating planar braided composite for smart civil infrastructures reinforcement." Construction and Building Materials 387 (2023): 131617. https://doi.org/10.1016/j.conbuildmat.2023.131617

[27] Mahboob, Amir, et al. "Evaluating the performance of hollow core slabs (HCS)-concrete and simplifying their implementation." Recent Progress in Materials 5.2 (2023): 1-15. http://dx.doi.org/10.21926/rpm.2302016

[28] D. E. Dixon et al., 'Standard practice for selecting proportions for normal, heavyweight, and mass concrete (ACI 211.1-91)', Farmington Hills: ACI, 1991

[29] Standard B. Testing hardened concrete. Compressive Strength Of Test Specimens, BS EN.2009;12390–12393.
[30] CEN (European Committee for Standardization). "Testing hardened concrete—Part 13: Determination of secant modulus of elasticity in compression." (2013).
[31] ASTM International Committee C09 on Concrete and Concrete Aggregates. Standard test method for splitting tensile strength of cylindrical concrete specimens1. ASTM international, 2017.
[32] Denneman, Erik, Elsabe P. Kearsley, and Alex T. Visser. "Splitting tensile test for fibre reinforced concrete." Materials and structures 44 (2011): 1441-1449. https://doi.org/10.1617/s11527-011-9709-x
[33] Standard A. Standard test method for slump of hydraulic-cement concrete. ASTM Annual Book of ASTM Standards; 2015.
[34] Peen, Woo Yian, Choong Kok Keong, and Omid Hassanshahi. "Behaviour of hollow circular section with multiple perforations under compression, flexure and torsion." Latin American Journal of Solids and Structures 16.02 (2019): e169. https://doi.org/10.1016/j.compstruct.2022.115912
[35] Taerwe L, Matthys S. Fib model code for concrete structures 2010. Berlin, Germany: Ernst & Sohn, Wiley; (2013).

J-Researchers

Journal of Civil Engineering Researchers

Journal homepage: www.journals-researchers.com

Investigating the Effect of Uncertainty in the Optimal Design of a Trapezoidal Channel

S. Pourbakhshian,[a*] F. Abdolrasuli,[a]

[a] *Department of Civil Engineering, Ramsar Branch, Islamic Azad University, Ramsar, Iran*

ABSTRACT

In this article, the optimal shape of the compound trapezoidal cross-section is presented by considering the deterministic constraints and the probabilistic constraint of channel flooding as uncertainty with the SPSA algorithm and with three flow discharge of 10, 50, and 120 m3/s. The objective function is to minimize the cost of excavation and lining, the design variables of depth and bed width of the canal, side slopes and constraints include uniform flow, maximum and minimum velocity, water surface width and the overtopping probability. The values of the freeboard and the slope of the channel bed are fixed and equal to 0.5 meters and 0.0028, respectively. The results show that with the increase in overtopping probability, the flow depth increases, but the side slopes, velocity and Froud number decrease. The cost of construction and the bed width, initially decreases with the increase of the overtopping probability, and at a certain value, the probability reaches its minimum value, and then with the increase of the overtopping probability, the cost of construction and bed width increases.

ARTICLE INFO

Received: October 17, 2024
Accepted: November 26, 2024

Keywords:
Open channels
Optimal design
SPSA algorithm
Overtopping probability
Uncertainty

DOI: 10.61186/JCER.6.4. 40
DOR: 20.1001.1.2538516.2024.6.4.5.0

1. Introduction

The optimal design of the cross section of the channel is necessary for the design discharge to convey through it and the least cost for its construction [1]. The optimal design of the composite channel cross-section was first addressed by Trout (1982) with the aim of minimizing lining costs with composite roughness for trapezoidal, rectangular, and triangular channels [2] .Guo, and Hughes, (1984) for the first time considered the free board as a design variable for the optimal design of the trapezoidal channel using the first principles of calculus and derivation and with the objective function of frictional resistance or the construction cost [3]. In Monadjemi's 's research (1994), the triangular section is the best hydraulic section among different sections such as rectangular, triangular, trapezoidal and round bottom triangular [4]. Swamee (1995) and Swamee et al. (2001, 2002, 2002) Presented optimal channels with triangular, rectangular, trapezoidal, and circular sections, considering water lost as seepage and evaporation losses, and using presented a non-linear method. The results showed that the cross-sectional area of the channel and losses due to seepage and evaporation in a trapezoidal channel are less than triangular and rectangular channels. The results of Babaeyan-Koopaei et al.'s research (2000) showed that the cross-sectional the wetted flow area and wetted perimeter

* Corresponding author. Tel.: +98-9113967847; e-mail: Sommayyeh. pourbakhshian@gmail.com.

of a triangular channel with a parabolic bottom is less than a channel with a triangular and parabolic cross-section. Das (2000) presented the optimal shape of the cross-section with composite roughness trapezoidal channel with freeboard using the method of Lagrange coefficients, taking into account the constraints of Manning's equation and the objective function of the construction cost [12]. Jain et al. (2004) presented the optimal design of the trapezoidal channel section by considering the velocity and top width constraints of the water surface using genetic algorithm. The cost of construction a channel using genetics algorithms is lower compared to the method of Lagrange multiplier. Bhattacharjya (2005) considered problem for optimal design of composite channel cross section of trapezoidal shape by investigating the constraint of freeboard and changes in the specific energy of the channel. [14]. Bhattacharjya (2006) optimized the trapezoidal channel section with nonlinear optimization model incorporating the critical flow condition of the channel. The results show that this method has a better and more favorable performance compared to the Lagrange method in the research of Das. [15]. Also, Bhattacharjya used the optimal shape of the open channel cross-section with the combined method of geneti algorithm and second-order sequential programming algorithm. The results showed the high efficiency of the mentioned method in the optimal and stable design of open channels. [16]. Das (2007) presented the optimal cross-section model of a trapezoidal channel with two objective functions of minimizing the overall cost of channel construction and minimizing the probability of overtopping and limiting the establishment of uniform flow using the first-order analysis method. The results of this research showed that with the decrease of overtopping probability, the flow depth decreases and the bed width increases. [17]. Bhattacharjya and Satish (2008) developed the model of Das (2007) by considering the freeboard as a design variable and also using genetic algorithm. The results indicate a direct relationship between the width of the channel and the cost of its construction, as well as the better efficiency of the genetic algorithm compared to the classical optimization. [18]. Reddy and Adarsh (2010) presented the optimal shape of the cross-section of the composite trapezoidal channel using the elitist-mutated particle swarm optimization (EMPSO) method with overtopping constrained design. The results show that the cost of construction the channel is lower than the method of Lagrange coefficients. [19]. While in the research of Das (2010), the mentioned clause was obtained through risk analysis. [20]. In another study, Reddy and Adarsh (2010) used two meta-heuristic methods such as Genetic Algorithm (GA) and Particle Swarm Optimization (PSO) algorithm to obtain the optimal shape of the channel section [21]. In a comprehensive research, Adarsh (2012) designed the optimal shape of the trapezoidal channel by taking into account the water loss in the form of seepage and evaporation using the meta-heuristic optimization technique namely probabilistic global search Lausanne (PGSL) [23]. Adarsh and Reddy (2013) presents a probabilistic multi-objective model for optimal design of composite channels that have across-sectional shape of horizontal bottom and parabolic sides with three objective functions including minimizing the cost of channel construction, maximizing the probability of the expected the channel capacity being greater than the design discharge and minimizing the overtopping using the particle swarm optimization method and Pareto-optimal. The results showed that the presented approach has good potential for other sections designs of open channels under input parameter uncertainty. In recent years, Easa (2011), Easa and Vatankhah, (2014), Han (2015), Han and Easa (2017), very extensive researches regarding the design of new general open channel cross-sections were introduced. The results show that the optimal section that minimizes construction cost is substantially better than the most hydraulically efficient section. [24-27]. Orouji et al. (2016) optimized the trapezoidal compound channel section using the frog leaping algorithm. The results show that the use of this algorithm is more economical compared to genetic algorithms, ants, etc. [28]. Roushangar et al. (2018) in their studies to provide the optimal shape of the composed trapezoidal channel using genetic algorithm showed that the application of depth, speed and Froud number constraints increases the construction cost, while the water surface width constraint reduces the cost. . [29]. Gupta et al. (2018) used Fish Shoal Optimization (FSO) for the optimal design of the trapezoidal channel section. which reduced the cost of channel construction compared to particle swarm algorithm (PSO) [30]. Farzin and Anarki (2020) using meta-heuristic methods, to the optimal and probabilistic design of the composed trapezoidal channel cross-section in which models are based on constant or variable freeboard, uniform or composite roughness coefficient, fixed and variable freeboard, and also velocity, Froude number and overtopping constraints using bat hybrid algorithm. The results showed that using HBP, compared to BA, PSO, LINGO, Lagrange multiplier method and shuffled frog-leaping algorithm, led to a 32% reduction in the cost of channel construction. Therefore, HBP has high potential for the optimal design of open channels. [31]. Pourbakhshian and Pouraminian (2021) presented some analytical models for the optimal design of trapezoidal composite channel cross-section. The objective function is the cost function per unit length of the channel, which includes the excavation and lining costs. To define the system, design variables including channel depth, channel width, side slopes, freeboard, and roughness coefficients were used. The constraints include the mannin-

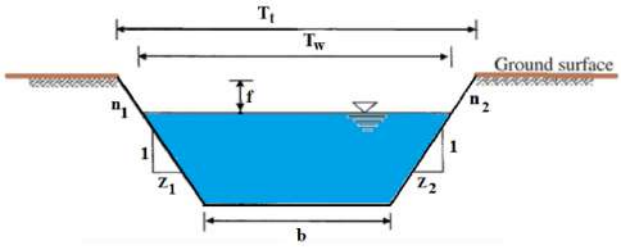

Figure 1. Representation of the cross-sectional geometry of the composite trapezoidal channel

Mg's equation, flow velocity, Froude number and water surface width, The Simultaneous Perturbation Stochastic Approximation (SPSA) algorithm was used to solve the optimization problem. The results are presented in three parts. In the first part, the optimal values of the design variables and the objective function are presented in different discharges. In the second part, the relationship between cost and design variables in different discharges is presented in the form of conceptual and analytical models and mathematical functions. Finally, in the third part, the changes in the design variables and cost function are presented as a graph based on the discharge variations. Result indicates that the cost increases with increasing water depth, left side slope, equivalent roughness coefficient, and freeboard. [32].

the optimal cross section of a composite parabolic channel by considering four models based on freeboard changes. The results show that increasing the discharge increases the flow depth, left and right-side slopes, total top width and water surface width, channel cross-sectional area and flow area, the total channel perimeter and wetted perimeters, flow velocity, Froud number and the cost increases. By examining the relationship between cost with design variables, constraints and geometric parameters of parabolic channel cross section in different iterations, the characteristic of the model that won the most number of iterations is based on the increase of left and right side slopes, total top width and water surface width, the cross-sectional area of the canal and the flow area, the total channel perimeter and the wetted perimeters, the Froud number, increase the cost, and in contrast, increasing the depth and flow velocity reduces the cost. Comparing the results of the four models with each other shows that the cost values in the first model are less than other models and in the third model are higher than all models. [33]. Since parameters such as discharge, longitudinal bed slope of the channel and roughness coefficients of the property have a stochastic nature, so that with the passage of time, the longitudinal bed slope of the channel and roughness coefficients will undergo changes due to the phenomenon of erosion and sedimentation compared to the initial values for the design and the amount Due to the occurrence of unauthorized rainfall, the discharge through the channel is higher than the design discharge of the channel, so there is uncertainty in determining the depth of the flow in the channel and the overtopping of the channel. As a result, considering the optimal design of irrigation channels limiting the possibility of overtopping reduces costs and damages. [34].

In this research, the optimal design of the cross-section of the composite trapezoidal channel by considering the deterministic constraints and the overtopping constraint and uncertainty by using the optimization algorithm of the Simultaneous Perturbation Stochastic Approximation (SPSA) in the flow discharge of 10, 50 and120 (m^3/s). Since it is necessary to design the optimal cross-section of open channels with the aim of passing the maximum flow and the minimum construction cost, in this regard, it is of great importance in terms of the possibility of overtopping due to the uncertainty of the design parameters including flow rate, longitudinal bed slope and flow roughness coefficients. In this research, for the first time, the SPSA algorithm has been used for the optimal design of composite trapezoidal channels by considering overtopping and uncertainty, and in this regard, the most important part of innovation is to include a complete set of definite constraints and the possibility of overtopping in the values of different flows.

2. Optimal design of open channels

2.1. Trapezoidal cross section

As shown in Fig. 1, $z_1: 1, z_2: 1$represent the side slopes of the channel corresponding to the left and right sides, n_1, n_2, n_3 are Manning's roughness coefficients on the left, right and bottom sides of the channel, b is bottom width, y is the flow depth, f is the freeboard, and s_0 is the longitudinal bed slope. where A_t and P_t are the is the total channel cross-sectional area and perimeter, respectively; $T_t$is the total top width of the channel cross-section; $A_w$and $P_w$are the channel wetted area and perimeter, respectively; $T_w$is the water surface width, P_{w1}, P_{w2}, and P_{w3} are wetted perimeters corresponding to the left, right and bottom sides of the channel respectively. P_{t1}, P_{t2}, and $P_{t3}$are perimeters corresponding to the left, right and bottom sides of the channel, respectively; R_w is the hydraulic radius; and $D$is

the hydraulic depth. Parameters *y*, *b*, z1, z2, and f are defined in Fig. 1 are related to the area (Eq 1), perimeter (Eq 2), and the overall width of the section (Eq 3):

$$A_t = b(y+f) + (z_1 + z_2)\,(y+f)^2/2 \quad (1)$$

$$P_{t1} = ({z_1}^2 + 1)^{(1/2)}.(y+f)$$

$$P_{t2} = ({z_2}^2 + 1)^{(1/2)}.(y+f)$$

$$P_{t3} = b$$

$$P_t = P_{t1} + P_{t2} + P_{t3} \quad (2)$$

$$P_t = \left\{\left[({z_1}^2 + 1)^{(1/2)} + ({z_2}^2 + 1)^{(1/2)}\right](y+f) + b\right\}$$

$$T_t = b + (z_1 + z_2)(y+f) \quad (3)$$

In the equations 1 to 3, by removing the freeboard in the equations, the corresponding water flow equations are obtained.

2.2. Design variable

According to the geometric model described in figure (1), design variables, description and their minimum and maximum values are given in Table 1.

Table 1.
Representation of design variables

X_i	unit	Design variables	X_L	X_R
$x_1 = y$	m	Depth of flow	0.5	15
$x_2 = b$	m	Channel bed width	1	20
$x_3 = z_1$	-	Channel right side slope	0.2	3
$x_4 = z_2$	-	Channel left side slope	0.2	3

2.3. Constraint

2.3.1. Deterministic constraint

According to Table 2, the constraint of uniform flow is considered to conduct the uniform flow in the channel [6]. Therefore, in this research, the Manning's equation constraint Horton's method was used to control uniform flow and to calculate the equivalent roughness coefficient [35]. Froud number constraint is included in order to avoid development of critical flow in the optimal design of the channel [14]. And the Channel top width is included to control the cost of land acquisition [12, 13, 21]. The minimum allowed velocity to prevent sedimentation is in the range of 0.6 to 0.9 m/s and the minimum velocity to prevent the growth of vegetation is 0.75 m/s [1]. The minimum velocity allowed in channel design is in the range of 0.75 to 0.9 [6]. In channels with a rigid boundary, the maximum allowable velocity (VL) is the velocity that does not cause erosion. Moreover, to ensure the conveyance of the discharge through the cross-section, the mean actual flow velocity in the channel should not exceed the maximum permissible velocity [8,13]. In this study, the minimum and maximum velocity values are 0.75 and 4 m/s, respectively.

Table 2
Representation of design variables

Equation	Describe	Constraint
$\Phi_1 = \left\lvert \frac{Q}{\sqrt{S_0}} - \frac{A_w^{5/3}}{\sum_{i=1}^{2} n_i P_{wi}^{1.5}} \right\rvert - \varepsilon \le 0$	Uniform flow	$\boldsymbol{\Phi_1}$
$\Phi_2 = \frac{F_r}{F_{r_{max}}}$	Sub Critical flow	$\boldsymbol{\Phi_2}$
$\Phi_3 = \frac{T_t}{T_{max}} - 1 \le 0$	Channel top width	$\boldsymbol{\Phi_3}$
$\Phi_4 = \frac{V_{min}}{V_{ave}} - 1 \le 0$	Minimum permissible velocity	$\boldsymbol{\Phi_4}$
$\Phi_5 = \frac{V_{ave}}{V_{max}} - 1 \le 0$	Maximum permissible velocity	$\boldsymbol{\Phi_5}$

2.3.2. Overtopping probability constrained

The overtopping probability constrained for the optimal design concept is used to design for safety against overtopping [20].

The phenomenon of erosion and sedimentation as well as runoff caused by unexpected rainfall can cause changes in the design values of longitudinal slope, channel roughness coefficients and flow discharge, which brings uncertainty in the depth of flow in the channel. Therefore, in this regard, from the first order analysis of uncertainty and assuming a normal distribution for the design parameters and the amount of flow passing through the channel due to the occurrence of precipitation, there may be changes compared to the initial design values that lead to uncertainty. The condition of the probability of overtopping is introduced as follows: The condition of the probability of overtopping is in the form of Eq. 4.

$$\Phi_6 = p(y > y + f) = P \quad (4)$$

$p(y > y + f)$, It is the probability of exceedance of flow depth over the freeboard which should be equal to the constant value of p.

The overtopping probability constraint is obtained in the order of the following steps:

1) Determination equation of Horton's equation in Manning's equation:

$$Q = \sqrt{S_0}\,\frac{A_w^{5/3}}{(\sum_{i=1}^{3} n_i P_{wi}^{1.5})^{\frac{2}{3}}} \quad (5)$$

2) Due to the probabilistic nature of flow discharge, bed slope and channel roughness coefficients, it is derived from the Eq. 6 to 8 with respect to parameters y, n_3, n_2, n_1, S_0:

$$\frac{dQ}{dy} = Q[\frac{5}{3}\frac{1}{A_w}\frac{dA_w}{dy} - \frac{2}{3}\frac{A_w^{5/3}}{(\sum_{i=1}^{3} {n_i}^{3/2}P_{wi})}\frac{d}{dy}((\sum_{i=1}^{3} {n_i}^{3/2}P_{wi})] \quad (6)$$

$$\frac{dQ}{dn_i} = -Q[\frac{2}{3}\frac{1}{(\sum_{i=1}^{3} {n_i}^{3/2}P_{wi})}\frac{d}{dn_i}((\sum_{i=1}^{3} {n_i}^{3/2}P_{wi})] \quad (7)$$

$$\frac{dQ}{dS_o} = \frac{Q}{2S_o} \quad (8)$$

3) According to Chow's (1988) research, the variance of y ($S^2{}_y$) is dependent on the variance of Q ($S^2{}_Q$), variance of n_1 ($S^2{}_{n_1}$), variance of n_2 ($S^2{}_{n_2}$), variance of n_3 ($S^2{}_{n_3}$) and variance of S_o ($S^2{}_{S_o}$).

$$S^2{}_y = \frac{1}{(\frac{dQ}{dy})^2}[S^2{}_Q + (\frac{dQ}{dn_1})^2 S^2{}_{n_1} + (\frac{dQ}{dn_2})^2 S^2{}_{n_2} + (\frac{dQ}{dn_3})^2 S^2{}_{n_3} + (\frac{dQ}{dS_o})^2 S^2{}_{S_o} \quad (9)$$

By arranging equation (9) based on dQ/dy, the Eq. (9) is written as Eq. (10):

$$\frac{dQ}{dy} = \frac{1}{S_y}[S^2{}_Q + (\frac{dQ}{dn_1})^2 S^2{}_{n_1} + (\frac{dQ}{dn_2})^2 S^2{}_{n_2} + (\frac{dQ}{dn_3})^2 S^2{}_{n_3} + (\frac{dQ}{dS_o})^2 S^2{}_{S_o}]^{\frac{1}{2}} \quad (10)$$

4) Therefore, by substituting Eq. (6), (7) and (8) in equation (10), the standard deviation of the flow depth is obtained according to the following equation:

$$S_y = \frac{3[\frac{S^2{}_Q}{Q^2} + \frac{1}{(\sum_{i=1}^{3} {n_i}^{3/2}P_{wi})^2}\sum {n_i}{P_{wi}}^2 S^2{}_{n_i} + \frac{1}{4{S_o}^2}S^2{}_{S_o}]^{\frac{1}{2}}}{\frac{5}{A}\frac{dA_w}{dy} - \frac{2}{(\sum_{i=1}^{3} {n_i}^{3/2}P_{wi})}\frac{d}{dy}((\sum_{i=1}^{3} {n_i}^{3/2}P_{wi})]} \quad (11)$$

5) Determining the standard deviation of the flow depth based on the normal standard variable.

The standard normal variable Z is defined as follows [6]:

$$Z = \frac{X - \mu}{\sigma} \quad (12$$

In statistical calculations, $\mu = \bar{X}$ $\sigma = S_x$ and $Z$is the standard normal distribution variable whose value is determined according to the overtopping probability values and interpolation in the cumulative distribution table of normal distribution probabilities. In this research, (y) is replaced for the variable. $(X - \mu)$, Therefore, the variable is defined as follows:

$$Z = \frac{y + f - y}{S_y} = \frac{f}{S_y} \quad (13)$$

In equation (13), f it is the freeboard of the channel, which in this research is equal to 0.5meters.

$$S_y = \frac{f}{Z} \quad (14)$$

By setting Eq. (14) and Eq. (11) equal, the overtopping constraint is defined as the following equation.

$$\frac{f}{Z} = \frac{3[\frac{S^2{}_Q}{Q^2} + \frac{1}{(\sum_{i=1}^{3} {n_i}^{3/2}P_{wi})^2}\sum {n_i}^2{P_{wi}}^2 S^2{}_{n_i} + \frac{1}{4{S_o}^2}S^2{}_{S_o}]^{\frac{1}{2}}}{\frac{5}{A}\frac{dA_w}{dy} - \frac{2}{(\sum_{i=1}^{3} {n_i}^{3/2}P_{wi})}\frac{d}{dy}((\sum_{i=1}^{3} {n_i}^{3/2}P_{wi})]} \quad (15)$$

Therefore, the constraint of overtopping probability is defined as Eq. (16).

$$\Phi_6 = \left|\frac{f}{Z} - \frac{3[\frac{S^2{}_Q}{Q^2} + \frac{1}{(\sum_{i=1}^{3} {n_i}^{3/2}P_{wi})^2}\sum {n_i}{P_{wi}}^2 S^2{}_{n_i} + \frac{1}{4{S_o}^2}S^2{}_{S_o}]^{\frac{1}{2}}}{\frac{5}{A}\frac{dA_w}{dy} - \frac{2}{(\sum_{i=1}^{3} {n_i}^{3/2}P_{wi})}\frac{d}{dy}((\sum_{i=1}^{3} {n_i}^{3/2}P_{wi})]}\right| - \varepsilon \leq 0 \quad (16)$$

2.4. Objective function

The first step in channel design is determining its optimal dimensions to transfer the flow discharge with the lowest construction cost. In this research, the total cost of constructing one meter of canal includes the costs of excavating (cross-sectional area) and lining the surfaces (perimeter).

$$MinimizeCost = Cost(y, b, z_1, z_2) \quad (17)$$

$$C_1 = C_e + C_L \quad (18)$$

Where C_e= Excavation cost is per unit of channel length and C_L= cost of channel lining is per unit of channel length.

$$C_e = c_e A_t \quad (19)$$

c_e= excavation cost per unit cross-sectional area for a unit length of the channel.

$$C_L = c_l P_t \quad (20)$$

c_l= lining costs per unit length of the perimeter.

$$C = c_e A + c_l P \quad (21)$$

C=objective function equal to the total construction cost of the channel consisting of excavation and lining cost.

2.5. Optimization algorithm

The SPSA algorithm is a powerful algorithm for the optimization of complex systems that was developed and expanded by SPAL in 1998. Among the features of the SPSA algorithm is that in each optimization iteration, regardless of the number of design variables, it only needs

to evaluate the objective function twice. Therefore, the use of this algorithm greatly reduces the volume of calculations and reduces the total optimization time. [36] SPSA algorithm has been effectively used in civil engineering, especially in arch dam optimization [37-43]. The SPSA algorithm is for optimization of unconstrained problems. Therefore, in order to use it in solving bounded problems with unequal constraints, it is necessary to replace the objective function with the pseudo-objective function obtained by using the method of external penalty functions:

$$w(X, r_p) = f(X) + r_p \sum_{j=1}^{m} \max[0, g_j(X)]^2 \Rightarrow f(\bullet) = w(\bullet) + \text{noise} \quad (22)$$

The above steps can be seen in the flowchart of Figure (2).

To use SPSA algorithm for solving constrained problems with inequality constraints $g_j \leq 0$ $(j = 1, \ldots, m)$, it is necessary to replace the quasi-objective function w obtained by the external penalty function method with the objective function f (Eq. 22). r_p is a penalty multiplier. The flow chart of the SPSA algorithm for the channel optimization problem can be shown in Figure 2.

3. Results and discussion

In this article, design steps of the optimal trapezoidal composite channel cross-section have been done by considering the overtopping probability constrained in different values of flow discharge using the SPSA optimization algorithm. The flow discharge values are 10, 50 and 120 m^3/s respectively. These steps are as follows:

- ***Step1:*** Das's method is used to verify the results was used to compare the results of the SPSA algorithm. The values of flow discharge, Manning roughness coefficients, bed slope, freeboard and constant cost values are as follows: $Q = 100\, {}^{m^3}/_{S}$, $n_1 = 0.015$ ، $n_2 = 0.015$, $c_1 = 0.5$, $c_2 = 0.3$, $c_3 = 0.35$, $c_4 = 0.4$, $f = 0.5m$, $S_0 = 0.0025$
  It should be noted that in the analytical model of Das (2000), only Manning's constraint is specified in the optimization process.

- ***Step2:*** Then, the model was developed with five very important constraints including, uniform flow constraint, Froud number constraint to control the subcritical flow in the channel, maximum velocity constraint to prevent scouring in the channel, minimum velocity constraint to control sedimentation in the channel and limiting the Channel top width were investigated to reduce the cost of the land area in order to provide the optimal shape of the channel section. The aforementioned restrictions are also called definite restrictions.

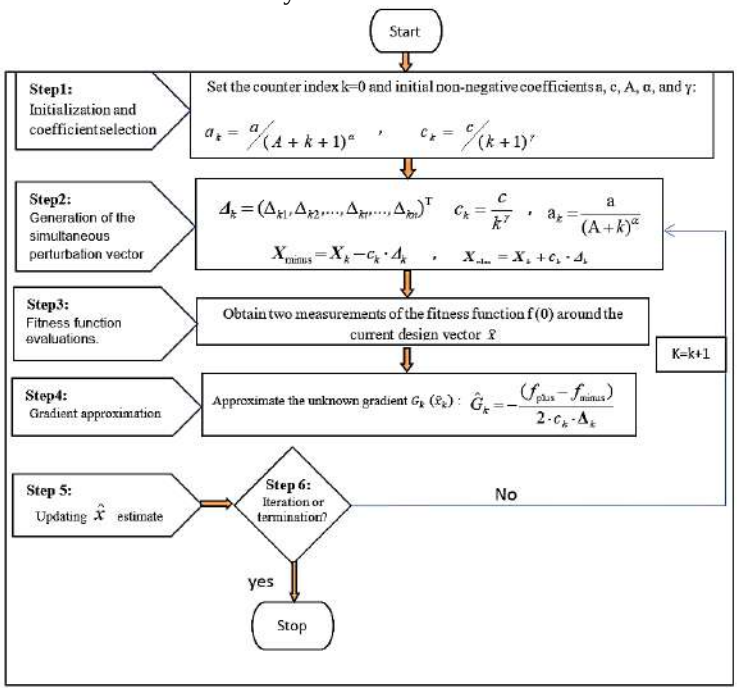

Figure 2. The flow chart of SPSA algorithm [32]

Table 3
Comparison of the optimization results of the trapezoidal composite channel section with the analytical model method of Das (2000)

Parameters / Model	y (m)	b(m)	Z1	Z2	f(m)	COST
Das (2000)	4.033	6.404	0.253	0.292	0.5	22.935
SPSA model (uniform flow)	4.0327	6.410	0.249	0.293	0.5	22.9354
SPSA model (total constraints)	4.013	6.305	0.305	0.297	0.5	22.9444

Comparing the results of the current model with the results of the analytical method of Das (2000) shows that the SPSA algorithm has a very good convergence in reaching the desired solution.

- ***Step3:*** After verifying and ensuring the correctness of the model in the first and second steps, the optimal shape of the compound trapezoidal channel section was obtained using the SPSA algorithm with the model of Das (2007), which input data of flow discharge values, roughness coefficients Manning, bed slope, freeboard and cost values in the validation section are as follows:
$Q = 120\, {}^{m^3}/_{S}$, $n_1 = 0.033$ ، $n_2 = 0.028$, $n_3 = 0.023$, $c_1 = 0.5$, $c_2 = 0.3$, $c_3 = 0.35$, $c_4 = 0.4$, $f = 0.5m$, $S_0 = 0.0025$
At this step, the values of the standard deviation of flow discharge, roughness coefficients and the bed slope of channel of the model (Das, 2007) are as follows:
$S_Q = 51.89414$, $S_{S_0} = 0.00356$, $S_{n_1} = 0.00572$, $S_{n_2} = 0.00445$, $S_{n_3} = 0.00356$
In Table 4, the comparison of the results obtained from the analytical model of Das (2007) with the results related to the optimization of the cross-section of the composed trapezoidal channel by considering Manning's constraint and the overtopping probability constraint corresponding to the minimum cost shows that the amount of cost using of the SPSA algorithm in similar optimization conditions is less than the analytical model of Das (2007).
- ***Step4:*** the optimization is considered with the overtopping probability by taking into account all the constraints to optimize the cross-section of the composed trapezoidal channel. that the input values are the same as the values of the third step and the optimal design is based on the flow discharge values of 10, 50, and 120 (m^3/s).
In this study, the optimization method was repeated by changing the flow discharge. The obtained results are summarized with tables and graphs.

Table 4
Comparison of the optimization results of the trapezoidal composite channel section with the analytical model method of Das (2007) by considering the possibility of flooding with the SPSA algorithm.

	COST	P	S_y
Das (2000)	4.033	6.404	0.253
SPSA model (uniform flow)	4.0327	6.410	0.249
SPSA model (total constraints)	4.013	6.305	0.305

Tables 5, 6 and 7, show the optimal values of flow depth, channel bed width, left and right-side slope of the channel, flow velocity, Froude number and channel construction cost at different overtopping probability values. The flow discharge values in this paper are 10, 50 and 120 m3/s and the freeboard value are 0.5 meters.

Table 5
Optimal values of design variables, constraints and objective function using SPSA algorithm for flow discharge Q=10 m^3/s

p	y(m)	b(m)	z_1	z_2	f	V(m/s)	Fr	Cost
0.01	1.756	2.167	0.613	0.597	0.5	1.763	0.490	6.565
0.05	1.834	2.119	0.502	0.564	0.5	1.762	0.476	6.491
0.1	1.887	2.092	0.443	0.534	0.5	1.758	0.467	6.456
0.15	1.928	2.069	0.438	0.484	0.5	1.754	0.460	6.436
0.2	1.977	2.048	0.385	0.469	0.5	1.749	0.452	6.418
0.25	2.036	2.045	0.334	0.426	0.5	1.742	0.440	6.400
0.3	2.084	2.033	0.305	0.397	0.5	1.736	0.432	6.395
0.35	2.124	2.031	0.291	0.358	0.5	1.730	0.424	6.392
0.4	2.175	2.037	0.253	0.329	0.5	1.722	0.415	6.394
0.45	2.199	2.044	0.261	0.288	0.5	1.718	0.410	6.395
0.5	2.238	2.057	0.217	0.279	0.5	1.711	0.402	6.403

Table 6
Optimal values of design variables, constraints and objective function using SPSA algorithm for flow discharge Q=50 m^3/s

p	y(m)	b(m)	z_1	z_2	f	V(m/s)	Fr	Cost
0.01	3.234	4.043	0.529	0.589	0.5	2.642	0.537	15.847
0.05	3.333	3.945	0.520	0.527	0.5	2.636	0.527	15.798
0.1	3.427	3.838	0.494	0.504	0.5	2.629	0.519	15.774
0.15	3.495	3.795	0.454	0.493	0.5	2.625	0.512	15.751
0.2	3.561	3.742	0.442	0.467	0.5	2.619	0.506	15.743
0.25	3.614	3.733	0.412	0.450	0.5	2.615	0.500	15.731
0.3	3.798	3.730	0.351	0.355	0.5	2.596	0.478	15.729
0.35	3.820	3.738	0.361	0.325	0.5	2.593	0.475	15.735
0.4	3.893	3.748	0.321	0.306	0.5	2.585	0.467	15.750
0.45	3.941	3.798	0.275	0.294	0.5	2.579	0.460	15.763
0.5	3.981	3.817	0.278	0.258	0.5	2.572	0.454	15.780

Table 7
Optimal values of design variables, constraints and objective function using SPSA algorithm for flow discharge Q=120 m^3/s

p	y(m)	b(m)	z_1	z_2	f	V(m/s)	Fr	Cost
0.01	4.306	6.450	0.465	0.444	0.5	3.314	0.566	26.763
0.05	4.348	6.439	0.443	0.428	0.5	3.313	0.562	26.733
0.1	4.386	6.387	0.436	0.420	0.5	3.311	0.559	26.722
0.15	4.500	6.170	0.430	0.418	0.5	3.302	0.553	26.717
0.2	4.561	6.084	0.426	0.405	0.5	3.297	0.548	26.714
0.25	4.666	5.947	0.402	0.400	0.5	3.289	0.541	26.710
0.3	4.808	5.898	0.354	0.360	0.5	3.278	0.528	26.705
0.35	4.861	5.924	0.328	0.338	0.5	3.273	0.522	26.707
0.4	4.913	5.942	0.317	0.308	0.5	3.267	0.517	26.718
0.45	4.946	5.984	0.286	0.300	0.5	3.264	0.512	26.725
0.5	4.956	6.021	0.267	0.298	0.5	3.262	0.510	26.728

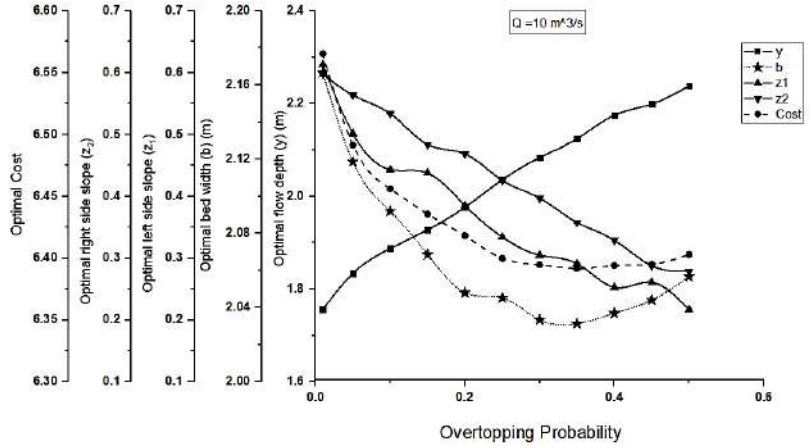

Figure 3. Results of optimization of composed trapezoidal cross-section using SPSA algorithm for flow discharge of 10 m^3/s

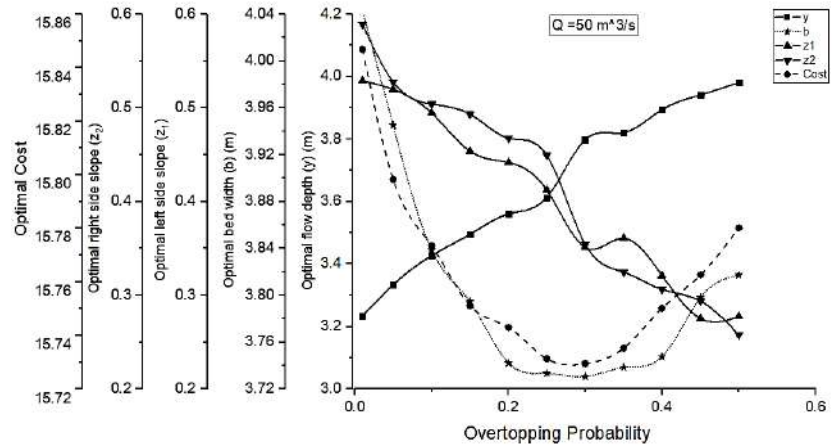

Figure 5: Results of optimization of composed trapezoidal cross-section using SPSA algorithm for flow discharge of 50 m^3/s

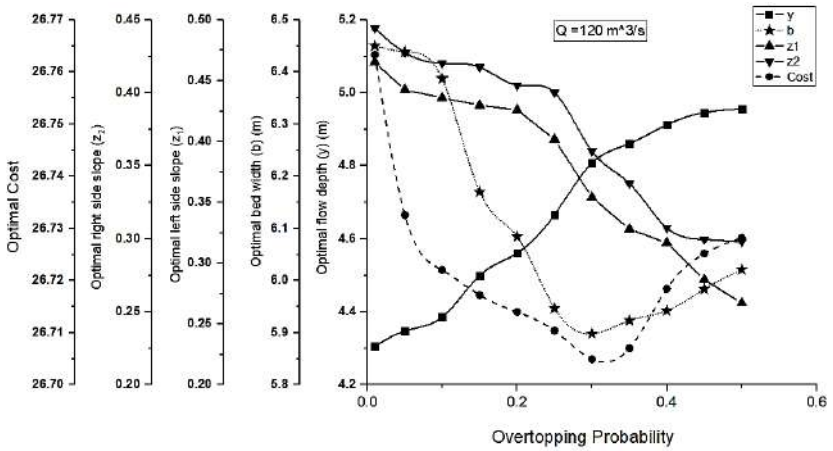

Figure 6. Results of optimization of composed trapezoidal cross-section using SPSA algorithm for flow discharge of 120 m^3/s

Figures 3 to 6 show the changes in the optimal values of flow depth, channel bed width, left and right-side slope of the channel, flow velocity, Froud number and channel construction cost with overtopping probability values using the SPSA algorithm. The result show that with increasing probability values, the flow depth increases and, in contrast, with the left and right-side slopes of the channel section, the flow velocity and Froud number decrease. These changes are also valid for all discharge values of 10, 50 and 120 m3/s. The values of the channel bed width and channel construction cost are first decreasing and then increasing. So that initially, with increasing overtopping probability values, the channel bottom width and construction cost decrease, but at a discharge of 10 m3/s from an overtopping probability value of 0.35 and above, and for flow discharge values of 50 and 120 m3/s from an overtopping probability value of 0.3 and above, the channel bottom width and construction cost increase with increasing overtopping probability values.

In Figure 7, the graph shows the changes in flow discharge values with overtopping probability values at flow values of 10, 50, and 120 m^3/s.

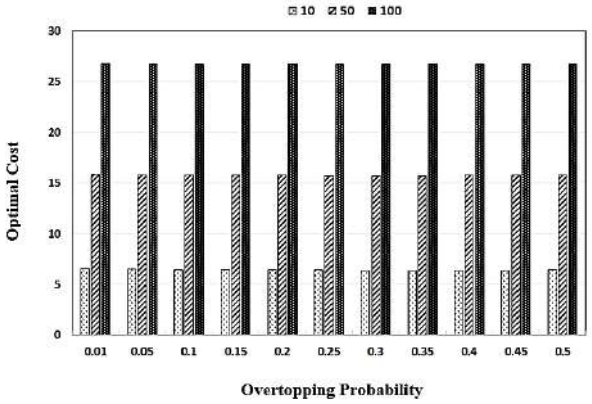

Figure 7: Comparison of the cost of constructing a compound trapezoidal canal for different overtopping probability values and discharge values of 10, 50, and 120 (m^3/s).

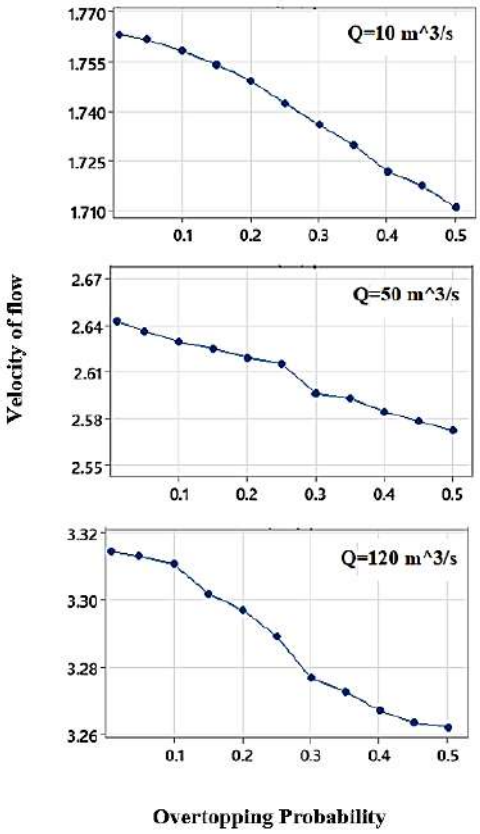

Figure 8: Optimal flow velocity values- overtopping probability relationship for different flow discharge values

Figure 8, shows the optimal values of flow velocity in a composed trapezoidal channel for different overtopping probability values (from 0.01 to 0.5) and flow discharge values of 10, 50, and 120 m^3/s. with the flow velocity decreasing as overtopping probability values increase.

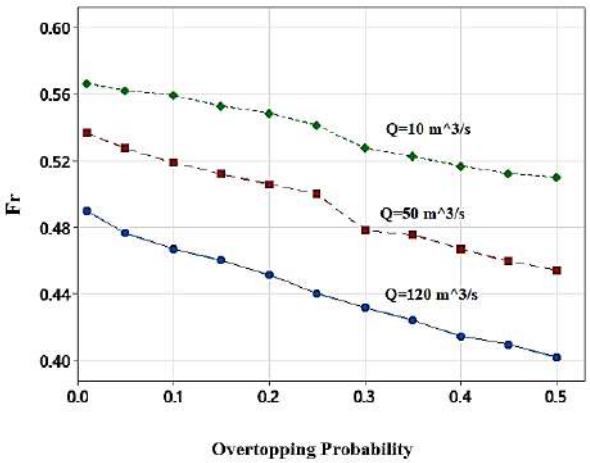

Figure 9: Optimal Froud values - overtopping probability relationship for different flow discharge values

Figure (8) shows the values of the Froude number in a composed trapezoidal channel for different overtopping probability values (from 0.01 to 0.5) and flow discharge values of 10, 50, and 120 m^3/s. As the overtopping probability values increase, the Froude number decreases.

4. Conclusion

In this study, the effect of uncertainty in the optimal design of a composed trapezoidal channel is presented. The effect of discharge is investigated by considering different values in these models on the design variables, constraints, objective function and geometric parameters and channel design, at different overtopping probability values. The results show that at a certain flow discharge value, with increasing overtopping probability values, the flow depth increases, but the left and right-side slopes, flow velocity and Froude number decrease. The changes in overtopping probability values are somewhat different with the channel bed width and cost function, so that the channel bed width and channel construction cost first decrease and then increase with increasing probability values. Accordingly, for a flow discharge of 10 m3/s and for an overtopping probability value of 0.35 and above, and for flow discharge values of 50 and 120 m3/s from an overtopping probability value of 0.3 and above, the channel bed width and construction cost increase with increasing overtopping probability values.

References

[1] Te Chow, Ven. Open channel hydraulics. 1959. New York: McGraw-Hill.

[2] Trout, Thomas J. "Channel design to minimize lining material costs." Journal of the Irrigation and Drainage Division 108.4 (1982): 242-249. https://doi.org/10.1061/JRCEA4.0001392

[3] Guo, Chwen-Yuan, and William C. Hughes. "Optimal channel cross section with freeboard." Journal of irrigation and drainage engineering 110.3 (1984): 304-314. https://doi.org/10.1061/(ASCE)0733-9437(1984)110:3(304)

[4] Monadjemi, Parviz. "General formulation of best hydraulic channel section." Journal of Irrigation and Drainage Engineering 120.1 (1994): 27-35. https://doi.org/10.1061/(ASCE)0733-9437(1994)120:1(27)

[5] Swamee, Prabhata K. "Optimal irrigation canal sections." Journal of Irrigation and Drainage Engineering 121.6 (1995): 467-469. https://doi.org/10.1061/(ASCE)0733-9437(1995)121:6(467)

[6] Swamee, Prabhata K., Govinda C. Mishra, and Bhagu R. Chahar. "Comprehensive Design of Minimum Cost IrrigationCanal Sections." Journal of irrigation and drainage engineering 126.5 (2000): 322-327. https://doi.org/10.1061/(ASCE)0733-9437(2000)126:5(322)

[7] Swamee, Prabhata K., Govinda C. Mishra, and Bhagu R. Chahar. "Minimum cost design of lined canal sections." Water Resources Management 14 (2000): 1-12. https://doi.org/10.1023/A:1008198602337

[8] Swamee, Prabhata K., Govinda C. Mishra, and Bhagu R. Chahar. "Design of minimum seepage loss canal sections with drainage layer

at shallow depth." Journal of irrigation and drainage engineering 127.5 (2001): 287-294. https://doi.org/10.1061/(ASCE)0733-9437(2001)127:5(287)

[9] Swamee, Prabhata K., Govinda C. Mishra, and Bhagu R. Chahar. "Design of minimum water-loss canal sections." Journal of Hydraulic Research 40.2 (2002): 215-220. https://doi.org/10.1080/00221680209499864

[10] Swamee, Prabhata K., Govinda C. Mishra, and Bhagu R. Chahar. "Optimal design of transmission canal." Journal of Irrigation and Drainage Engineering 128.4 (2002): 234-243. https://doi.org/10.1061/(ASCE)0733-9437(2002)128:4(234)

[11] Babaeyan-Koopaei, K., E. M. Valentine, and D. C. Swailes. "Optimal design of parabolic-bottomed triangle canals." Journal of Irrigation and Drainage Engineering 126.6 (2000): 408-411. https://doi.org/10.1061/(ASCE)0733-9437(2000)126:6(408)

[12] Das, Amlan. "Optimal channel cross section with composite roughness." Journal of irrigation and drainage engineering 126.1 (2000): 68-72. https://doi.org/10.1061/(ASCE)0733-9437(2000)126:1(68)

[13] Jain, Ashu, Rajib Kumar Bhattacharjya, and Srinivasulu Sanaga. "Optimal design of composite channels using genetic algorithm." Journal of Irrigation and Drainage Engineering 130.4 (2004): 286-295. https://doi.org/10.1061/(ASCE)0733-9437(2004)130:4(286)

[14] Bhattacharjya, Rajib Kumar. "Optimal design of open channel section considering freeboard." ISH Journal of Hydraulic Engineering 11.3 (2005): 141-151. https://doi.org/10.1080/09715010.2005.10514808

[15] Bhattacharjya, Rajib Kumar. "Optimal design of open channel section incorporating critical flow condition." Journal of irrigation and drainage engineering 132.5 (2006): 513-518. https://doi.org/10.1061/(ASCE)0733-9437(2006)132:5(513)

[16] Bhattacharjya, Rajib Kumar, and Mysore G. Satish. "Optimal design of a stable trapezoidal channel section using hybrid optimization techniques." Journal of irrigation and drainage engineering 133.4 (2007): 323-329. https://doi.org/10.1061/(ASCE)0733-9437(2007)133:4(323)

[17] Das, Amlan. "Flooding probability constrained optimal design of trapezoidal channels." Journal of irrigation and drainage engineering 133.1 (2007): 53-60. https://doi.org/10.1061/(ASCE)0733-9437(2007)133:1(53)

[18] Bhattacharjya, Rajib Kumar, and Mysore Satish. "Flooding probability-based optimal design of trapezoidal open channel using freeboard as a design variable." Journal of irrigation and drainage engineering 134.3 (2008): 405-408. https://doi.org/10.1061/(ASCE)0733-9437(2008)134:3(405)

[19] Reddy, M. Janga, and S. Adarsh. "Overtopping probability constrained optimal design of composite channels using swarm intelligence technique." Journal of irrigation and drainage engineering 136.8 (2010): 532-542. https://doi.org/10.1061/(ASCE)IR.1943-4774.0000217

[20] Das, Amlan. "Cost and flooding probability minimization based design of HBPS channel." Water resources management 24 (2010): 193-238. https://doi.org/10.1007/s11269-009-9444-z.

[21] Janga Reddy, M., and Sankaran Adarsh. "Chance constrained optimal design of composite channels using meta-heuristic techniques." Water resources management 24 (2010): 2221-2235. https://doi.org/10.1007/s11269-009-9548-5

[22] Adarsh, S. "Modeling parametric uncertainty in optimal open channel design using FORM-PGSL coupled approach." Stochastic environmental research and risk assessment 26 (2012): 709-720. https://doi.org/10.1007/s00477-011-0539-8

[23] Sankaran, Adarsh, and Janga Reddy Manne. "Probabilistic multi-objective optimal design of composite channels using particle swarm optimization." Journal of hydraulic research 51.4 (2013): 459-464. https://doi.org/10.1080/00221686.2013.777372

[24] Easa, Said M. "New and improved channel cross section with piecewise linear or smooth sides." Canadian Journal of Civil Engineering 38.6 (2011): 690-697. https://doi.org/10.1139/l11-037

[25] Easa, Said M., and Ali R. Vatankhah. "New open channel with elliptic sides and horizontal bottom." KSCE Journal of Civil Engineering 18 (2014): 1197-1204. https://doi.org/10.1007/s12205-014-0559-2

[26] Han, Yan-Cheng. "Horizontal bottomed semi-cubic parabolic channel and best hydraulic section." Flow Measurement and Instrumentation 45 (2015): 56-61. https://doi.org/10.1016/j.flowmeasinst.2015.04.001

[27] Han, Yan-Cheng, and Said M. Easa. "New and improved three and one-third parabolic channel and most efficient hydraulic section." Canadian Journal of Civil Engineering 44.5 (2017): 387-391. https://doi.org/10.1139/cjce-2016-0535

[28] Orouji, Hossein, et al. "Shuffled frog-leaping algorithm for optimal design of open channels." Journal of irrigation and drainage engineering 142.10 (2016): 06016008. https://doi.org/10.1061/(ASCE)IR.1943-4774.0001059

[29] Roushangar, Kiyoumars, et al. "A cost model with several hydraulic constraints for optimizing in practice a trapezoidal cross section." Journal of Hydroinformatics 19.3 (2017): 456-468. https://doi.org/10.2166/hydro.2017.081

[30] Gupta, Sanjay K., et al. "Fish shoal optimization for identification of the most suitable revetment stone for design of minimum cost earthen canals carrying sediment-laden flow." ISH Journal of Hydraulic Engineering 24.2 (2018): 172-189. https://doi.org/10.1080/09715010.2017.1402211

[31] Farzin, Saeed, and Mahdi Valikhan Anaraki. "Optimal construction of an open channel by considering different conditions and uncertainty: application of evolutionary methods." Engineering Optimization 53.7 (2021): 1173-1191. https://doi.org/10.1080/0305215X.2020.1775825

[32] Pourbakhshian, Somayyeh, and Majid Pouraminian. "Analytical models for optimal design of a trapezoidal composite channel cross-section." Civil and Environmental Engineering Reports 31.1 (2021). https://doi.org/10.2478/ceer-2021-0009

[33] Pourbakhshian, S., and P. Fasih. "OPTIMIZATION OF COMPOSI TE PARABOLIC CHANNEL CROSS-SECTION BASED ON CH ANGES IN DISCHARGE AND FREEBOARD." Sharif Journal of Civil Engineering 38.1.2 (2022): 155-167. https://doi.org/10.24200/J30.2022.58880.3011

[34] Farzin, Saeed, et al. "Optimization Modelling of Irrigation Channel Considering Flooding Conditions and Uncertainty." Irrigation and Water Engineering 9.1 (2018): 46-60. https://doi.org/10.1080/0305215X.2020.1775825

[35] Horton, Robert E. "Separate roughness coefficients for channel bottom and sides." Eng. News-Rec 111.22 (1933): 652-653.

[36] Spall, James C. "An overview of the simultaneous perturbation method for efficient optimization." Johns Hopkins apl technical digest 19.4 (1998): 482-492.

[37] Seyedpoor, Seyed Mohammad, et al. "Optimal design of arch dams subjected to earthquake loading by a combination of simultaneous perturbation stochastic approximation and particle swarm algorithms." Applied Soft Computing 11.1 (2011): 39-48. https://doi.org/10.1016/j.asoc.2009.10.014

[38] Pourbakhshian, S., and M. Ghaemain. "Shape optimization of arch dams using sensitivity analysis." KSCE Journal of Civil Engineering 20 (2016): 1966-1976. https://doi.org/10.1007/s12205-015-0135-4

[39] Pourbakhshian, S., M. Ghaemain, and A. Jogatae. "The shape optimization of concrete arch dams considering stage construction."

Scientia Iranica 23.1 (2016): 21-35. https://doi.org/10.24200/SCI.2016.2094

[40] Pouraminian, Majid, and Somayeh Pourbakhshian. "SPSA Algorithm based optimum design of longitudinal section of bridges." Indian Journal of Science and Technology 7.9 (2014): 1327-1332. https://doi.org/10.17485/ijst/2014/v7i9/59472

[41] Pouraminian, Majid, and Somayyeh Pourbakhshian. "Shape optimization of concrete arch dams with SPSA algorithm and post-analysis of pareto front for selection the best alternatives." Journal of Hydraulic Structures 6.3 (2020): 59-82. https://doi.org/10.22055/JHS.2020.33293.1137

[42] Pouraminian, Majid, and Mohsen Ghaemian. "Shape optimisation of concrete open spandrel arch bridges." Građevinar 67.12. (2015): 1177-1185. https://doi.org/10.14256/JCE.1223.2015

[43] Rahgozar, Navid, Majid Pouraminian, and Nima Rahgozar. "Structural optimization of vertical isolated rocking core-moment frames." Journal of Vibration and Control 29.15-16 (2023): 3451-3460. https://doi.org/10.1177/10775463221096882

J-Researchers

Journal of Civil Engineering Researchers

Journal homepage: www.journals-researchers.com

Pre-Feasibility Project for the Creation of a High-Traffic Pavers Factory for the Decentralized Autonomous Government of Sigchos Canton

Mohammadfarid Alvansazyazdi,[a,b,c*] Gabriel Alejandro Molina Gomez,[d] Luis Miguel Leon Torres,[e]

[a] *Institute of Science and Concrete Technology, iCiTECH, Universitat politècnica de València,Spain*

[b] *Carrera de ingeniería Civil, Universidad Central del Ecuador, av. Universitaria, Quito 170521, Ecuador*

[c] *Facultad ingeniería, industria y Construcción, Carrera ingeniería Civil, Universidad Laica Eloy alfaro de Manabi,Manta, Ecuador*

[d] *Maestría en Construcciones de Obras Civiles Mención Gestión y Dirección, Facultad de ingeniería y Ciencias aplicadas, Universidad Central del Ecuador, av. Universitaria*

[e] *Benito Juarez University, 36th Street Nte. 1609, Christopher Columbus, 72330 Heroic Puebla de Zaragoza, Pue., Mexic*

ABSTRACT

The objective of this study is to determine the technical, legal, and economic feasibility of establishing a heavy-duty paver block factory for the Municipal Decentralized Autonomous Government of Sigchos Canton. The methodology used included a non-experimental research approach, with an explanatory, descriptive, and correlational design. Surveys were conducted with the legal representatives of the parish councils to gather primary information, while secondary information was obtained through bibliographic and documentary review.

The results from the market study reveal significant demand and acceptance from the parish representatives toward the production of vehicular pavers, supporting the need to improve local road infrastructure and economic development. A market opportunity was identified both in government projects and private initiatives, with an estimated daily demand of 2,800 paver units.

As for the technical study, efficient production processes were designed, with rigorous quality control measures and an annual production capacity of 2,880,000 pavers. The administrative-legal analysis reflects a comprehensive and proactive approach to meeting legal and regulatory requirements, including the decision to establish a Corporation (S.A.) and obtaining the necessary permits for the factory's operation.

Finally, the financial study results indicate that the project is economically viable, with a positive Net Present Value (NPV), Internal Rate of Return (IRR), Payback Period (PBP), average profitability (AP), and Benefit-Cost Ratio (BCR), supporting the project's feasibility.

ARTICLE INFO

Received: October 17, 2024
Accepted: November 11, 2024

Keywords:
Economic feasibility
Paver block factory
Municipal Decentralized Autonomous Government of Sigchos Canton
Technical legal

DOI: 10.61186/JCER.6.4.52
DOR: 20.1001.1.2538516.2024.6.4.6.1

[*] Corresponding author. Tel.: +593987026212; e-mail: moal13m@doctor.upv.es or faridalvan@uce.edu.ec or farid.alvan@uleam.edu.ec .

1. Introduction

The planning and execution of road infrastructure projects are crucial for the sustainable development of local communities. In this context, the Municipal Decentralized Autonomous Government of Sigchos Canton, located in the province of Cotopaxi, faces the need to improve its road network to meet the growing mobility demands of its population [1-3].

In line with this need, the establishment of a Heavy-Duty Paver Block Factory presents a strategic opportunity for Sigchos Canton. research highlighted that, "the production of pavers not only improves road infrastructure but can also have a significant impact on local economic development"[4] .

In response to this situation, this thesis aims to examine the feasibility of developing a Heavy-Duty Paver Block Factory for the Municipal Decentralized Autonomous Government of Sigchos Canton. The study seeks to apply a methodology that determines the technical and financial feasibility of this project. It is expected that the implementation of best practices from this guide will have a positive impact on the project's success. The feasibility study will address various studies and factors involved in assessing the viability of a project of this nature [5].

1.1. Research Methodology

The main objective of this research chapter is to evaluate the feasibility of establishing a heavy-duty paver block factory for the Municipal Decentralized Autonomous Government of Sigchos Canton, analyzing the impact of macroeconomic variables on the production sector. Specifically, it seeks to identify opportunities and threats for the project, determine its economic viability through key indicators, and calculate the necessary investment. The research, classified as non-experimental, descriptive, explanatory, and correlational, uses a quantitative approach.

A survey was conducted with the legal representatives of the Parochial GADs to collect primary data, complemented by a bibliographic review. The population corresponds to Sigchos Canton and its 4 parishes, while the sample will be selected by convenience, defined according to Leiner [6] as a method adopted by researchers in which market study data is collected from a conveniently available group of respondents. It is the most commonly used sampling technique because it is fast, simple, and economical. In many cases, members are selected based on their accessibility to form part of the sample, and the researcher chooses members simply based on proximity;-

Table 1
Product Characteristics

PEDESTRIAN PAVER	VEHICULAR PAVER
Dimensions: 20 centimeters in length, 10 centimeters in width, and 8 centimeters in height.	Dimensions: 23 centimeters in length, 17 centimeters in width, and 8.5 centimeters in height.
Strength: Supports a load of 350 kilograms-force.	Strength: Capable of supporting a load of 400 kilograms-force.
Ingredients for manufacturing 120 units:	Materials required to manufacture 50 units:
Fine macadam: 91 kilograms	
Stone: 91 kilograms	Sand: 91 kilograms
Cement: 50 kilograms	Gravel: 91 kilograms
Water: 21 liters	Cement: 50 kilograms
	Water: 21 liters
	

using this technique, habits, opinions, and viewpoints can be observed in the easiest possible way. Therefore, in this project, the sample will correspond to the presidents.

The data analysis was based on descriptive statistics to assess the supply and demand of the project. Through an analytical-synthetic analysis, the entire production process was studied, from supply to distribution, in order to identify improvements and optimize production.

1.2. Data Analysis

The initial analysis was based on the product characteristics (Table 1), where, thanks to primary sources at the GAD, it was possible to establish the requirements and specifications for the product in accordance with demand.

The cobblestone can be considered an effective road and social solution due to its durability, resistance, and ability to enhance urban aesthetics. Additionally, its use can promote social interaction by creating more pleasant and safer spaces for pedestrians. In rural areas, cobblestones can also be beneficial by improving accessibility and road infrastructure, thus contributing to local development.

The Decentralized Autonomous Municipal Government of Sigchos, as part of its responsibilities, is in charge of the proper maintenance of the urban road circuit of the canton. Most of these roads currently consist of unpaved or gravel surfaces (figure 1), which need to be improved through the implementation of vehicular cobblestones with a resistance of 350 kg/cm². To achieve this goal, the execution of additional subprojects will be required.

The demand for cobblestones is based both on the paving requirements presented by the Decentralized Autonomous Government (GAD) and on additional needs that may arise from private projects. To determine the demand for cobblestones from the GAD, the following projects for the next 5 years were considered, as shown in Table 2.

On the other hand, the demand from private companies was considered. The three representatives interested in acquiring vehicular cobblestones are distributed as shown in Table 3.

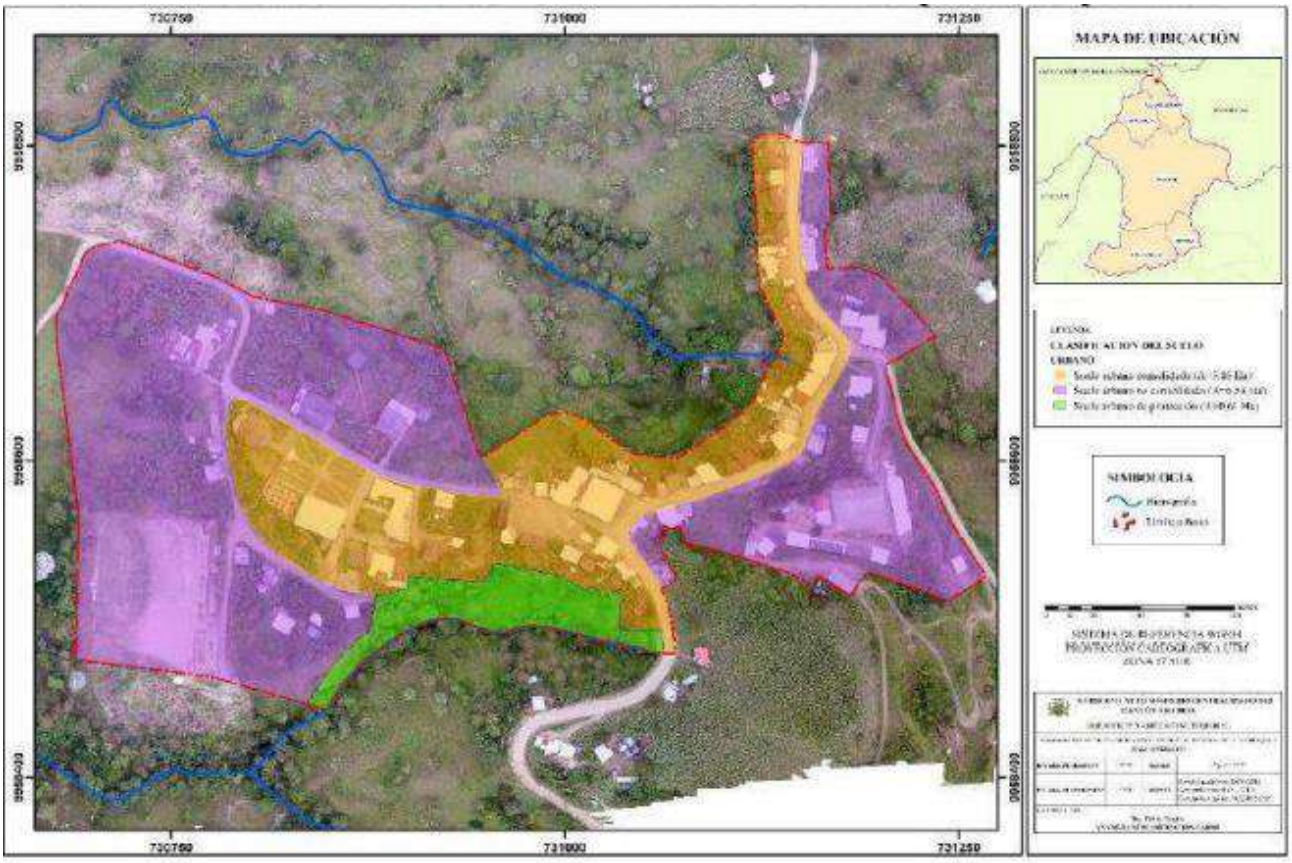

Fig. 1 Current Demand

Table 2

Requirements for Vehicular Cobblestones from GAD Projects in Sigchos

NO.	Location	Length (M)	Width (M)	Area (M²)	Cobblestones (Units)
1	Chugchilán	152.4	9.5	1447.8	30404
2	Guayaquil	265	8.6	2279	47859
3	Topaliví	352	8.06	2837.12	59580
4	Culacusig	72	6	432	9072
5	Dr. Rodrigo Borja	172	7	1204	25284
6	Vía al Calvario	305	6	1830	38430
TOTAL		1318.4		10029.92	210629

Table 3

Requirements for Vehicular Cobblestones from the Representatives of Sigchos

Number of Representatives	Quantity of Cobblestones per Month	Total Cobblestones per Month	Total Cobblestones per Day
15	3500,00	52500 ,00	2625,00

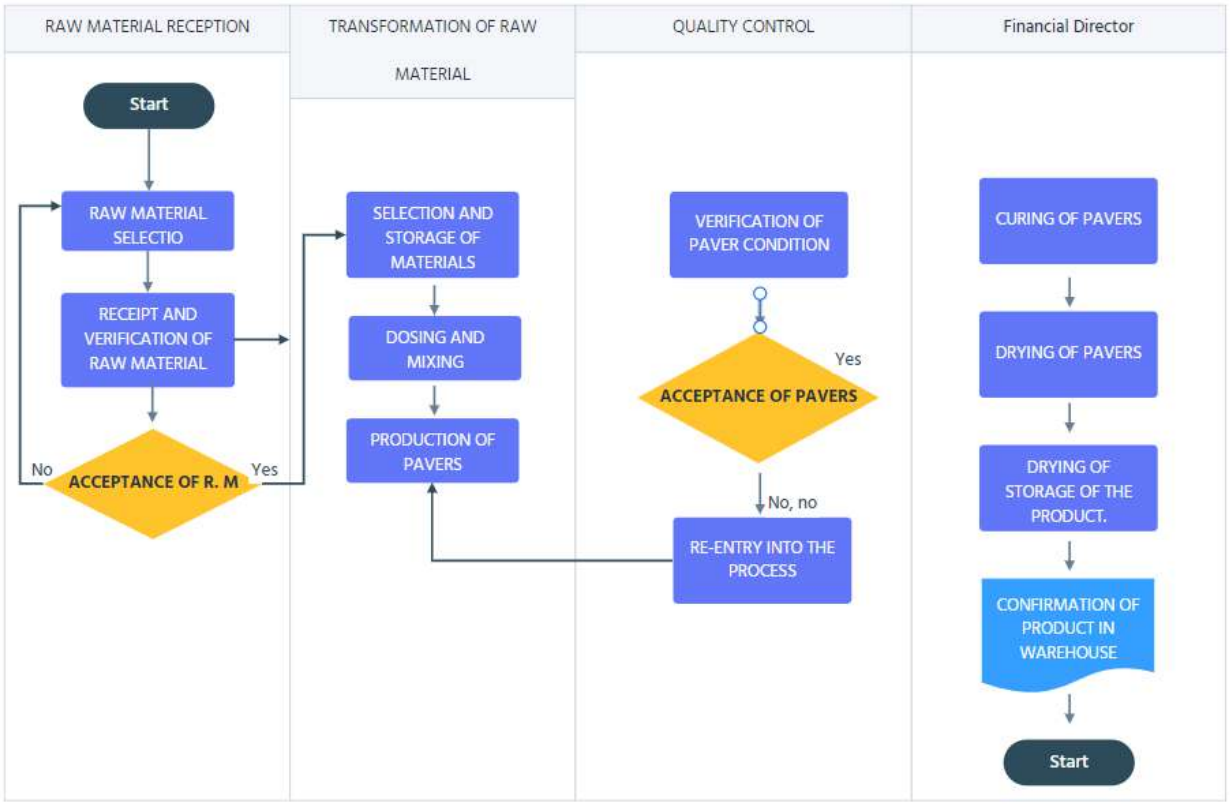

Fig.2 Proceso de producción

This demand corresponds to 2,625 vehicular cobblestones per day to meet the needs of private companies, as no interest was observed in purchasing pedestrian cobblestones. The current project exclusively addresses the production of vehicular cobblestones. Additionally, considering the projects of the GAD, the total number of cobblestones required daily is 2,800 units.

1.3. Performance Indicators

The fundamental purpose of incorporating the project's feasibility evaluation is to optimize the production process, making the most of the available resources and achieving a high-quality final product at a reduced cost.

To standardize the product requirements, we will rely solely on the INEN 3040 standard for Concrete Cobblestones [7], which establishes the necessary requirements and testing methods. This standard will be the main guide in our research project, ensuring that our product meets the quality and strength standards required in the industry (Fig. 2).

The production process of the paving stone, taking into account the raw material specifications and design established in the product architecture, is described as follows:

1. Preparation of raw materials: The process begins with the selection and purchase of high-quality materials that meet the specifications of the INEN 3040 standard. A crushing and mixing process of the materials, such as cement, aggregates, and water, is carried out to obtain a homogeneous mixture.

2. Dosage of aggregates: This is a critical step in the paving stone production process, as it ensures that the mixture has the appropriate properties to meet quality standards.

3. Preparation of the mixture: This determines the physical and chemical properties of the final product.

4. Manufacturing of paving stones: This involves the production of concrete blocks designed for paving surfaces. It includes the preparation of the concrete mixture, the molding of the blocks, and their curing to ensure strength and durability.

5. Setting of the paving stone: During setting, the concrete undergoes a chemical reaction known as hydration, where cement combines with water to form a gel that binds the aggregates. This process is fundamental for the strength and durability of the paving stones.

6. Curing of the paving stone: This is the process of maintaining adequate moisture and temperature in the freshly made paving stones to allow the concrete to achieve its optimal strength and durability. This process typically lasts several days and can be carried out using methods such as air curing, steam curing, or mist water curing.

7. Storage of paving stones: It is important that storage is carried out in a flat, firm area, away from moisture and protected from the elements to prevent damage. Paving stones should be stacked in a way that prevents warping or cracking, and it is recommended to use spacers between layers to avoid them sticking together.

Table 4
Annual Production of Paving Stones

Raw Material	Total Daily Paving Stones	Total Annual Paving Stones
Cement		
Stone Dust	4,000 daily (2 lines would be 8,000 daily)	2.880.000,00
Gravel type 3/8		
Water		

2. Development of the Financial Analysis

An instrument that measures the time required for the net cash flows of an investment to recover its initial cost or investment is the Payback Period.

$$PAYBACK = \frac{(TOTAL\ INVESTMENT - NET\ CASH\ FLOW\ YEAR\ 1)}{NET\ CASH\ FLOW\ YEAR\ 2} \quad (1)$$

$$PAYBACK = \frac{(\$85344{,}73 - \$238625{,}52)}{\$234710{,}95}$$

$$PAYBACK = 0.065 \times 360$$

$$PAYBACK = 6\ MONTHS\ 5\ DAYS$$

The payback period for the investment will occur in 6 months and 4 days, which is feasible since it falls within the project's useful life.

The Net Present Value (NPV) is a procedure that calculates the present value of specific future cash flows generated by an investment. It is defined as the difference between the revenues and expenses at updated values, or the difference between net income and the initial investment. In other words, the net present value is simply the updated sum of all benefits, costs, and investments of the project. Practically, it is the updated sum of the net cash flows for each period [8].

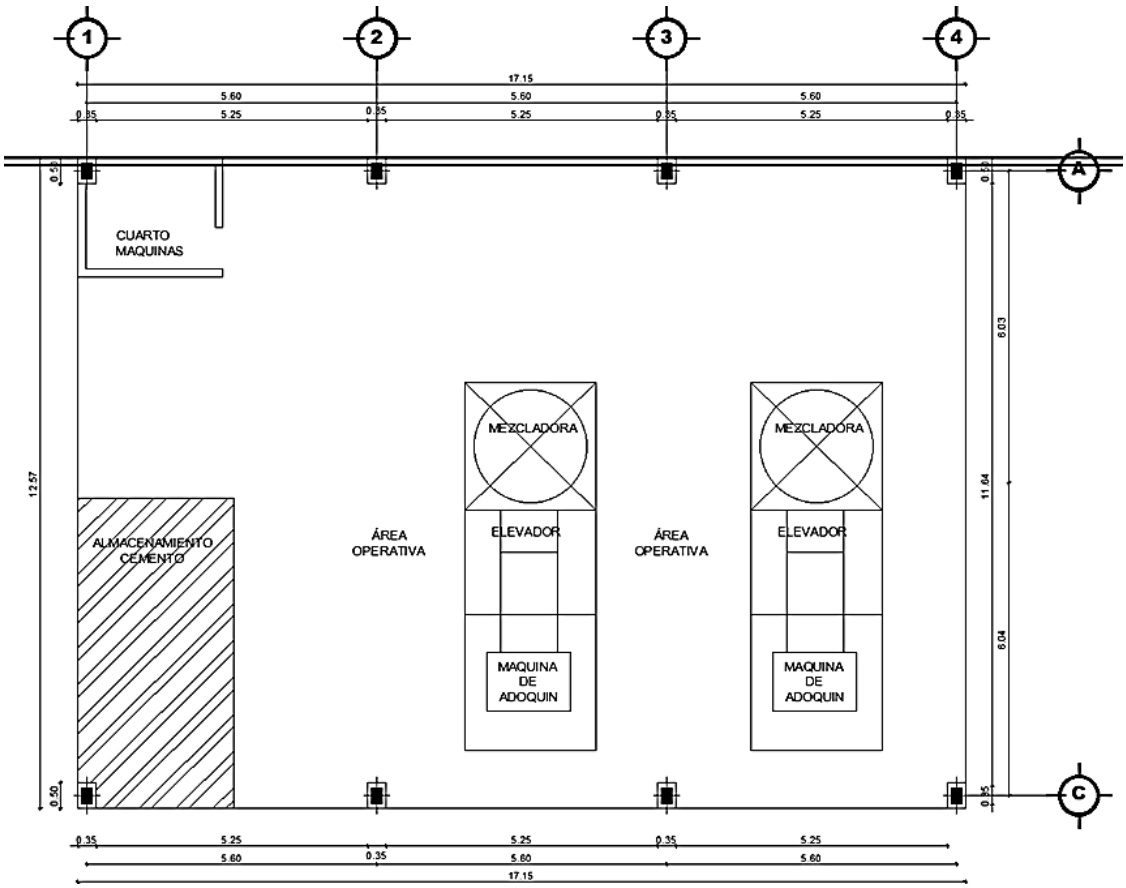

Fig. 3 Plant View of the Project (Production Area)

Table 5

Payback Period of the studied project

Period (year)	Investment ($)	Net Cash Flow ($)	Cumulative Net Cash Flow ($)
0	85,344.73 $		
1		238,625.52 $	238,625.52 $
2		234,710.95 $	473,336.47 $
3		233,811.20 $	707,147.67 $
4		232,564.04 $	939,711.71 $
5		230,160.75 $	1,169,872.46 $
6		223,725.73 $	1,393,598,19 $
7		219,542.89 $	1,613,141.08 $
8		212,576.01 $	1,825,717.09 $
9		208,807.18 $	2,034,524.27 $
10		202,241.00 $	2,236,765.27 $
Total	85,344.73 $		

For the calculation, an update factor of 3.20% is used, which corresponds only to the estimated inflation for the year 2025 as provided by the Central Bank, since the Municipal GAD of the Sigchos Canton is not an investor; therefore, the passive rate offered by the financial system for savings is not taken into account.

The NPV (Net Present Value) can be calculated as follow:

$$NPV = \sum(Updated\ Net\ Cash\ Flow - Updated\ Investment) \quad (2)$$

$$NPV = 1{,}812{,}081.54\ \$$$

The net present value of the project is $1,812,081.54, which is a figure greater than zero, indicating that the investment will yield returns above the required rate of return (Table 6).

The benefit-cost ratio is an indicator that separates the updated revenues and expenditures of the project and the relationship between them (Table 7). It determines how many times the revenues exceed the expenditures.

The Benefit-Cost Ratio can be calculated as follow:

$$BC = \frac{\sum(Net\ Cash\ Flow)}{Current\ Investment} \quad (3)$$

$$BC = 22.23$$

The profitability of a project is a financial indicator that measures the project's ability to generate economic benefits in relation to the initial investment made

Table 6
NPV (Net Present Value) of the studied project

Period	Current Values		Discount Factor	Updating Factor	
	Investment	Net Cash Flow		Investment	Net Cash Flow
0	85,344.73 $		1	85,344.73 $	
1		238,625.52 $	0.969		231.228.13
2		234,710.95 $	0.939		220.393.58
3		233,811.20 $	0.91		212.768.19
4		232,564.04 $	0.882		205.121.48
5		230,160.75 $	0.854		196.557.28
6		223,725.73 $	0.828		185.244.90
7		219,542.89 $	0.802		176.073.40
8		212,576.01 $	0.777		165.171.56
9		208,807.18 $	0.753		157.231.81
10		202,241.00 $	0.73		147.635.93
Total		2,236,765.27 $		85,344.73 $	1,897,426.27 $

Table 7
Benefit-Cost Ratio

Period	Investment	Net Cash Flow Updated Cash
0	85,344.73 $	
1		231.228.13
2		220.393.58
3		212.768.19
4		205.121.48
5		196.557.28
6		185.244.90
7		176.073.40
8		165.171.56
9		157.231.81
10		147.635.93
Total	85,344.73 $	1,897,426.27 $

Table 8
Project Profitability

Profitability	
Project Cost	561,712.88 $
Sale Cost	792,000.000 $
Profit USD$	230,287.12 $
Profitability	41.00 %

The table demonstrates that with an initial investment (project cost) of $561,712.88, the brick factory generated sales amounting to $792,000.00, resulting in a profit of $230,287.12. This translates to a profitability of 41% (Table 8).

3. Results and Discussion

The market study reveals a strong demand and acceptance among representatives of the parishes in the Sigchos canton for the production of vehicular pavers, supporting the need to enhance local road infrastructure and promote economic development. Additionally, a market opportunity is identified in both government projects and private initiatives, with an estimated daily demand of 2,800 units of vehicular pavers. The absence of local manufacturers presents a significant opportunity for establishing a paver factory in the region, which can leverage direct marketing channels to effectively reach consumers.

In summary, the study suggests a favorable outlook for the production and marketing of vehicular pavers in Sigchos canton, backed by robust demand and the lack of local competition. The technical study focused on the product architecture and production process of both vehicular and pedestrian pavers, adhering to standards such as INEN 3040. Efficient processes were designed, covering everything from material selection to the storage of finished products, with an annual production capacity of 2,880,000 pavers. Rigorous quality control measures and balances of raw materials and personnel were established, while fixed asset and manufacturing costs were meticulously analyzed. A retail price was determined with a 30% profit margin, following validation of its acceptance through a survey, and specific areas were allocated within the manufacturing plant to ensure operational efficiency.

The administrative-legal analysis conducted for the establishment and operation of the high-traffic paver factory in Sigchos canton reflects a comprehensive and proactive approach to meeting legal and regulatory requirements. The decision to form a Corporation (S.A.) is based on the separation of responsibilities between shareholders and the company, providing stability and flexibility in business management. Furthermore, the need to complete legal processes such as obtaining the Unique Taxpayer Registry (RUC), Land Use Permit, Municipal License, and Environmental Permit demonstrates a

commitment to legality and environmental respect. Additionally, the analysis of labor obligations established in the Labor Code ensures the protection of workers' rights.

The financial study results indicate that the project is economically viable, as evidenced by positive outcomes in the Net Present Value (NPV), Payback Period (PP), and Benefit-Cost Ratio (BCR). Moreover, the short payback period of six months and the high profitability of 41% further corroborate its financial viability.

4. Conclusion

The conducted study demonstrates the high viability of establishing a high-traffic paver factory in Sigchos canton. The unmet demand from local parishes, combined with the absence of direct competitors, creates a potentially lucrative market. From a technical perspective, an efficient and high-quality production process has been designed, complying with current regulations. Additionally, the administrative-legal analysis ensures adherence to all legal and labor requirements. Finally, the financial assessment reveals the project's robustness, with positive economic indicators supporting its short-term profitability. In conclusion, the establishment of this factory not only addresses a local infrastructure need but also represents an opportunity for economic development in Sigchos canton.

References

[1] Van Damme, O., H. Van Geelen, and P. Courange, The evaluation of road infrastructure development projects. Transportation Research Procedia, 2016. 14: p. 467-473.

[2] Džumhur, Saša, Žanesa Ljevo, and Jasmina Marić. "BIM Project Execution Planning Suited for Road Infrastructure Pilot Project in Bosnia and Herzegovina." Advanced Technologies, Systems, and Applications II: Proceedings of the International Symposium on Innovative and Interdisciplinary Applications of Advanced Technologies (IAT). Springer International Publishing, 2018. https://doi.org/10.1007/978-3-319-71321-2_50

[3] Alvansazyazdi, Mohammadfarid, et al. "Exploring Crack Reduction in High-Performance Concrete: The Impact of Nano-Silica, Polypropylene, and 4D Metallic Fibers."

[4] Gonzalez-Navarro, Marco, and Climent Quintana-Domeque. "Paving streets for the poor: Experimental analysis of infrastructure effects." Review of Economics and Statistics 98.2 (2016): 254-267.

[5] Shen, Li-yin, et al. "Project feasibility study: the key to successful implementation of sustainable and socially responsible construction management practice." Journal of cleaner production 18.3 (2010): 254-259. https://doi.org/10.1016/j.jclepro.2009.10.014

[6] Leiner, Dominik. "Convenience samples from online respondent pools: A case study of the SoSci Panel." Studies in Communication| Media (SCM) 5.4 (2014): 367-396.

[7] INEN, N., 3040, IE de N.(2016). Adoquines de Hormigón NTE INEN 3040. Instituto Ecuatoriano de Normalización. 45.

[8] Córdoba Padilla, M., Formulación y evaluación de proyectos. 2011, Ecoe ediciones.

Author Guidelines EditEdit Author Guidelines

GENERAL GUIDELINES FOR AUTHORS

Journal of civil engineering researches invites unsolicited contributions of several forms: articles, reviews and discussion articles, translations, and fora. Contributions should fall within the broad scope of the journal, as outlined in the statement of scope and focus. Contributors should present their material in a form that is accessible to a general anthropological readership. We especially invite contributions that engage with debates from previously published articles in the journal.

Submissions are double-blind peer-reviewed in accordance with our policy. Submissions will be immediately acknowledged but due to the review process, acceptance may take up to three months. Submissions should be submitted via our website submission form (see links above for registration and login). Once you login, make sure your user profile has "author" selected, then click "new submission" and follow the instructions carefully to submit your article. If problems arise, first check the FAQ and Troubleshooting guide posted below. If you are still experiencing difficulty, articles can be submitted to the editors as email attachments.

Each article should be accompanied by a title page that includes: all authors' names, institutional affiliations, address, telephone numbers and e-mail address. Papers should be no longer than 10,000 words (inclusive of abstract 100-150 words, footnotes, bibliography and notes on contributors), unless permission for a longer submission has been granted in advance by the Editors. Each article must include a 100 words "note on contributor(s)" together will full institutional address details, including email address. We request that you submit this material (title page and notes on the contributors) as "supplementary files" rather than in the article itself, which will need to be blinded for peer-review.

We are unable to pay for permissions to publish pieces whose copyright is not held by the author. Authors should secure rights before submitting translations, illustrations or long quotes. The views expressed in all articles are those of the authors and not necessarily those of the journal or its editors. After acceptance, authors and Special Issue guest editors whose institutions have an Open Access library fund must commit to apply to assist in article production costs. Proof of application will be requested. Though publication is not usually contingent on the availability of funding, the Journal is generally under no obligation to publish a work if funding which can be destined to support open access is not made available.

Word template and guidelines

Our tailored Word template and guidelines will help you format and structure your article, with useful general advice and Word tips.

(La)TeX template and guidelines

We welcome submissions of (La)TeX files. If you have used any .bib files when creating your article, please include these with your submission so that we can generate the reference list and citations in the journal-specific style

Artwork guidelines

Illustrations, pictures and graphs, should be supplied with the highest quality and in an electronic format that helps us to publish your article in the best way possible. Please follow the guidelines below to enable us to prepare your artwork for the printed issue as well as the online version.

Format: TIFF, JPEG: Common format for pictures (containing no text or graphs).

EPS: Preferred format for graphs and line art (retains quality when enlarging/zooming in).

Placement: Figures/charts and tables created in MS Word should be included in the main text rather than at the end of the document.

Figures and other files created outside Word (i.e. Excel, PowerPoint, JPG, TIFF, EPS, and PDF) should be submitted separately. Please add a placeholder note in the running text (i.e. “[insert Figure 1.]")

Resolution: Rasterized based files (i.e. with .tiff or .jpeg extension) require a resolution of at least 300 dpi (dots per inch). Line art should be supplied with a minimum resolution of 800 dpi.

Colour: Please note that images supplied in colour will be published in colour online and black and white in print (unless otherwise arranged). Therefore, it is important that you supply images that are comprehensible in black and white as well (i.e. by using colour with a distinctive pattern or dotted lines). The captions should reflect this by not using words indicating colour.

Dimension: Check that the artworks supplied match or exceed the dimensions of the journal. Images cannot be scaled up after origination

Fonts: The lettering used in the artwork should not vary too much in size and type (usually sans serif font as a default).

Authors services:

For reformatting your manuscript to fit the requirement of the Journal of Civil Engineering Researchers and/or English language editing please send an email to the following address:

researchers.services@gmail.com

Noted: There is a fixed charge for these mentioned services that is a function of the manuscript length. The amount of this charge will be notified through a reply email.

FAQ AND TROUBLESHOOTING FOR AUTHORS

I cannot log in to the system. How do I acquire a new user name and password?

If you cannot remember your username, please write an email to (journals.researchers@gmail.com), who will locate your username and notify you. If you know your username, but cannot remember your password, please click the "Login" link on the left-hand menu at homepage. Below the fields for entering your username and password, you will notice a link that asks "Forgot your password?"; click that link and then enter your email adddress to reset your password. You will be sent an automated message with a temporary password and instructions for how to create a new password. TIP: If you do not receive the automated email in your inbox, please check your SPAM or Junk Mail folder. For any other issues, please contact our Managing Editor,Kamyar Bagherinejad (admin@journals-researchers.com).

How do I locate the online submission form and fill it out?

First you need to register or login (see above). Once you are logged in, make sure the "roles" section of your profile has "Author" selected. Once you assign yourself the role of "Author," save your profile and then click the "New Submission" link on your user home page.

Once you arrive at the submission form page, please read the instructions carefully filling out all necessary information. Unless specified otherwise by the editors, the journal section to be selected for your submission should be "Artlcles." Proceed to the remaining sections, checking all boxes of the submission preparation checklist, and checking the box in the copyright notice section (thus agreeing to journals-researchers's copyright terms). Once the first page is completed, click "Save and Continue." The next page allows you to upload your submission. Use the form to choose your file from your computer. Make sure you click "Upload." The page will refresh and you may then click "Save and Continue." You will then proceed to a page for entering the metadata for your article. Please fill out all required fields and any further information you can provide. Click "Save and Continue." The next page allows you to upload supplementary files (images, audiovisual materials, etc.). These are not required, but if you wish to provide supplementary materials, please upload them here (do no forget to click "Upload." Then click "Save and Continue." This brings you to the final page of the submission form. Please click "Finish Submission" in order to close the

submission process. You wil then be notified by email that your article has been successfully submitted. TIP: If you do not receive the automated email in your inbox, please check your SPAM or Junk Mail folder. For any other issues, please contact our Managing Editor, Kamyar Bagherinejad (admin@journals-researchers.com).

Why am I not receiving any email notifications from HAU?

Unfortunately, some automated messages from Open Journal Systems arrive in users' Spam (or Junk Mail) folders. First, check those folders to see if the message was filtered into there. You may also change the settings of your email by editing your preferences to accept all mail from [jcer] and related journals-researchers.com email accounts.

I am trying to upload a revised article following an initial round of peer-review, but I cannot locate where to upload the article. Where do I submit a revised article?

Follow the login process outlined above and when you successfully login you will see on your user home page a link next to "Author" for "active" articles in our system (usually it is only one article, but if you have mulitple submissions currently in our system, the number could be higher. Click the "Active" link and you will be led to a page that lists your authored articles currently in our system. Click the link under the column labeled "Status" and this will take you to a page showing the current review status of your article. At the very bottom of the screen, you will see an upload form under the heading "Editor decision." Here you may upload your revised article. An automated email will be sent to the editors and you may also notify them directly via email. You may then logout.

I successfully submitted an article; how long will it take for the editors to respond to me with a decision.

For all articles that are recommended for peer-review, the editors of JCER strive to notify authors of a decision within 4-6 weeks. You may contact JCER's Managing Editor, Kamyar Bagherinejad (admin@journals-researchers.com). if you have any questions relating to the review process and its duration.

For all other inquiries, please contact: Kamyar Bagherinejad (Managing Editor)

Privacy Statement

The names and email addresses entered in this journal site will be used exclusively for the stated purposes of this journal and will not be made available for any other purpose or to any other party.

Articles

Section default policy

Make a new submission to the Articles section.

Copyright Notice EditEdit Copyright Notice

Journal of Civil Engineering Researchers follows the regulations of the International Committee on Publication Ethics (COPE) and the ethical principles of publishing articles in this journal are set based on the rules of this committee, and in case of problems, it will be treated according to these rules.

Privacy Statement EditEdit Privacy Statement

The names and email addresses entered in this journal site will be used exclusively for the stated purposes of this journal and will not be made available for any other purpose or to any other party.

Scholars Pavilion

Scholars Pavilion or **Scholars Chartagi** is a monument donated by the Islamic Republic of Iran to the United Nations Office at Vienna. The monument architecture is claimed by the Islamic Republic News Agency of Iran to be a combination of Islamic and Achaemenid architecture, although the latter clearly predominates in the decorative features, with Persian columns and other features from Persepolis and other remains from the Achaemenid dynasty. The Chahartaq pavilion form runs through the architecture of Persia from pre-Islamic times to the present.

Statues of four famous Persian medieval scholars, Omar Khayyam, Al-Biruni, Muhammad ibn Zakariya al-Razi and Ibn-Sina are inside the pavilion. This monument donated in June 2009 in occasion of Iran's peaceful developments in science.

J-Researchers